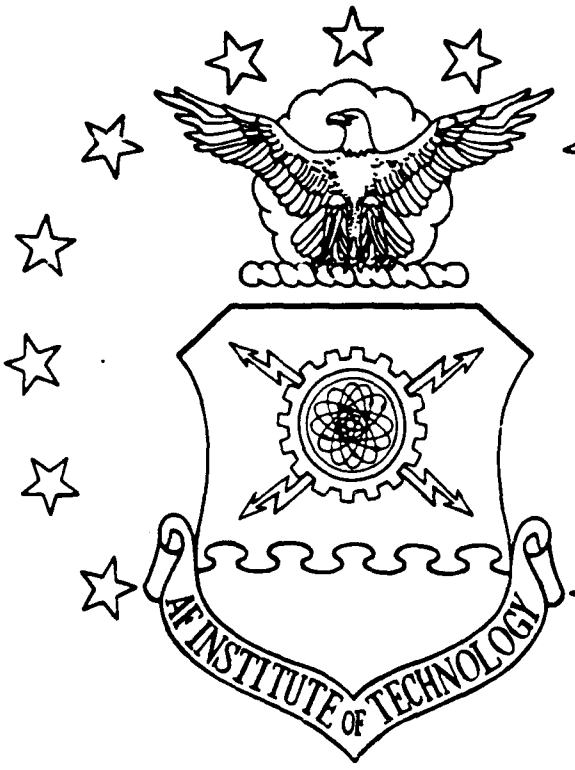

INVESTIGATION OF THE FAILURE MODES IN A METAL MATRIX COMPOSITE UNDER THERMAL CYCLING

THESIS

Paul G. Ermer
Captain, USAF

AFIT/GAE/ENY/89D-07

DEPARTMENT OF THE AIR FORCE
AIR UNIVERSITY
AIR FORCE INSTITUTE OF TECHNOLOGY

Wright-Patterson Air Force Base, Ohio

AFIT/GAE/ENY/89D-07

INVESTIGATION OF THE FAILURE MODES IN A METAL MATRIX COMPOSITE UNDER THERMAL CYCLING

THESIS

Presented to the Faculty of the School of Engineering

of the Air Force Institute of Technology

Air University

In Partial Fulfillment of the

Requirement for the Degree of

Master of Science in Aeronautical Engineering

Paul G. Ermer

Captain, USAF

December 1989

Preface

The first objective of this thesis was to develop a Thermal Fatigue (TF) testing system for Metal Matrix Composites (MMCs). I could not have accomplished this task without the help of Jay Anderson, John Pernot, and the rest of the technicians in the Aero Lab. They helped with the connections of all the components of the system and trouble-shooting the computer software.

I would also like to thank Dr. A. Nagar of the Flight Dynamics Laboratory and Mr D. A. Harmon of McDonnell Douglas St. Louis for providing the material. I am indebted to my thesis advisor Dr. Shankar Mall, for all his help and patience he has given me during this project and to Mr. Ted Fecke of the Propulsion Laboratory for his financial support in purchasing some necessary equipment.

Most of all I wish to thank my wife, Catherine, for her divine understanding during the past 18 months, and especially for her help in typing and editing this work. Lastly, thanks goes to our daughter Amanda who always added sunshine to the day.

Paul G. Ermer

Table of Contents

List of Figures

List of Tables

Abstract

There is currently wide interest in producing a vehicle capable of hypersonic flight. Structural materials in such a vehicle must be able to withstand high temperatures and retain high stiffness. Metal matrix composites (MMCs) are rapidly becoming the strongest candidates for these applications and concurrently, the need to study the effects of thermal cycling on them. This study emphasizes the development of a computer-controlled testing system that thermally fatigues a specimen under a variety of thermal conditions.

A titanium matrix composite with silicon carbide fibers (SCS_6/Ti-15-3) is the object of this study. To demonstrate the capability of this system, ten thermal fatigue tests were completed. The MMC was cycled from 300°F to 800°F while collecting strain and temperature data. A systematic study was undertaken to investigate the initiation and progression of the damage and its effect on mechanical properties as a function of applied thermal stresses.

Results show that for up to 16,750 cycles, material properties remain unchanged and do not correlate with thermal cycling. Interior damage begins at 500 cycles as deformation of the fiber/matrix interface. Exterior damage begins at 1,500 cycles as delamination cracks along the ply seams.

INVESTIGATION OF THE FAILURE MODES IN A METAL MATRIX COMPOSITE UNDER THERMAL CYCLING

I. Introduction

There is currently wide interest in producing a vehicle capable of hypersonic flight (24:2). Such a vehicle under consideration is the National Aerospace Plane (NASP). One of the key technology areas in the NASP Program is the development of high temperature materials.

In order to achieve hypersonic flight, materials are required which will experience both monotonic and cyclic thermal loadings which are unprecedented (19:1). Structural materials in such a vehicle must be able to withstand high temperatures and retain high stiffness while carrying significant stresses (24:2). As an example, the leading edge airfoil surfaces of the NASP are expected to see thermal loads in excess of 2000°F, and must maintain significant load bearing capability at these extreme temperatures (19:1). Missiles and structural applications of new generation propulsion systems have similar requirements (8:1388). Turbine disk temperature and load limit profiles experienced during a typical flight cycle are shown in Figure 1 (31:240).

Because of their unique combinations of properties, both continuous filament and discontinuously reinforced metal matrix composites (MMCs) are being developed for use in advanced DoD

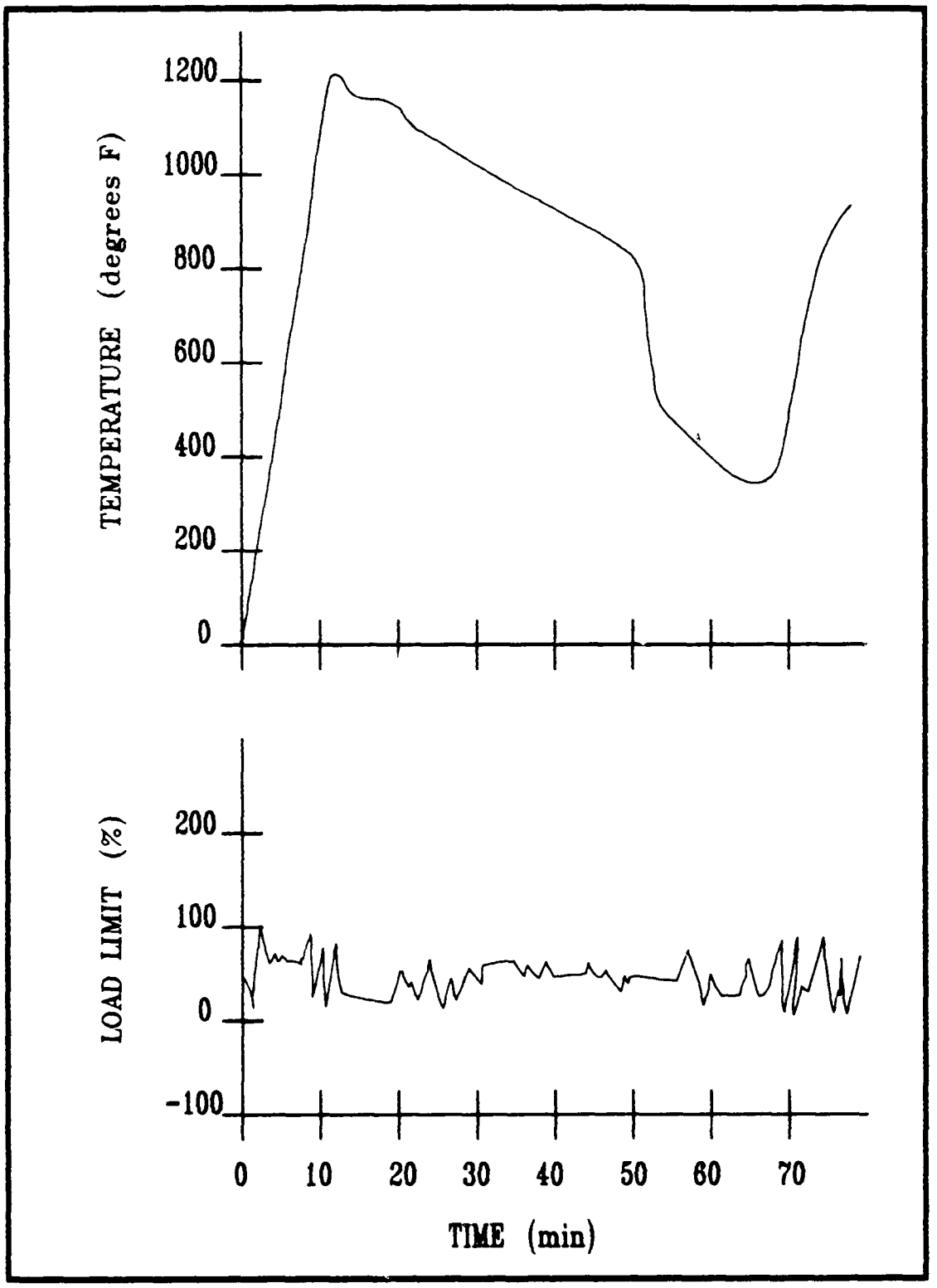

Figure 1. Temperature and Load Limit Profiles of Turbine Disk During Typical Flight Cycles

structural applications (11:19-1). Continuous fiber reinforcement is expected to maintain reasonable stiffness and strength and limit creep at elevated temperatures. The metal matrix offers toughness, especially during takeoff, where foreign object impact is of concern to the NASP (25:89).

Other desirable properties include high moduli, low coefficients of thermal expansion (CTE), long term dimensional stability and good fracture, fatigue and corrosion resistance. Of much current interest to the DoD are MMCs fabricated using aluminum, titanium, magnesuim, and copper alloy matrix materials with various reinforcements of graphite, silicon carbide, boron or alumina (16:1).

Titanium reinforced with continuous silicon carbide fibers is a metal matrix system that has been considered for high temperature applications. The particular system of interest in this study is designated as SCS6/Ti-15-3. As a material system, SCS6/Ti-15-3 MMC has a potential for application at temperatures up to 1300°F, although oxidation effects could limit use temperatures. SCS6/Ti-15-3 is a good model material, and may be considered the forerunner of more advanced titanium aluminide based MMCs.

What differentiates the composite system from other low temperature composites such as Al-Boron, is its higher temperature capability, significantly higher matix and interface strengths, and presence of reaction zones at the fiber-matrix interfaces. Because of the extreme reactivity of Ti, the reaction zone is extremely difficult

to avoid in Ti based composites, including the new generation of aluminide based composites (26:2). Thus, the work presented here should have a broad validity in the rapidly developing field of high temperature MMCs.

In order to better design MMC components in high temperature application, one must assess a complete picture of their performance in high temperature environments. Among the high temperature environments, thermal cycling is known to cause significant degradation in most MMC systems (25:89).

The degradation of thermally cycled MMCs has been primarily attributed to the mismatch of CTEs between fiber and matrix and also to the formation of reaction products at fiber/matrix interfaces. These result in microscopic level degradation in MMCs; the formation of microvoids in W/Cu composites, the roughing and cracking of the interfaces in B/Al composites, Al_2O_3 composites, Al_2O_3/Mg composites and SiC/Ti composites (25:90). The microscopic level degradation always associated with the fiber matrix interfaces leads to the macroscopic level degradations, a reduction in mechanical properties, and changes in size (25:90).

In a recent study of the room temperature behavior of laminates composed of Ti-15-3-3 matrix reinforced by continuous SCS6 silicon carbide fibers, Johnson et. al. (19:40) reported nonlinear elastic material response and significant degradation in mechanical properties resulting from the separation of the fiber and matrix (25:89). Before

the investigation, failure of the fiber/matrix interface was not expected, as it had not been observed in a silicon carbide/aluminum composite. However, since the yield stress of the titanium is much larger than the yield strength of aluminum, the fiber/matrix interface in the titanium matrix system must sustain much higher stresses before matrix yielding. In order to improve the performance of metal matrix composites, the reaction of the interface to thermal cycling and its correspondence with the fatigue failure of the MMC must be known.

Fatigue failure in continuous filament MMCs usually originates at stress concentrations located at the specimen surface, at broken fiber ends, or at the fiber/matrix interface as already mentioned. The mechanisms leading to failure occur by combinations of the following steps (11:3).

1) Fatigue hardening of the matrix
2) Crack initation and propagation in the matrix
3) Localized separation of the filaments from the matrix
4) Fracture of overloaded filaments
5) Transfer of load to unbroken filaments causing overload and fracture of neighboring filaments
6) Rupture

The first goal of this effort was to develop a thermal fatigue (TF) testing system for the SCS6/Ti-15-3 MMC. This material is expensive and rare to come by; therefore, the test system must be capable of testing small specimens. There is also a current need for

an apparatus to test material in a safe and relatively inexpensive manner. The TF system uses quartz lamps to heat the specimen and a strain-gage type of extensometer to measure strain. The complete system is explained later in this thesis.

This system was successfully used to support the second goal of this work, TF testing of SCS6/Ti-15-3 metal matrix composite. For this purpose, a systematic study was undertaken to investigate the initiation and progression of the thermal fatigue damage and its effect on the mechanical properties as a function of applied thermal stresses. A series of 300°F to 800°F TF tests were conducted which are described in detail in subsequent chapters.

II. Thermal Fatigue of MMCs

Thermal Fatigue Testing

Fatigue refers to a material's deterioration caused by repeated loading. Components can be stressed beyond their elastic limits, as in the case of those subjected to thermal stresses induced by temperature oscillations. The test systems used to measure a material's resistance to thermal fatigue utilize an external heating and cooling source that can rapidly heat and cool localized areas of samples. Typically the sample sports a sharp edge that is designed to be the initiation site for cracks. The compact tension (CT) specimen is an example.

MMCs are not as adaptable to the measurement of crack growth as CT specimens. Investigators of MMCs are more concerned with where and how damage initiates and how it progresses. TF testing is used to understand MMCs and their failure modes so they can better be used in modern applications.

TF testing equipment requires a mechanical holding device and a temperature controlling system. They must be capable of subjecting the material to a variety of temperature profiles. Figure 2 shows several temperature profiles of interest.

Most equipment used for TF testing consists of closed loop temperature systems. The equipment usually includes a mechanical holding device that has been modified by some means to heat the specimen. The holding device can customarily load the material for

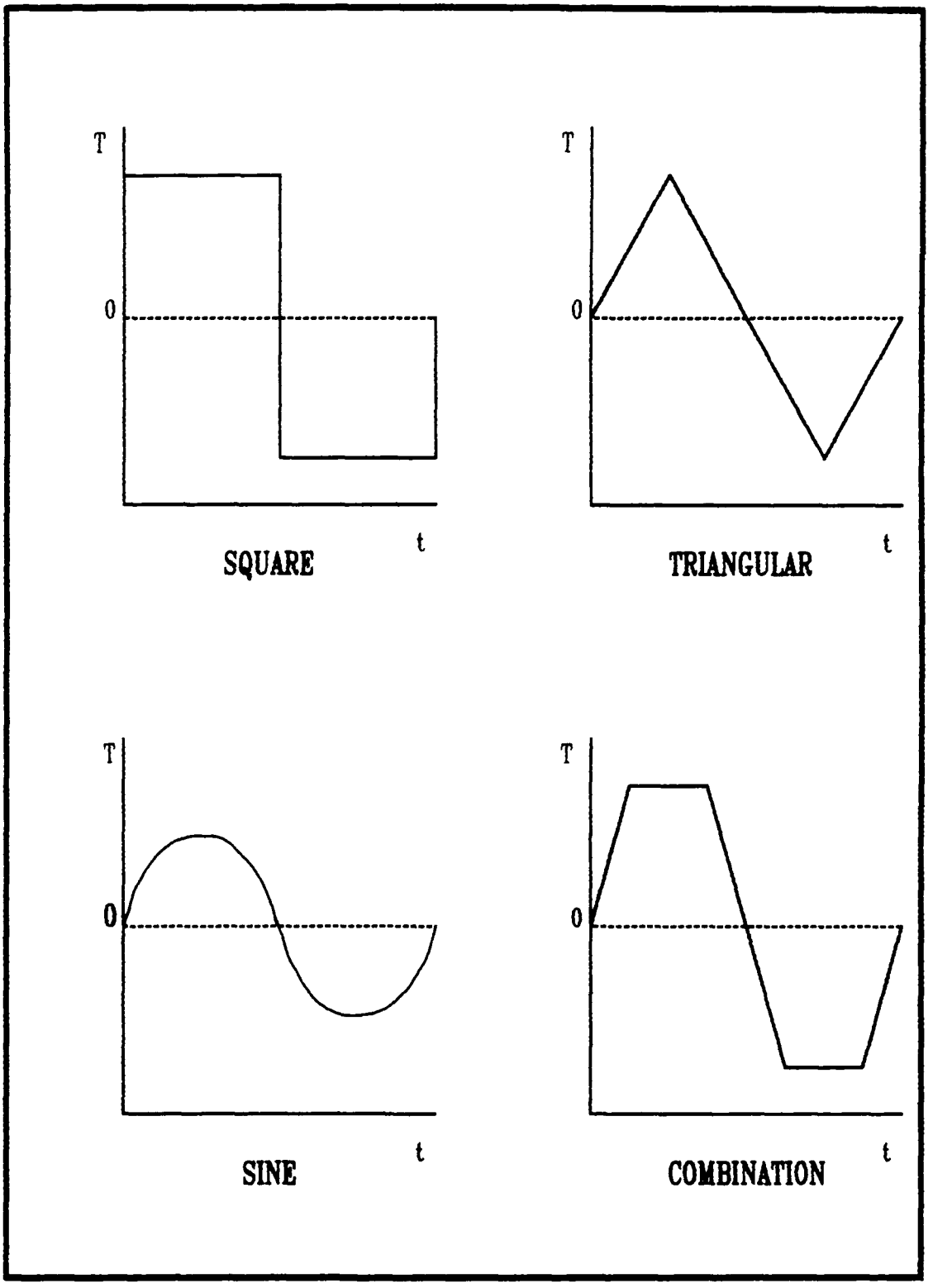

Figure 2. TF Temperature Profiles

post TF test analysis such as Ultimate Tensile Strength (UTS), Young's Modulus, Poisson's Ratio, etc. There are four basic means for transferring heat to and from the specimen: (1) fluidized bed, (2) radiation, (3) resistance heating, and (4) radio frequency induction (16:35).

The hot fluidized bed technique can be used to heat specimens at a very high rate. Heating and cooling is possible by alternately immersing the specimens in hot and cold fluidized beds. The bed has been used extensively by Mowbray and Woodford (16:36) in an attempt to identify alloys with the greatest thermal fatigue resistance.

Radiation heating lamps can be used for thermal testing applications. This method is chosen by some researchers since it is clean and relatively easy to control. Heil (18:20,23) used four quartz lamp heaters to perform TF tests. Heating and cooling rates of 14.4°F per second were used to cycle temperatures between 800°F and 1200°F. Compressed air cooled the specimen. Heil welded type-K thermocouple wire to the specimen for feedback and control.

Oleinik, Pogrebnyak, and Zmil (33:321-323) have designed a device that uses radiation heating to achieve specimen temperatures up to 3272°F for fatigue tests. The heating is produced by passing high current through a 0.24 inch diameter molybdenum rod wound in a four-loop spiral around a cylindrical test specimen. Specimen temperature is measured by platinum/rhodium - platinum/rhodium (type PR-30/6) thermocouples welded along the working zone. The temperature variation

in this zone is 2 percent, but a high frequency regulator can control temperatures to within 3.6°F. This device is limited to a heating rate of 72°F per minute.

Passing high current through a specimen can result in high heating rates with a great amount of control. Wilson and Warren (37:3) of Pratt and Whitney used current up to 1200 amps between 0 and 3 volts AC to achieve heating rates of 100°F per second using closed loop control. Temperatures of center crack tension (CCT) specimens ranged from 200°F to 1000°F. This heating method can be dangerous, since high current is constantly applied to the specimen. A major disadvantage of the method is it creates a non-uniform temperature field around the crack tip.

Pelloux and Marchand (34:A4) have used the radio frequency technique for thermo-mechanical fatigue tests of nickel-based superalloys. They have found that low frequency heaters produce lower wall thickness gradients and have fewer grounding problems than the high frequency heaters. They use thermocouples for temperature measurements and feedback, and a thermistor for a stabe cold junction required for control of the system.

Majumdar and Newaz (26:5) measured strains with a strain-gage type of extensometer. Strain was monitored over a 1 inch gage length. The extensometer was modified for high temperatures by adding ceramic probes that were spring loaded laterally against the edge of the specimen.

MMC Testing

The promising attributes of metal matrix composites are well known and have motivated interest in the potential use of these materials in a number of aerospace and other high technology applications. These attributes include high stiffness to density ratio, low thermal expansion coefficient, high thermal conductivity, and good environmental resistance. However, along with these characteristics there are certain unique response characteristics that require attention. In particular, these include nonlinear thermo-mechanical response which is generally exhibited in a stress-strain curve or in a strain-temperature curve. In addition it has been observed that fracture toughness may be a problem for these systems.

The selection of the suitable metal matrix composites for a particular application is influenced by the need to consider these special characteristics and also by the existence of a large number of candidate systems in the form of different constituents, different fabrication processes, and different internal material geometry. In view of the complexity of the situation, a sound approach to evaluating different metal matrix composites for selection for a particular application requires a combination of theory and experiment for both material and structural evaluation.

Fatigue of metal matrix composites can be quite complex. The matrix, because of its relatively high strength and stiffness compared to the fiber, plays a very active role compared to a polymer matrix.

Fatigue damage in a metal matrix can reduce the laminate stiffness by as much as 50 percent without causing laminate failure (23:9).

Fatigue failure modes in continuous fiber reinforced metal matrix composites are controlled by the fiber and matrix and by the fiber/matix interfaces. The relative strains to fatigue failure of the fiber and matrix will determine the failure mode provided the fiber/matrix interface is strong enough to support the required load. If the matrix requires much less cyclic strain to fatigue than the fiber, then the matrix damage will dominate. If on the other hand, the fiber requires less cyclic strain to fail than does the matrix, the fiber damage will dominate. This composite will fail rather suddenly in fatigue with little warning, provided that fiber/matrix interface is strong enough to transfer load into the broken fibers. The fiber/matix interface may be unable to carry the required stress and may fail, causing the fiber/matrix separation. This is likely to occur in those MMC systems with high yield strength matrices that cause high load transfer between fiber and matrix in the off-axis plies. Lastly, if both the fiber and matrix require approximately the same cyclic strain for fatigue failure and the fiber/matrix interface is sufficiently strong, self-similar crack growth, as found in metals, may result. Self-similar crack growth is also possible when the matrix is strong enough to create a high stress concentration in the fiber ahead of the matrix crack. Thus, by starting the fatigue damage in the matrix, the crack can propagate across the fibers (23:2).

As new continuous fiber-reinforced metal matrix composites are hypothesized and developed, projection of their fatigue behavior can be made by understanding the relative strengths of the fiber, matrix and fiber/matrix interface.

The role of the interface between the fiber and matrix of a composite has received a great deal of attention regarding its effects upon mechanical performance. Most recently, the interface condition has been extensively studied and discussed within the context of its effect upon toughness and energy dissipation during the fracture process of brittle composites. For example, Budiansky, Hutchinson and Evans (7) examine several interface parameters associated with these effects including Coulomb friction coefficient, fiber/matrix debonding energy and fiber/matrix interface pressure. Their work draws upon previous modeling reported by Aveston, Cooper and Kelly (1). One philosophy drawing heavily on such understanding and applied during development of new composite materials where toughness is an issue, has been to engineer so-called "weak" interfaces which promote energy absorption through fiber/matrix bonding and frictional processes (32:2).

Of course, in addition to an energy dissipation mechanism during failure, the fiber/matrix interface is also essential to the normal transfer of load throughout the composite, thus contributing to both stiffness and strength. As a result, other authors have focused on the mechanical effects of interface integrity upon average composite

stiffness and strength properties. Chen and Lin (32:3) considered the behavior of completely bonded and completely unbonded interface conditions and examined their effects upon transverse modulus and strength. A unit-cell finite element model of a regular packed array of fibers imbedded in a matrix was applied in that study. Results for both conditions were compared with experiments conducted on a boron-aluminum composite system and the authors concluded from comparing analysis and experiment that the boron-aluminum composite behaved like a well bonded system. More recently, Takahashi and Chou (32) reported on the effects of these same two bounding conditions for interface integrity using a cavity formation model. These authors show that a vanishingly weak interface results in lower transverse composite modulus and strength. In an effort to model a more general interface condition. Aboudi (32) formulated a model which characterized interface integrity with two parameters quantifying the degree of adhesion in the normal and tangential direction. A common assumption in all three of these investigations is to ignore the effects of process-induced residual stresses.

Review of recent work suggests that most of the high temperature isothermal fatigue and thermo-mechanical fatigue work to date were confined to unidirectional SCS6/Ti-15-3 composites. Gayda et. al. (15) observed that while on a stress range basis, the isothermal fatigue life (at 572°F and 1022°F) of a 0-degee uniaxial SCS6/Ti-15-3 composite was higher than the matrix alloy, the reverse was true when fatigue

life was compared on a strain range basis. It was suggested that fatigue life was probably not matrix dominated, but more likely it was governed by fiber/matrix interface characteristics. In reference (14), isothermal and in-phase and out-of-phase load-controlled bithermal TMF experiments were performed on the same material between 572°F and 1022°F. Both in-phase and out-of-phase fatigue lives were found to be shorter than IF life when data were compared on a stress basis. On a strain range basis, in-phase and out-of-phase fatigue lives fell on the same curve, indicating no differences. It was suggested that this behavior was because TMF life was interface controlled. However, in reference (15), the matrix fatigue life on a strain range basis was fairly constant over the used temperature range, so that the authors' contention of interface controlled life might need further mechanical validation. In reference (24), Johnson et. al. studied the tensile and fatigue behavior of uniaxial and angle-ply SCS6/Ti-15-3 composites at room temperature. The authors suggested that in the angle-ply system, the 0-degree plies played a significant role in controlling fatigue life.

Majumdar and Newaz (26) investigated the thermo-mechanical fatigue (TMF) response of a quasi-isotropic SCS6/Ti-15-3 angle ply. Load controlled in-phase TMF experiments were performed over the temperature range 600-1200°F, and parallel isothermal fatigue (IF) experiments were conducted at 1200°F. It was observed that the total strain range stabilized to a fairly constant value within a relatively short number

of fatigue cycles. For the TMF specimens, a good correlation was obtained between the total measured strain range and TMF life. On a stress range basis, TMF life was found to be significantly shorter than IF life. Damage mechanisms showed transverse microcracks oriented perpendicular to the loading axis in IF specimens. In TMF specimens significant inter-ply delamination type of damage, parallel to the loading axis, was observed both near and away from the fracture surface. Inter-ply delamination cracking also was significant in thermally cycled specimens, but not in IF specimens. Most of the microcracks were found to originate at the fiber/matrix interface or in the fiber/matrix reaction zone.

Metal Matrix Composite Analyzer: METCAN

The computer program, called METCAN, was used to analyze the response of the MMC in this study. A description of the code follows.

The multi-cell model (MCM) is composed of a unique set of micromechanics equations for the analysis of high temperature metal matrix composites developed by Hopkins and Chamis (20). The set is comprised of closed-form expressions to predict equivalent pseudo homogeneous properties for the unidirectional fiber reinforced ply. The multi cell is formulated to predict lamina and laminate properties and stress-strain behavior in an average sense. The multi-cell model has been incorporated into the computer program METCAN (27) by Murphy and Hopkins.

In formulating the MCM, the principles of displacement compatibility and force equilibrium were used. The periodic structure of a unidirectional metal matrix composite ply is approximated by a square array unit cell model, as shown in Figure 3. Figure 3 also indicates the three subregions (A, B, C) which are defined to characterize the through-the-thickness nonuniformity of the constituent stresses and material properties. In Figure 3, D is the fiber diameter and D_0 is the diameter of the interface region.

The micromechanics equations used in a multi-cell model are derived for the case of a transversely isotropic (isotropic in the x_2-x_3 plane) ply assuming the constituents are also isotropic or transversely isotropic.

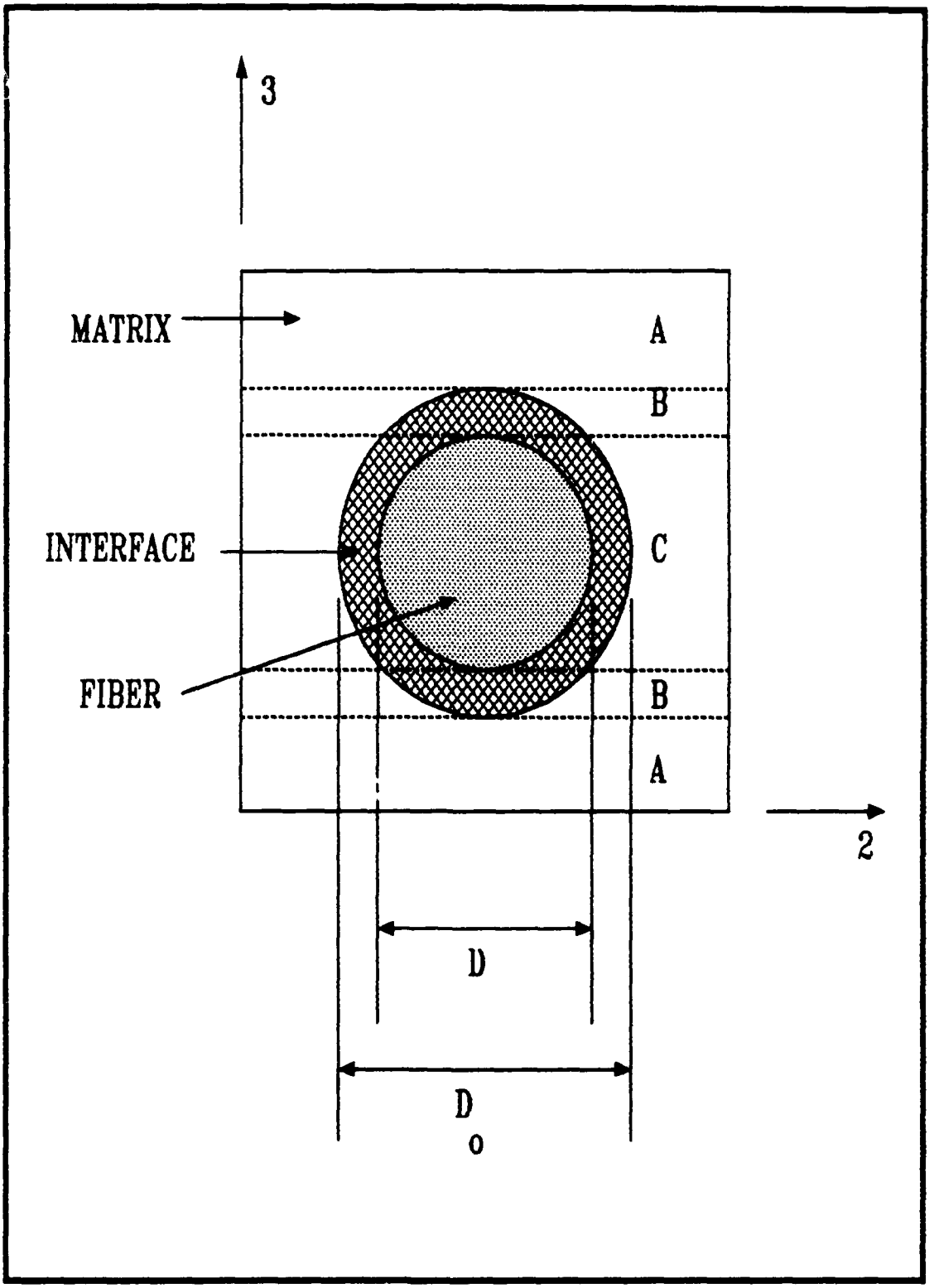

Figure 3. Multi-Cell Model Showing Subregions

The micromechanics equations used in the MCM are summarized in (20). These equations include expressions for ply equivalent mechanical properties, ply equivalent thermal properties, ply inplane uniaxial strengths, and thermomechanical constituent stresses. Reference 15 also presents the procedure in deriving the micromechanics equations. For illustrative purposes, selected equations are included in this report.

Ply mechanical properties (longitudinal modulus):

$$E_{111} = v_m E_{m11} + v_f \left[\left[1 - \left[\frac{D}{D_o} \right]^2 \right] E_{d11} + \left[\frac{D}{D_o} \right]^2 E_{f11} \right] \quad (1)$$

Ply thermal properties (longitudinal coefficent of thermal expansion):

$$\alpha_{111} = v_m \frac{E_{m11}}{E_{111}} \alpha_{m11} + v_f \left[1 - \left[\frac{D}{D_o} \right]^2 \right] \frac{E_{d11}}{E_{111}} \alpha_{d11} + \quad (2)$$

$$\left[\frac{D}{D_o} \right]^2 \frac{E_{f11}}{E_{111}} \alpha_{f11}$$

Constituent stresses (longitudinal fiber and matrix):

$$\sigma_{f11} = \left[\frac{\sigma_{111}}{E_{111}} + \delta T \left[\alpha_{111} - \alpha_{f11} \right] \right] E_{f11} \qquad (3)$$

$$\sigma_{m11} = \left[\frac{\sigma_{111}}{E_{111}} + \delta T \left[\alpha_{111} - \alpha_{m11} \right] \right] E_{m11} \qquad (4)$$

In these equations, the subscripts f, m, d, and l indicate fiber, matrix, interface, and lamina properties respectively. The terms E, α and v are the modulus, coefficient of thermal expansion and volume fraction, respectively. δT is the temperature change.

METCAN (METal Matrix Composite ANalyzer) is a computer code (27) developed at the NASA Lewis Research Center to perform nonlinear analysis of fiber-reinforced metal matrix composites. The METCAN program is primarily focused for use with large structural analysis programs where one material system may be used in a variety of structural configurations. For example, the standard output is set up to interface with NASTRAN by printing the laminate material property cards in a correct format for NASTRAN. The METCAN code is compatible with FORTRAN 77 standards and is fairly machine independent. The program uses the MCM in a multifactor-dependent nonlinear relationship

to predict mechanical properties, thermal properties, and constituent stresses, among other things.

METCAN also incorporates thermoviscoplastic nonlinear constitutive relationships (TVP-NCR) that consist of products of terms with unknown exponents (9). These relationships were formulated for METCAN by Chamis and Hopkins. The exponents are determined for the specific materials and type of nonlinear dependence. The exponents are determined from available experimental data or estimated from anticipated behavior of the particular term.

The generic form for the TVP-NCR is as follows:

$$\frac{P}{P_o} = \left[\frac{T - T_F}{T_F - T_o}\right]^n \left[\frac{S - \sigma_F}{S - \sigma_F}\right]^m \left[\frac{\dot{S} - \dot{\sigma}_F}{\dot{S} - \dot{\sigma}_F}\right]^l \cdots \left[\frac{\dot{T} - \dot{T}_F}{\dot{T} - \dot{T}_F}\right]^k \left[\frac{N_{MF} - N_M}{N_{MF} - N_{Mo}}\right]^q \left[\frac{N_{TF} - N_T}{N_{TF} - N_o}\right]^r \left[\frac{t - t_F}{t - t_F}\right]^s \cdots \tag{5}$$

where

P denotes the property of interest

P_o is the corresponding property at reference

T is the current temperature

T_o is the reference temperature at which P_o is determined

N_M are the mechanical cycles

N_T are the temperature cycles

S_F is the fracture stress determined at T_o conditions

σ_o is the reference stress at which P_o is determined

σ is the current stress state

The subscripts F, o, M, T. denote the final or characteristic property, reference, mechanical and thermal, respectively. The superscript · indicates rate of change in time of the underlying variable. The exponents n, m, l, k, q, r, s are determined from observed or expected behavior. The terms with these exponents represent the effects of temperature, stress, stress rate, temperature rate, mechanical cycles, thermal cycles and time, respectively.

Each term on the right hand side of the above equation describes a monotonic functional dependence of P/P_o from some initial property value to a terminal or ultimate material state. The specific shape of the function depends on the exponent; thus, a variety of functional dependences can be simulated using the TVP-NCR equation.

One advantageous feature of the METCAN computer code is its resident databank of constituent (fiber, matrix, and interface) material properties. By storing the appropriate information in the databank, the user merely has to specify the corresponding code name to access the properties for the specific fiber, matrix or interface. In addition to the material properties, the databank also stores the exponents and initial values of stresses for each constituent.

The loading is input into the program through tabular input representing discrete points on the loading curve. Temperature and mechanical loads (inplane stresses, inplane moments, transverse shear loads, and surface pressures) can be applied.

Although the micromechanical model employed in METCAN is that of a unidirectional ply, the program can analyze a composite laminate of any stacking sequence. The program has an output option feature so that the user may control the type and quantity of output.

III. Experimental Equipment

As previously mentioned, the first objective of this study was to develop a thermal fatigue (TF) testing system to study the SCS6/Ti-15-3 metal matrix composite. The capability of the system was demonstrated by performing a series of TF tests on $[0]_6$ ply layup MMC. The testing system is described here.

Test System

The test system required for TF studies consists of a mechanical holding device, thermal control unit, and a strain measurement instrument. Figures 4 and 5 are pictures of the actual system. A main computer is used to record all cyclic temperature and strain data. Figures 6 shows a block diagram of the entire system. The mechanical holding of the specimen is produced by a Material Testing System (MTS) servohydraulic loading and control system. Proper temperature is maintained by heating and cooling the specimen. The heating is provided by two quartz lamp heaters controlled by a microprocessor that uses thermocouples for feedback. The specimen is cooled by jets of compressed air regulated by both manual and process-controlled electric valves. Strains are monitored using a strain-gage type of extensometer, with quartz probes that are spring loaded against the middle portion of the specimen's gage length. Although this system was designed for testing strips of MMC, it can easily be modified for use

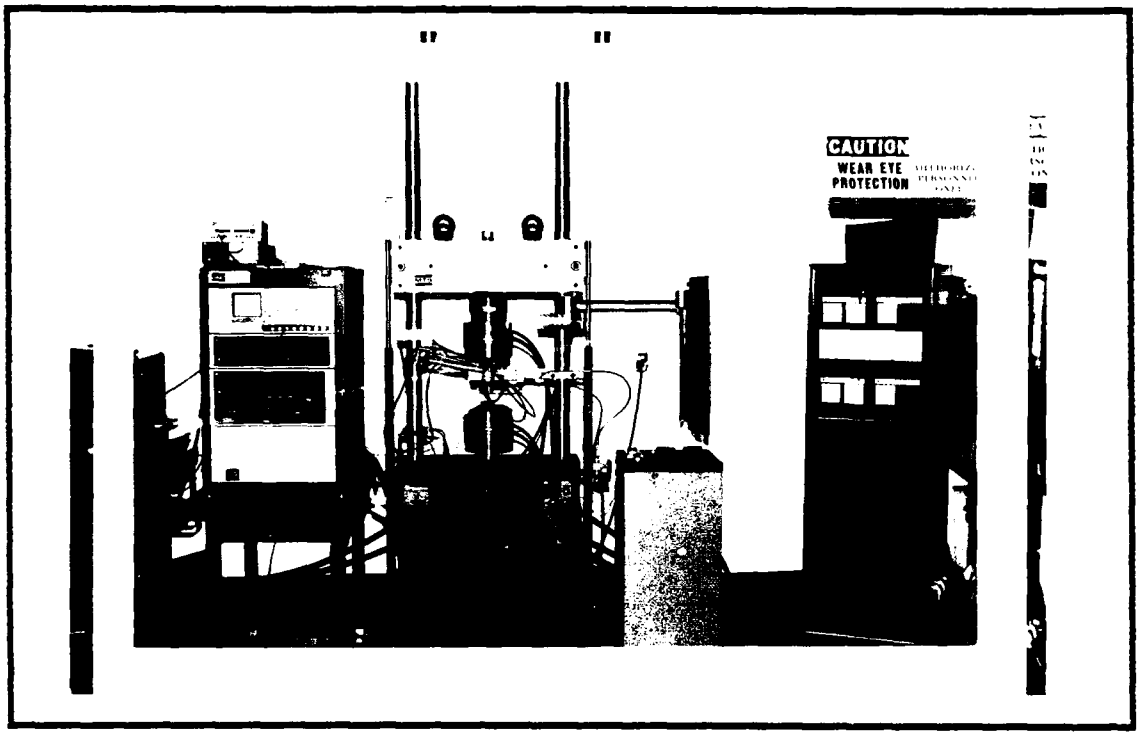

Figure 4. TF Test System

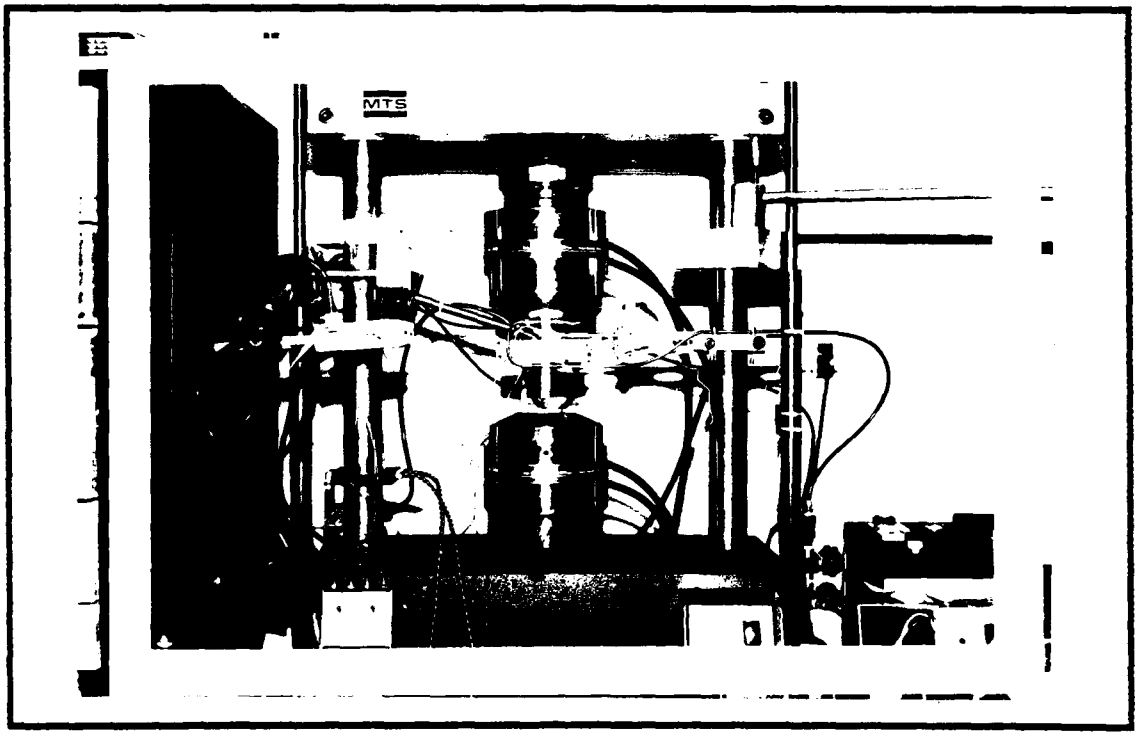

Figure 5. MMC Ready for TF Testing

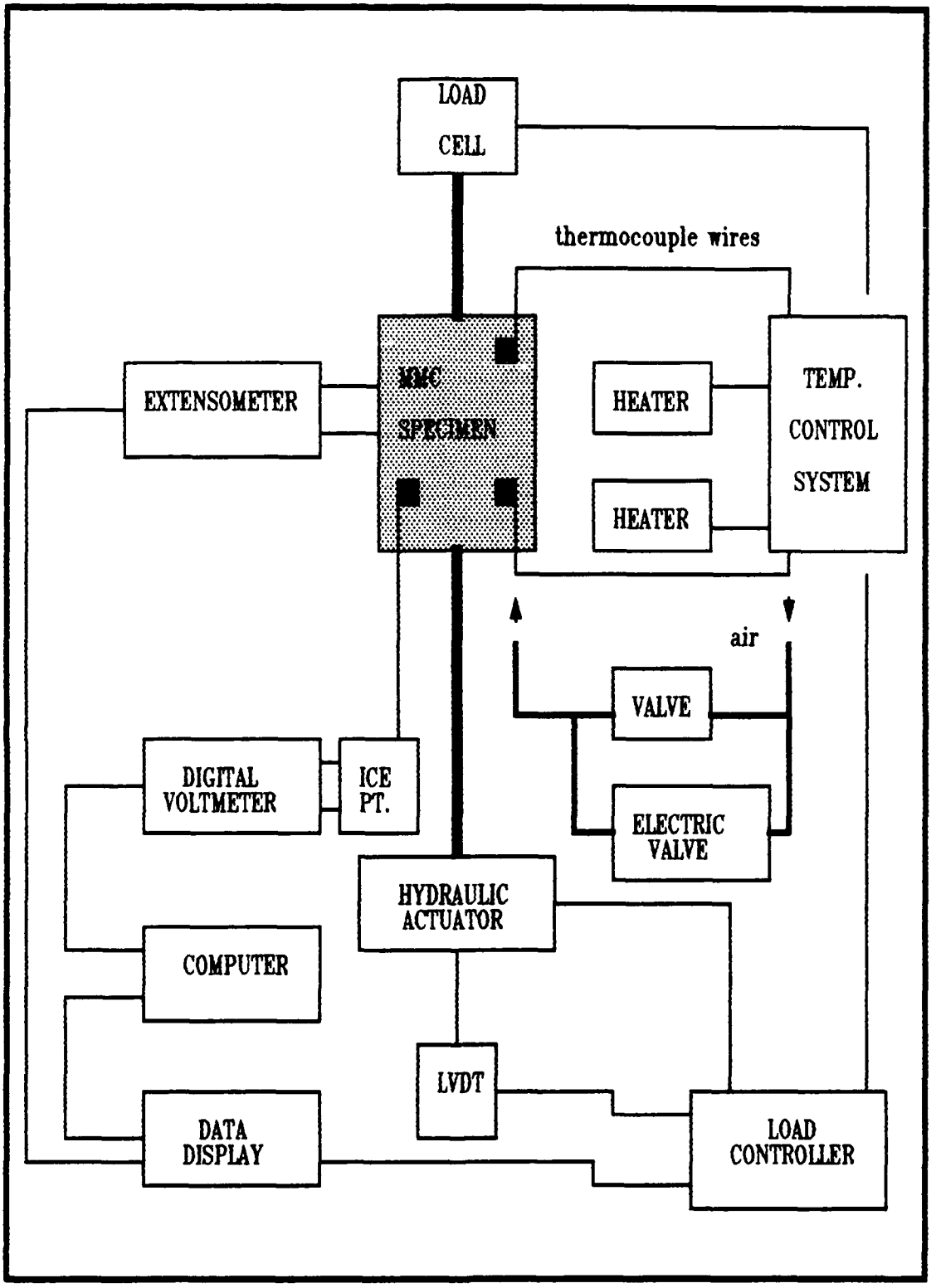

Figure 6. Block Diagram of Testing System

with other geometries. All components of the testing system will be described in detail.

Mechanical Holding System

The major components of the system that mechanically hold the specimen are shown in Figure 7. They include:

1) 22 kip MTS model 810 servohydraulic machine
2) MTS model 458 MicroConsole
3) MTS model 464 Data Display
4) High temperature hydraulic grips

The 22 kip MTS loading machine was used to suspend the specimen between the quartz lamp heaters with its upper grip while TF testing took place. After the TF testing portion was complete, the lamps were swung aside and the lower grip was raised into position to load the sample to collect Young's modulus and Poisson's ratio. The MTS machine was operated in the 10,000 lb. maximum load-control range using the load cell for feedback. The data display reads load and displacement from the controllers and displays it for recording. The load cell was calibrated to within 0.5 percent for the 10,000 lb. range setting.

To isolate the hydraulic gripping devices and load cell from any extreme temperature gradients, special high temperature wedge grips were used. The stainless steel grips were manufactured to allow for

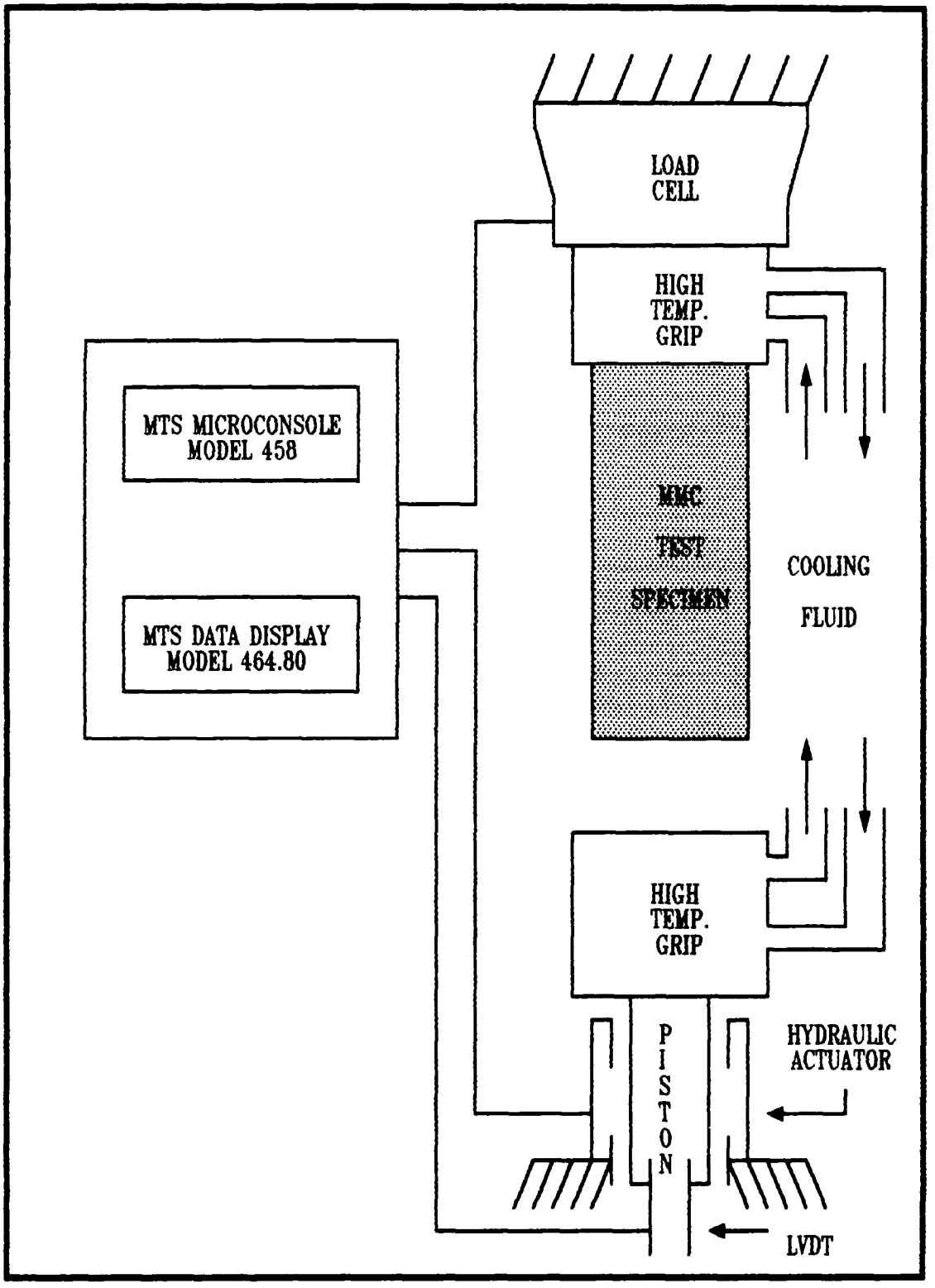

Figure 7. Mechanical Holding Device

the circulation of cooling fluid. Distilled water was pumped through the grips and constantly cooled to room temperature with a water conditioning unit. The high temperature grips prevented conductive heating of both the load cell and the hydraulic piston. The other modification to the MTS machine was a tinted plexiglas safety shield. The shield was mounted on the load frame to block the instense radiation emitted from the quartz lamp heaters, while safely allowing an observer to watch the TF testing. The shield could swing out of the way for access to the specimen.

Temperature Control System

The components used for temperature control of the specimen are shown in Figure 8. The major components of the system are:

1) Micricon 82300 process control system
2) Two quartz lamp heaters
3) HP 3437A digital voltmeter
4) Zenith 248 computer
5) Manual and process-controlled cooling air system
6) Cooling water arrangement

The specimen was heated with two quartz lamp heaters. The lamp heaters used were of the parabolic strip type with a 1000 watt tungsten-filament quartz lamp. The parabolic surface of each heater reflects

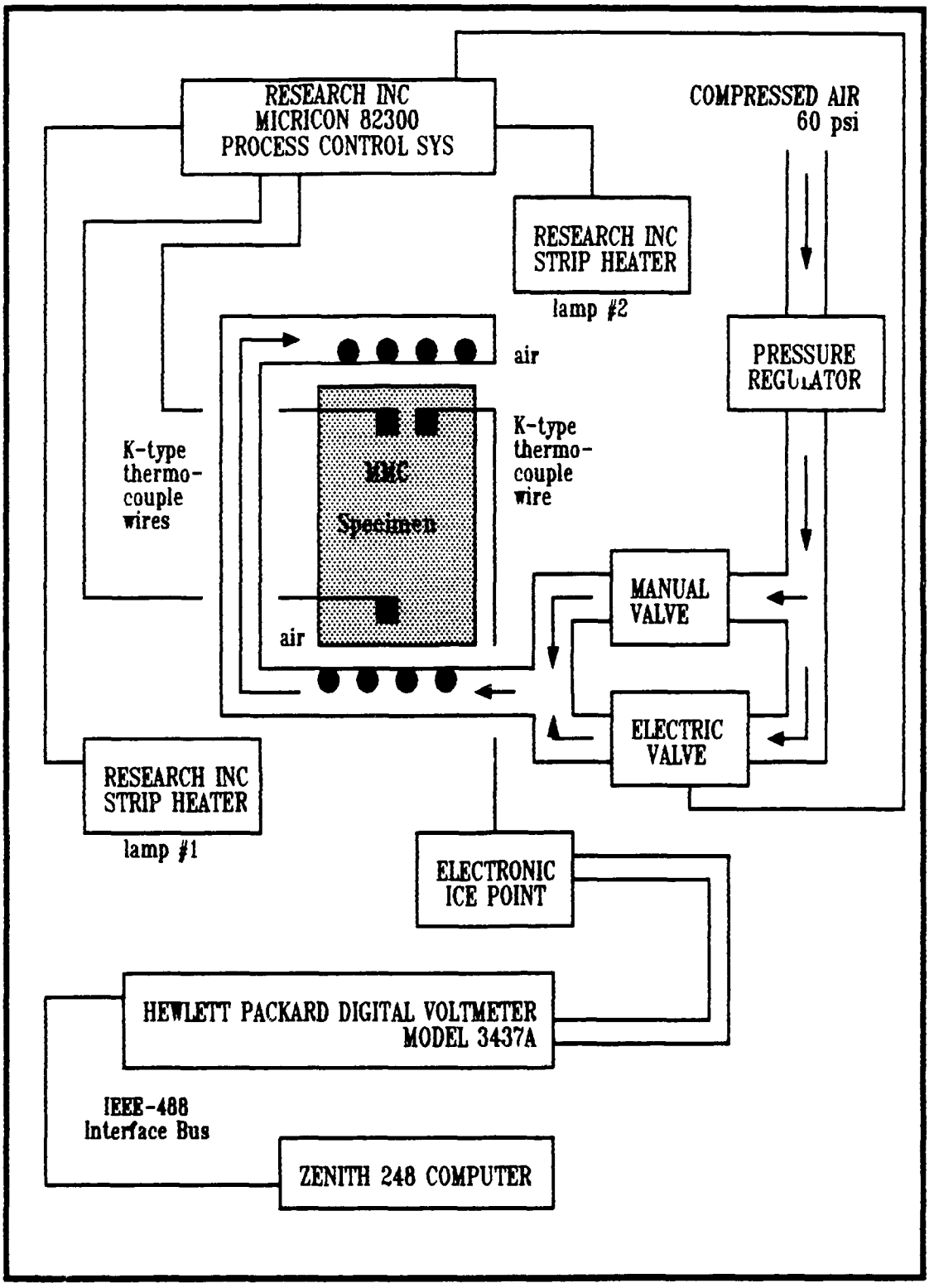

Figure 8. Temperature Control System

radiant energy onto a 1 inch section of the specimen. The specimen absorbs the infrared radiant energy and converts it to heat energy. A major advantage of this heating method is that the energy passes through the air without heating it; therefore, most of the energy is transmitted directly to the specimen. A disadvantage of this method is that to operate most efficiently, a specimen should be dark and nonreflective to absorb more energy, but for this test the heating rates and temperatures were adequate for the natural surface condition of the specimen.

The heaters are mounted on aluminum brackets and connected to the MTS load frame with a rod and knuckle type arrangement as shown in Figure 9. The main mounting bracket is clamped to the frame of the MTS machine, and the mounting knuckle is allowed to rotate in order to swing the lamps away from the specimen when required. The rods and knuckles can rotate and translate as shown in order to position the lamps to obtain the proper heating coverage of the specimen. This arrangement provided the flexibility to heat a small specimen. When the lamps are in a position that provides a uniform temperature distribution across the specimen, the adjustment screws can be tightened to prevent further movement.

One lamp was positioned horizontally on each face of the specimen. The number one lamp was placed on the front face of the specimen slightly higher than center and the number two lamp was placed on the back face of the specimen slightly lower than center. The areas

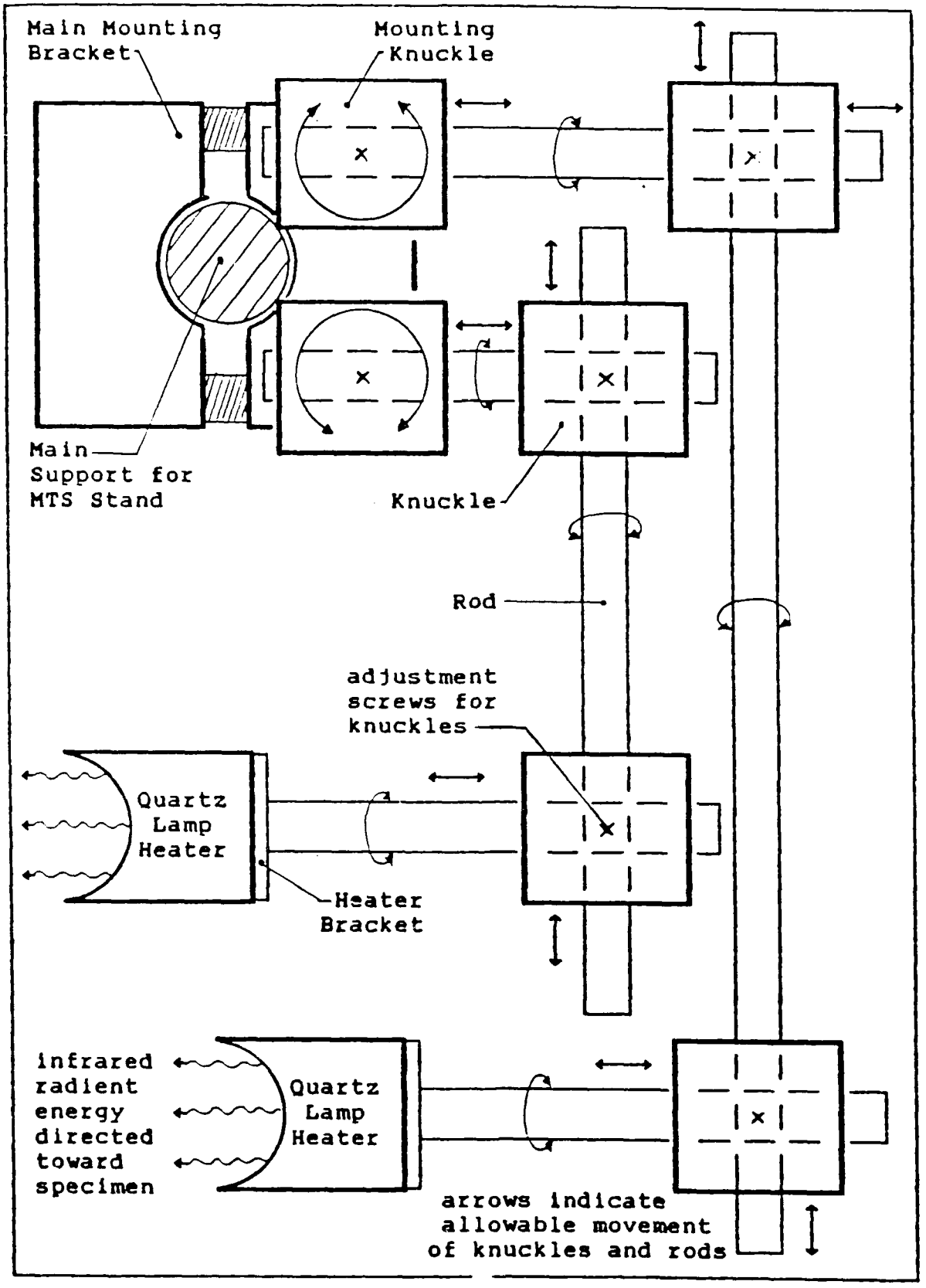

Figure 9. Top View of Mounting Assembly for Heating Lamps

overlapped in the center for complete coverage. Heil (18:21) used similiar lamp configurations to heat center crack tension specimens. During temperature cycling, Heil was able to maintain temperature variations of 5°C (9°F) or less.

During temperature cycling, forced convective cooling was required to reduce specimen temperatures in the desired time. Jets of air were blown across the front and back of the specimen as illustrated in Figure 10. Initial experimentation showed that low levels of air flow used during heating resulted in less temperature variation across the specimen and smooth temperature transition during cycling. This brought about a need for two levels of air flow, one for use during heating of the specimen and the other for cooling. The two levels of air flow are described for Figure 11. The manual valve is adjusted to achieve the desired level of air flow for the heating portion of the cycle. During cooling, the electric valve opens, allowing secondary air flow to pass over the specimen. To regulate the air flow, a pressure regulator was placed in the flow before the two valves. With this two-level cooling process, heating and cooling rates of 20.8°F per second were achieved (300°F to 800°F cycles in 48 second periods).

A Micricon 82300 process control system was used to control and power the heating lamps and to open the electric valve for the cooling air. Three sets of Chromel-Alumel (type-K) thermocouple wires were welded to the specimen at the locations shown in Figure 12 for feedback and temperature readings. These positions were chosen after trying

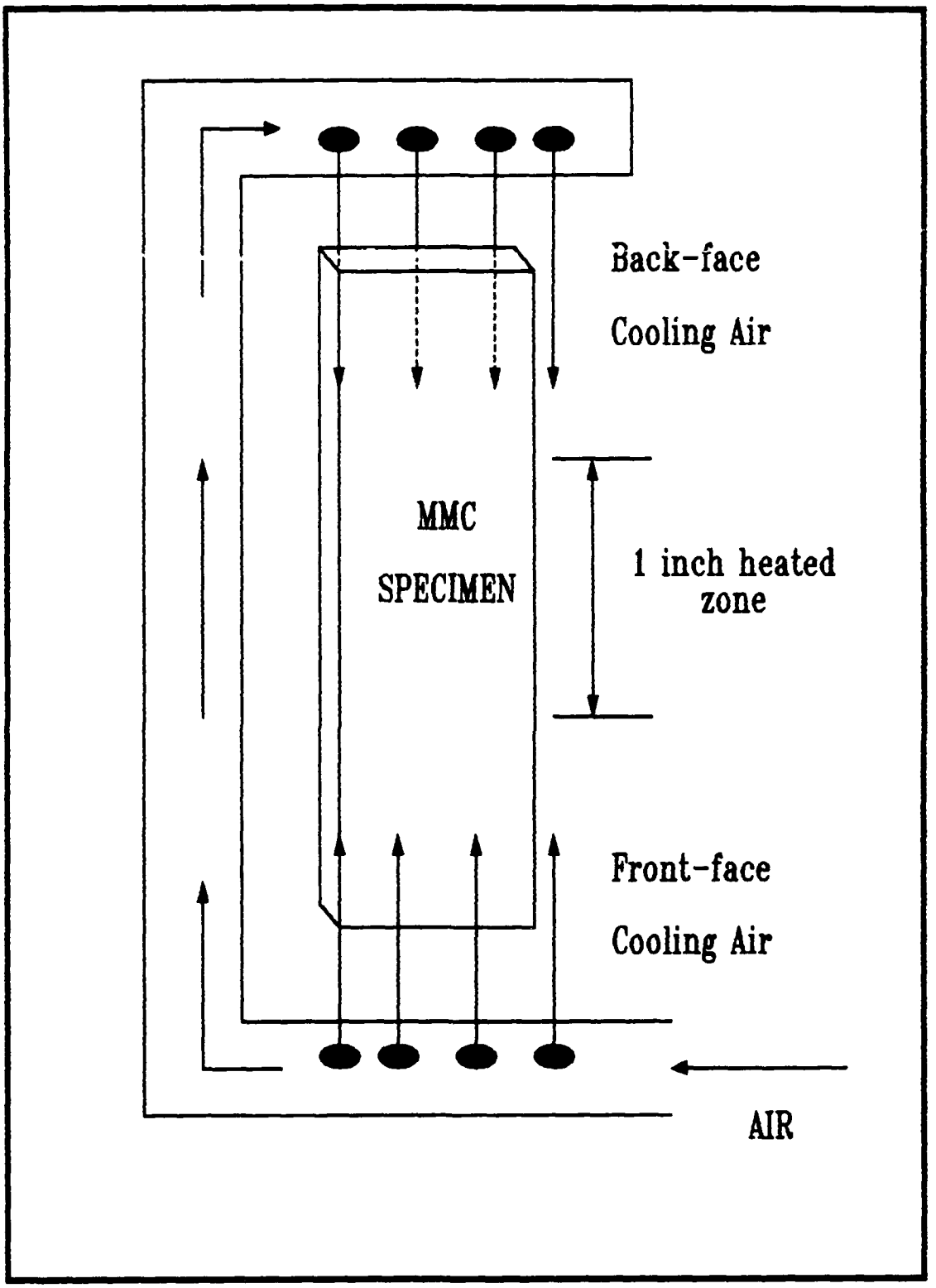

Figure 10. Compressed Air Cooling Jets

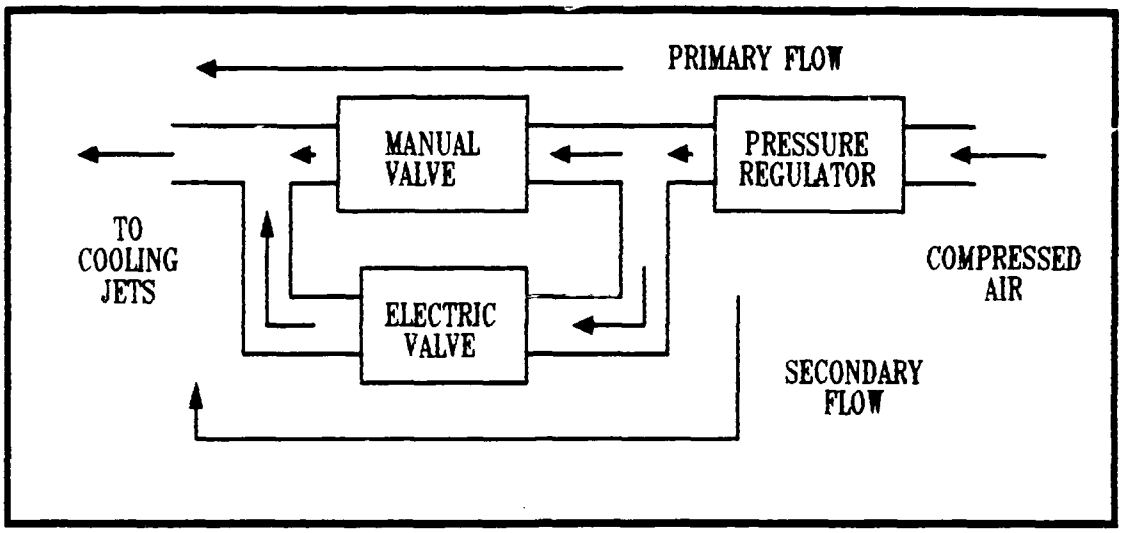

Figure 11. Primary and Secondary Air Flow to Cooling Jets

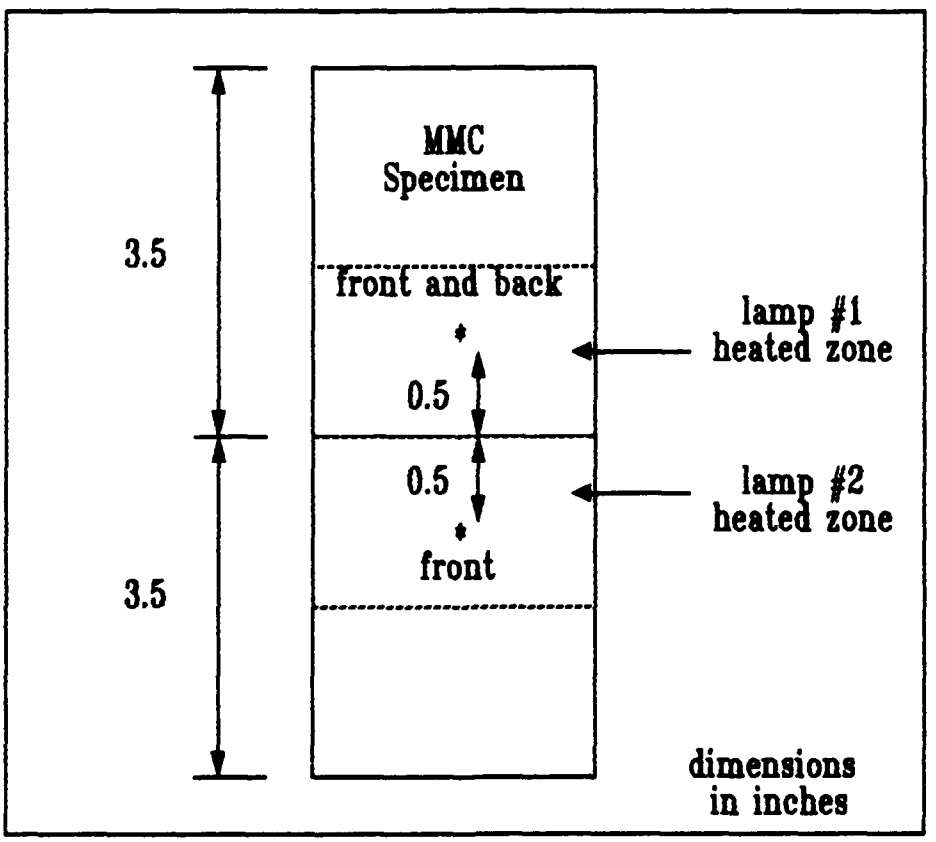

Figure 12. Thermocouple Locations on the MMC Specimen

various locations. The two thermocouples used for feedback to the Micricon were placed at the center of the heating lamps radiation area but on the face opposite the lamp. At these locations, the temperature deviations across the gage length were at the most 1 percent during temperature cycling tests between 300°F and 800°F.

Besides operating the lamps, the Micricon 82300 has a programming capability to directly control the thermal cycling of the specimen. The cycling can be input into the Micricon as a series of command segments (140 total), each describing one step in the heating and cooling process. Each segment requires as inputs the temperature to be reached, and the specified time to reach it. The Micricon calculates a setpoint temperature every second of the segment and controls the lamp appropriately to match the feedback thermocouple temperature to the setpoint temperature. A sequence of segments can be programmed to first heat the specimen and then allow it to cool linearly over the chosen period. The sequence can be repeated for a maximum of 250 cycles. Groups of sequences can be programmed to increase the number of cycles. Every segment includes an alarm to be identified which activates a specified relay at the rear of the Micricon. Closing the relay sends power to the electric valve allowing air to blow over the specimen during the cooling portion of the cycle.

The Micricon 82300 uses three-mode, proportional, integral, and derivative (PID), control. PID control in the Micricon is described in Figure 13. The proportional factor, or gain, determines how the output

of the controller will vary with a change in the error signal. The gain setting can be adjusted between 0.0 and 128.0 (29:1.4,2.9). During preliminary experiments with the Micricon, gain settings between 20.0 and 60.0 were used to create cyclic temperature profiles of 300°F to 800°F with a period of 48 seconds.

Integral, or reset, adds to or subtracts from the gain to determine the final output. Reset is used to correct the steady state error (offset) when using PID control (13:7). The reset control for the Micricon can be set between 0.0 and 60.23 repeats per minute to correct the offset in the maximum (peak) temperature (29:2.9).

The derivative factor, or rate, takes into account the time lag in the system (13:11). Rate values ranging from 0.0 to 8.5 minutes can be set.

Research Inc., manufactures of Micricon, suggest that gain and reset be set first, simultaneously (28:5). The gain should be set as high as possible without creating large oscillations of lamp output. Preliminary tests showed that an increase in output resulted in an instantaneous increase in temperature; therefore, rate was not required for control of the lamps. After the gain was set, the reset was used to eliminate the offset. According to Research Inc., reset values that are too large cause oscillations of the lamp output as in the case of too much gain. However, oscillation of the lamp output did not occur for any value of reset used. A gain value of 21.0 and reset value of 55.0 worked well for the temperature cycling tests. Rate was

not used since only proportional and integral (PI) control was required for the quartz lamp heaters. The specified values of gain and reset allowed for sharp peaks and valleys at the setpoint temperatures without any oscillations of lamp output. These oscillation must be avoided since they drastically reduce the life of the tungsten-filament lamp.

The minimum (LO LMT) and maximum (HI LMT) output sent to the lamps can be controlled by the Micricon 82300. LO LMT and HI LMT values of 4.0 and 85.0 percent were used during cycling tests to extend the bulb's life. Using the LO LMT and HI LMT setting prevents large jumps in current output to the lamps.

As previously mentioned, three thermocouples were welded to the specimen. The thermocouple not used for Micricon feedback was used to record the thermocouple voltage through the HP3437A voltmeter. The voltmeter's resolution was not high enough to accurately measure the thermocouple's voltage at the lower temperatures; therefore, an amplifier was built to magnify the voltage ten times before being input to the voltmeter. The voltage was then converted to temperature using the relation obtained from the thermocouple manufacturer, Omega Engineering Inc. (10:T.12).

$$T(^{\circ}C) = (C_0 + C_1x + C_2x^2 + \ldots + C_8x^8)/10 \qquad (6)$$

where the constants are defined as:

$C_0 = 0.226584602$ $C_1 = 24152.109$

$C_2 = 67233.4248$ $C_3 = 2210340.682$

$C_4 = -860963914.9$ $C_5 = 4.83506 \times 10^{10}$

$C_6 = -1.18452 \times 10^{12}$ $C_7 = 1.38690 \times 10^{13}$

$C_8 = -6.33708 \times 10^{13}$

and:

x = voltage read by the voltmeter in volts

Temperature is converted to °F by:

$$T(°F) = 32.2 + (9/5)T(°C) \qquad (7)$$

The recorded temperature was used to generate temperature versus time plots.

The final component of the temperature control system is the water cooling arrangement in Figure 14. The high temperature grips and the quartz lamps both require coolant, in this case distilled water, to be pumped through them. Distilled water was used to prevent corrosion of the components. A water conditioner reduced the water temperature after it circulates through all the components and returns to the

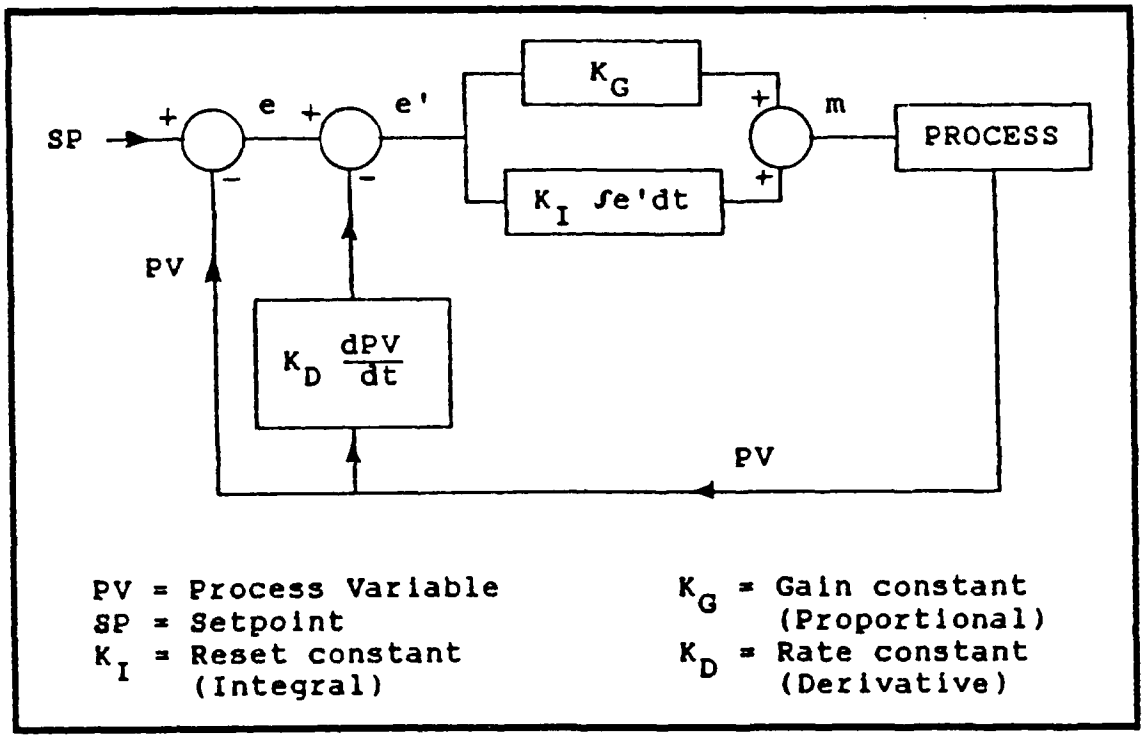

Figure 13. PID Control in the Micricon 82300

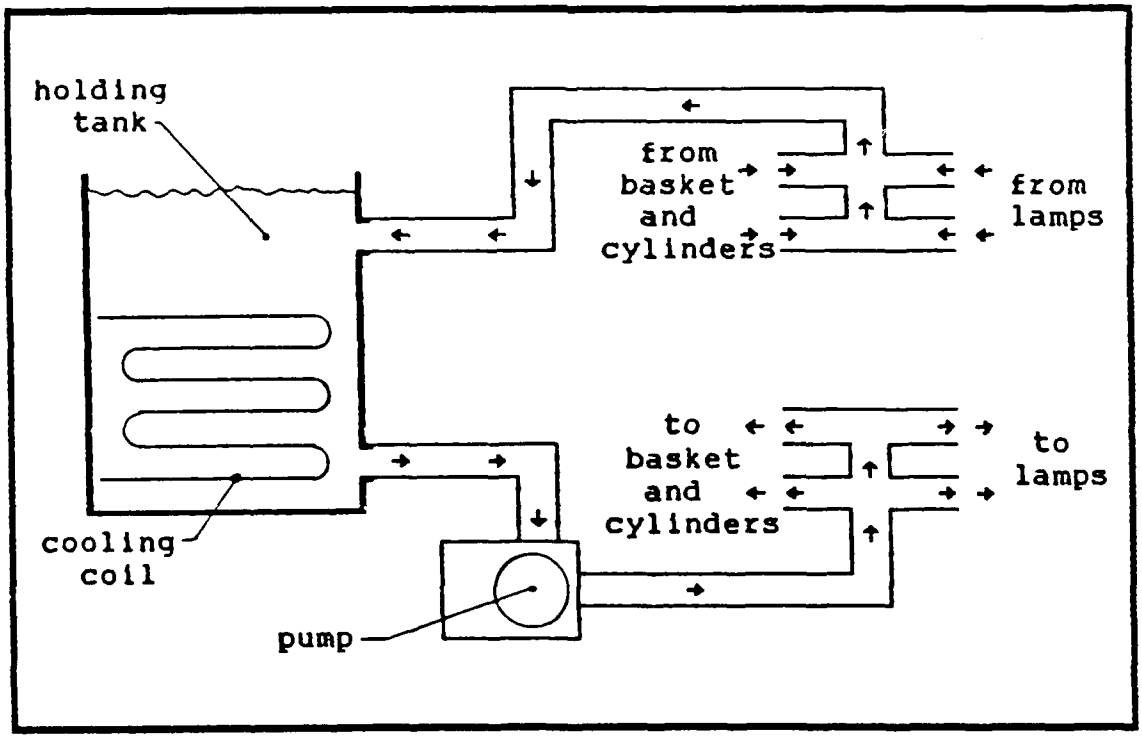

Figure 14. Water Cooling System

holding tank.

If leaks occur in the system and a large quantity of coolant is lost, sévere damage can be done to the lamps and pump. To protect these components, a relay system is being developed to shut down the pump and Micricon control unit if the water in the tank drops below a specified level. This system uses a cork float attached to a microswitch that closes under the float's weight when the tank water level drops. A diagram of this relay system is shown in Figure 15.

Strain Measurement Device

The strain measurement system is shown in Figure 16. Strains were calculated from the displacement measurement of a strain gage type of extensometer. Because the extensometer is meant to operate in high temperature environments, it is furnished with 4 inch long quartz rod probes. The MTS extensometer was designed so its rods fit into notches cut in the edge of a compact tension (CT) specimen giving a 0.5 inch gage length. The quartz rods are spring loaded to maintain constant contact against the CT notches. The extensometer mounts in a specially designed holder that clamps to the frame of the MTS loading machine. The holder applies lateral pressure against the specimen so no slippage occurs during opening and closing of the crack. The holder is also equipped with an air hose fitting and baffling system to allow air to blow across the extensometer to keep it cool for thermal-mechanical fatigue tests.

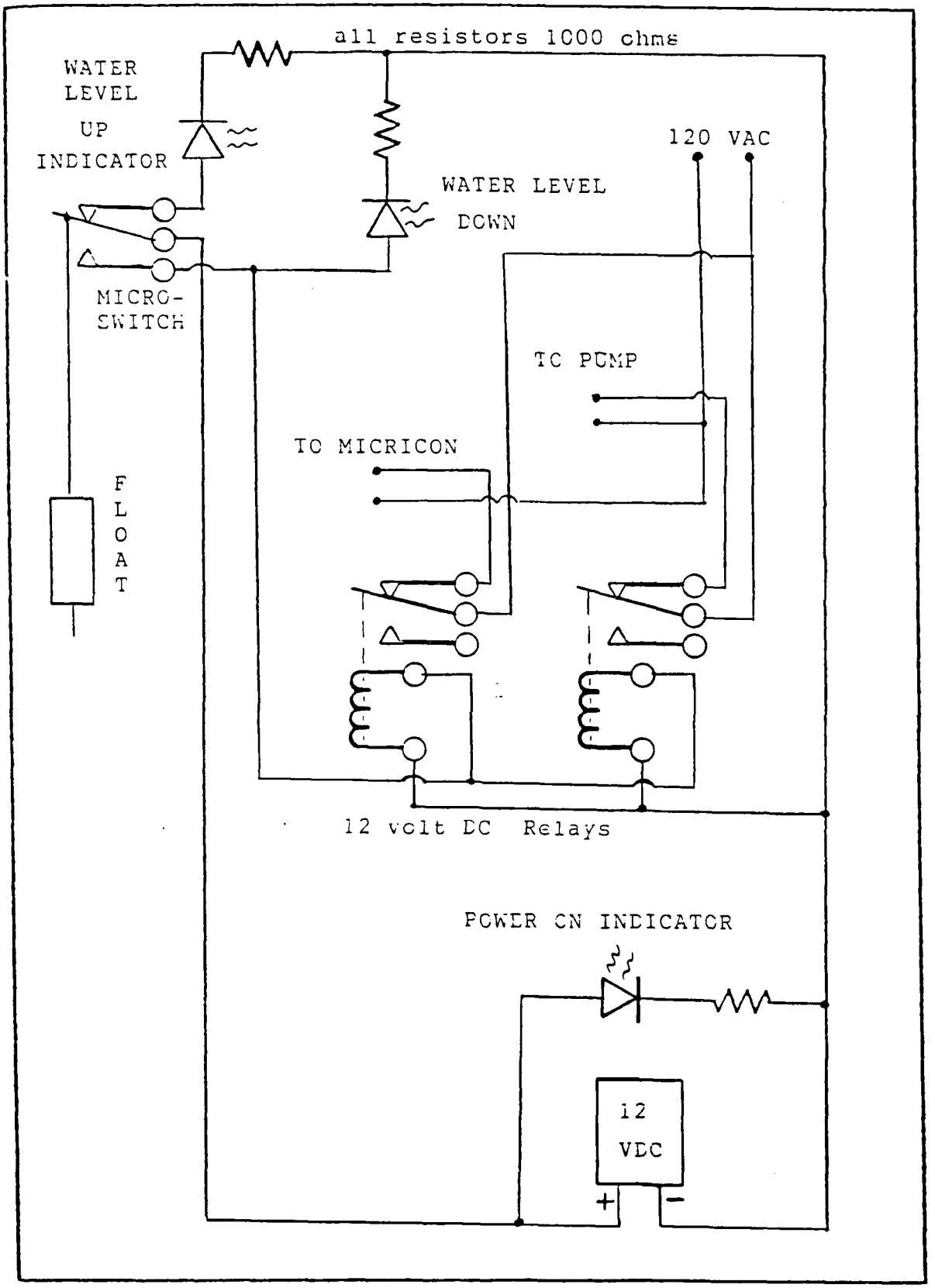

Figure 15. Protective Relay System

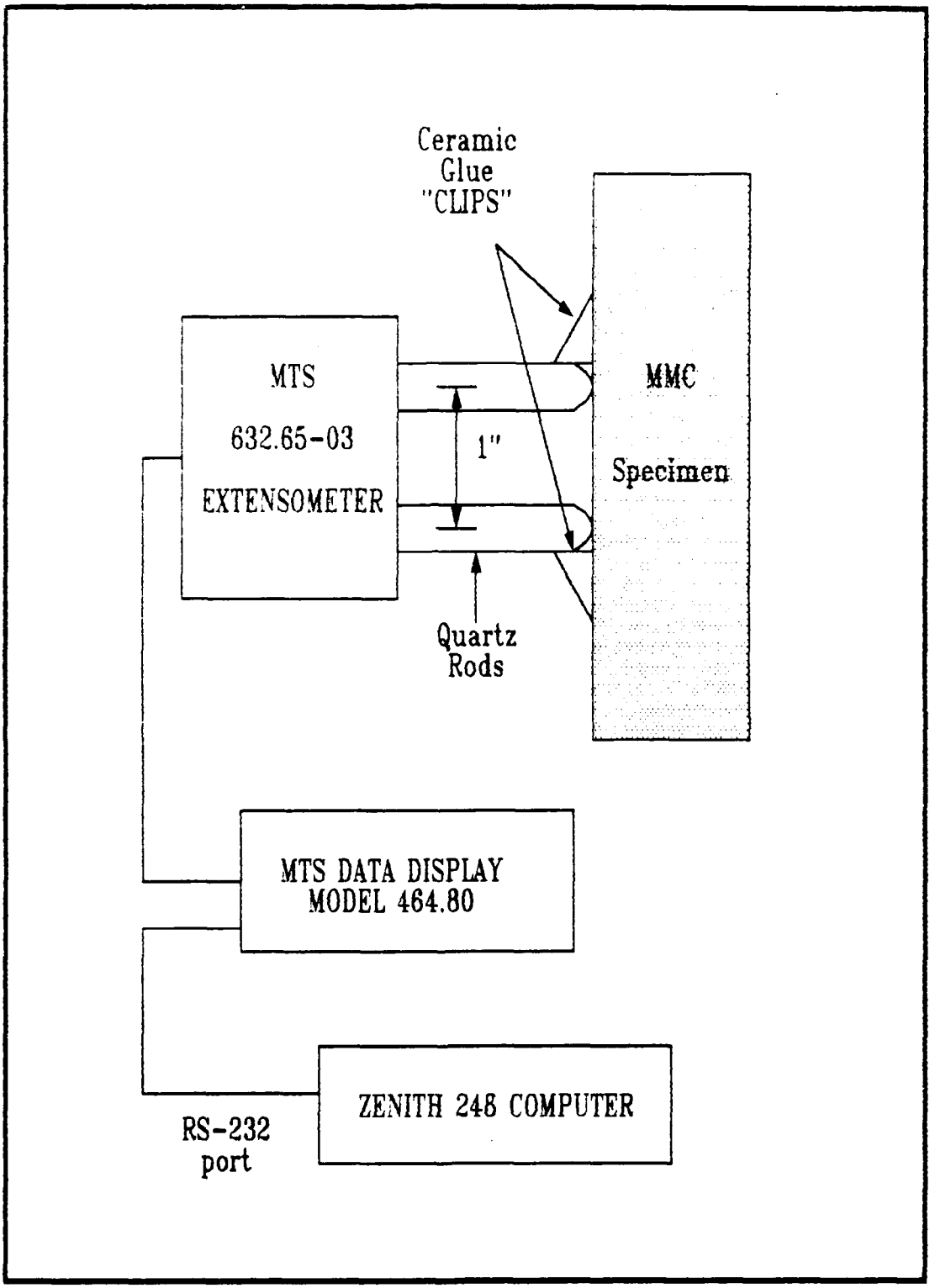

Figure 16. Strain Measurement System

The extensometer was modified in two ways for use in TF testing of the metal matrix composite. Figure 17 illustrates the modifications. First, since a 1.0 gage length was desired rather than a 0.5 inch gage length, the lower curved quartz rod was replaced with a straight rod. This increased the gage length to 1.0 inch. Secondly, to avoid any stress concentrations in the MMC, no notches could be cut in the specimen to accept the quartz rods, and the lateral pressure of the holder was not great enough to prevent the rods from slipping against the specimen edge. Therefore, some type of stops had to be attached to the specimen.

This was accomplished by molding small "clips" on the edge of the specimen with high temperature ceramic glue. The proper curvature of the "clip" was maintained by molding the glue around wooden dowels fitted over the specimen edge. The dowels and quartz rods had the same diameter. The correct gage length was achieved by aligning the dowels on the specimen with a Gaertner telemicroscope and digital position readout.

As mentioned earlier, the quartz rods are loaded by an internal matallic element. Resistance-type strain gages are bonded to the element to form a Wheatstone bridge circuit. Elongation or compression of the specimen causes movement of the quartz rods. This motion is transmitted to the metallic element causing it to bend, thus changing the resistance of the bonded strain gages. This change in the balanced condition of the Wheatstone bridge circuit causes an output voltage

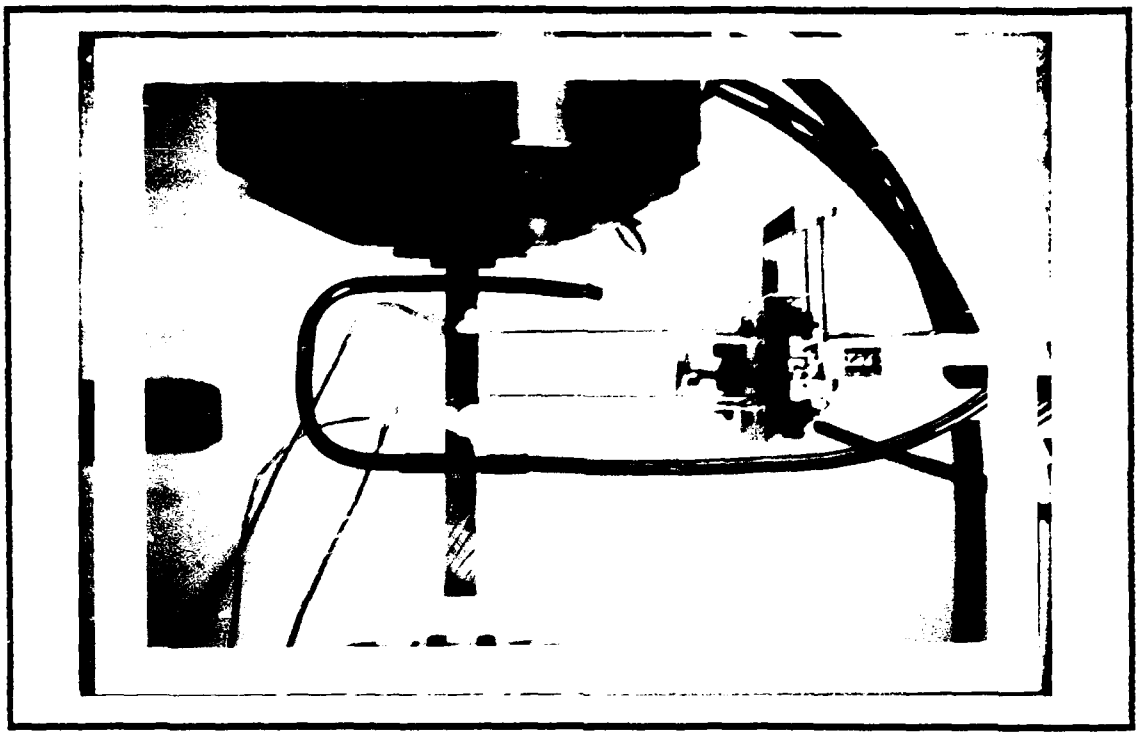

Figure 17. Extensometer in the Ceramic Glue Clips

that is proportional to the displacement of the rods (36:1-2). The voltage is sent to the data display for recording.

Calibrating the voltage from the data display to the displacement of the quartz rods was executed with a MTS extensometer calibration instrument. Because the extensometer was modified, a special set of aluminum clasps were constructed to hold the extensometer in place in the instrument. The linear relation between extensometer voltage and rod tip displacement found from the calibration is given in the following equation:

$$D = 0.025950x + 1.2672 \qquad (8)$$

where:

x = extensometer voltage read from the data display in volts

D = displacement of the rod tips in inches

Finally, thermal strain was calculated by comparing the change in the displacement from an elevated temperature to the room temperature displacement and dividing the difference by the room temperature displacement.

Computer Data Acquisition

Both thermocouple and extensometer voltage were collected by a Zenith 248 computer and then converted to temperature and strain. The computer was programmed to read data from the volmeter and data dislplay. Figure 6 shows the complete arrangement of the computer and the electronic components. The voltmeter was connected to the computer by a IEEE-488 (GPIB) data bus. A Qua Tech Inc. MXI-241 multifunction board was installed in the Zenith 248 to provide an interface with the GPIB-compatible component. The data display sent information to the computer through a RS-232 port.

The computer software to control the data acquisition is given in Appendix A. A block diagram of the program is given in Figure 18. Initially, the program requires the extensometer room temperature voltage to be used as a baseline for the strain calculation, filenames

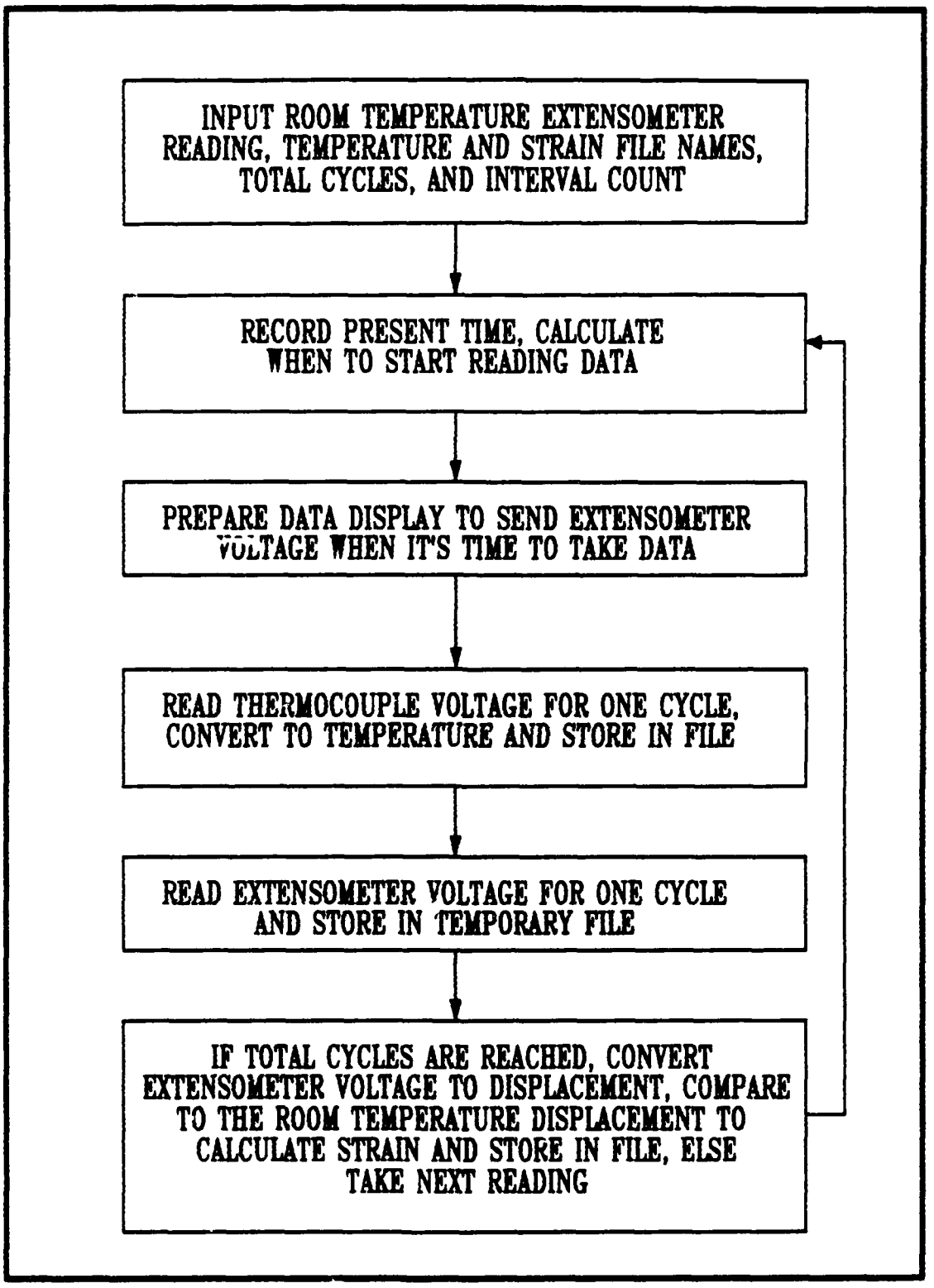

Figure 18. Block Diagram of the TF Testing Program

to store the temperature and strain cycle data, total number of cycles, and an interval count that tells the computer how often to read data. Using the period duration (48 seconds) and interval count, the program begins by calculating the amount of time between data recording. Comparing these times to its internal clock triggers the computer to send a message to the data display preparing it for transfer of the extensometer voltage.

The computer cannot receive data from the voltmeter and data display at the same time so thermocouple voltage over one thermal cycle is sent first, converted to temperature, and stored in the specified file. Immediately following this step, the program commands the data display to send the extensometer voltage and stores it in a temporary file. The program continues this process until the total number of thermal cycles is reached; whereupon, the extensometer voltage is converted to displacement and compared to the room temperature reading to calculate strain. The strain is then stored in the given file.

IV. Experimental Procedure

Specimen Details

The specimen employed in this investigation was the SCS6/Ti-15-3 metal matrix composite. Ti-15-3, a shortened designation for Ti-15V-3Cr-3Al-3Sn, is a rather new metastable beta strip alloy used where cold formability and high strength are desired (24:2). Because it is cold formable, rather thin sheets of Ti-15-3 can be made much more economically than alpha-beta alloys. Due to its availability in thin gage foils and its good mechanical properties, Ti-15-3 has been considered as a reasonable matrix material for high temperature MMCs.

The composite laminate was made by hot-pressing Ti-15-3 foils between unidirectional tapes of silicon carbide fibers designated as SCS6. The fiber diameter is 0.0056 inch. Several pieces of panels having six plies of 0 degree fibers were supplied by McDonnel-Douglas Aircraft Company. Each laminate was approximately 0.046 inches thick with a fiber volume fraction of 0.4. Material properties for the fiber and matrix are given in Table 1.

Table 1 Material Properties of SCS6/Ti-15-3 (23:12)

	Fiber	Matrix
Density	0.110 lb/in^3	0.172 lb/in^3
Youngs Modulus	58.0 x 10^6 psi	13.4 x 10^6 psi
CTE	2.290 x 10^{-6}/°F	4.36 x 10^{-6}/°F
Poissons Ratio	0.250	0.360
UTS	500.0 ksi	130.0 ksi

Each panel was cut into 0.5 inch by 7.0 inch rectangular specimens by using a diamond cutoff wheel. Figure 19 shows two specimens, one before TF testing and one after. The dark area is the formation of oxidation on the specimen. The 0° fibers were in the length-wise direction. The faces were left in the as-fabricated condition, whereas the edges were wet ground with successively finer grades of silicon carbide discs (180, 240, 400, 600 grit) on a 12 inch disc grinder. The edges were then polished on a rexmet polishing cloth with lapping oil and diamond paste: 15 micron down to 1 micron. This made it possible to view the edges under a high possible optical microscope and assess the baseline (uncycled) damage to the specimen due to cutting. After thermal cycling, the specimen edge could easily be viewed to see the progression of any damage. If any permanent record of the damage was desired, the edge was easily repolished for optical photography.

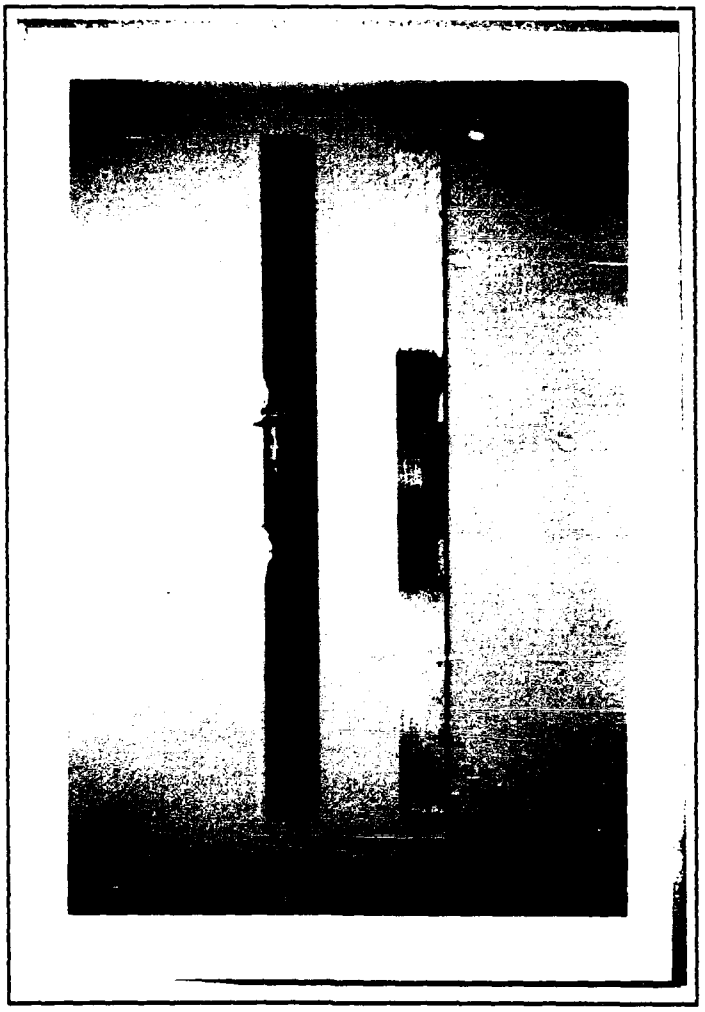

Figure 19. MMC Before and After Thermal Cycling

Figures 20 through 23 are representative of the baseline specimen edge. Even before any thermal cycling, there is characteristic damage due to manufacturing and sample preparation. Note that the specimen has many surface scratches. These are due to the inadequacies of the polishing technique of such a long narrow specimen.

Usually, a small piece is cut from the sample and mounted in epoxy resin before polishing. Mounting aids in handling the specimen and maintaining the specimen flat against the polishing surface. The mounted specimen is easier to clean and the smaller size obtains a more uniform polish compared to a large specimen. The best optical pictures are taken of a specimen which is perfectly flat, immaculately clean and highly polished. Because the MMC still needed to undergo thermal cycling it could not be permenantly mounted in epoxy; therfore, it was difficult to keep the sample absolutely perpendicular on the grinding wheel at all times.

The nature of the silcon carbide fibers makes it extremely hard to polish. Only diamond pastes could be used to smooth the fibers. Any contamination in the diamond paste ruins the total polishing effort by scratching the surface. Since the matrix is softer than the fibers, it is worn away easier. Thus, the focal plane is different for the fiber and the matrix, making the photographs appear fuzzy. The scratched surface is an inconvenience, but the damage is evident and easy to discern.

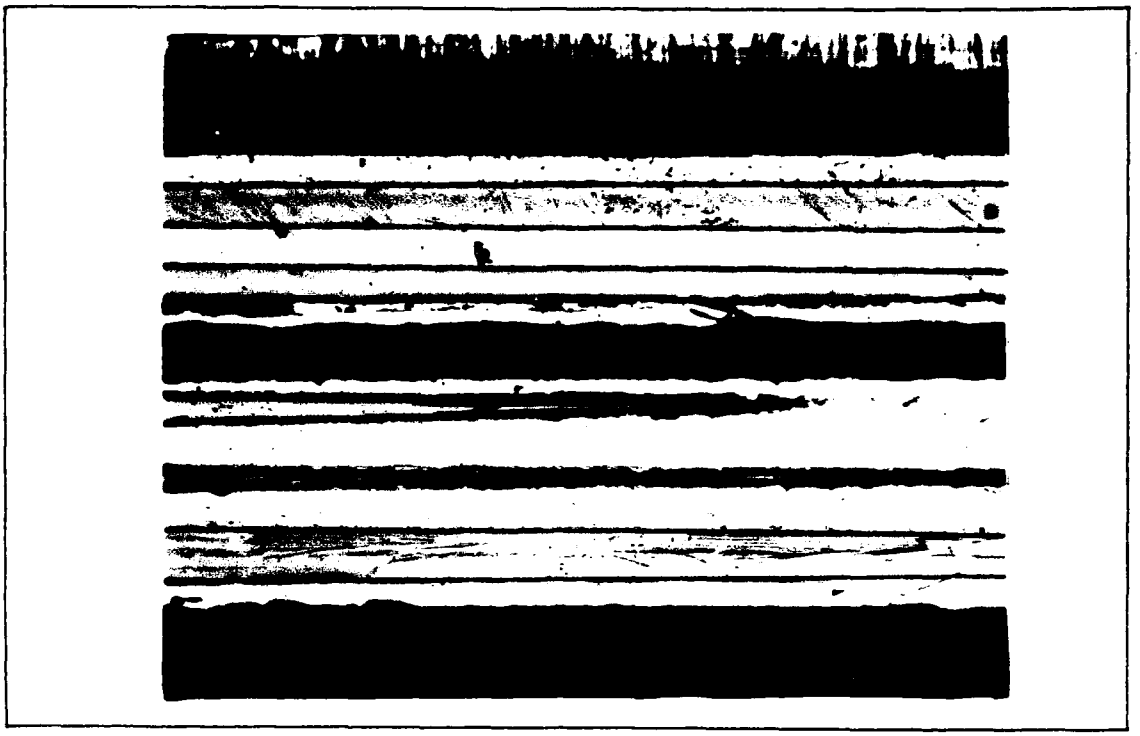

Figure 20. Typical Edge Damage of an Uncycled Specimen (50X)

Figure 21. Typical Edge Damage of an Uncycled Specimen (50X)

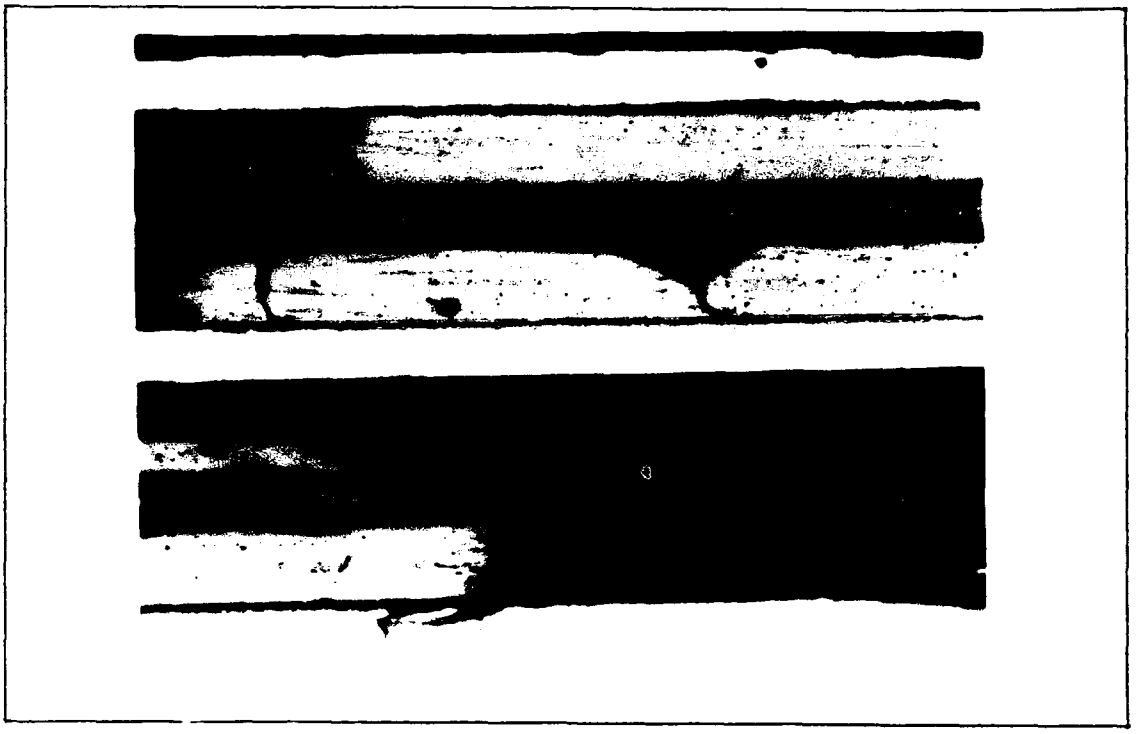

Figure 22. Fiber Pullout Damage of an Uncycled Specimen (200X)

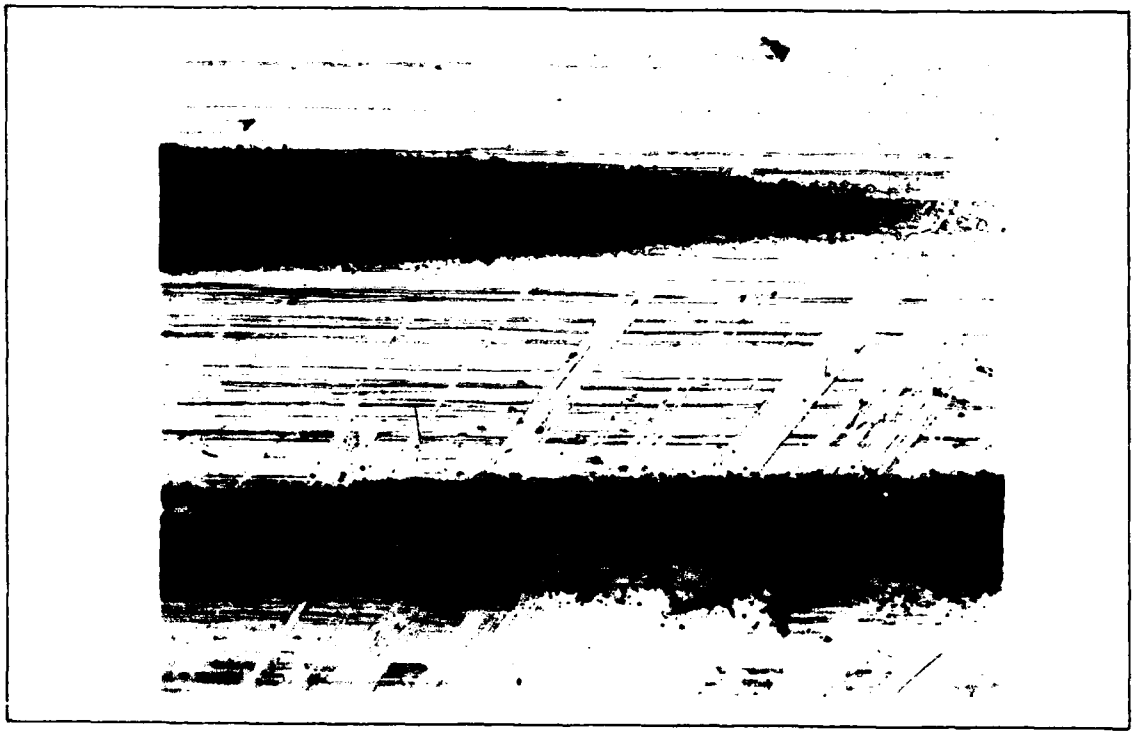

Figure 23. Fiber Tip Damage of an Uncycled Specimen (200X)

The most common baseline damage is fiber breakage and pullout. In Figures 20 through 23 the lightest areas are the titanium matrix, the gray areas are the longitudinal fibers and the dark areas are the cavities where the fiber was pulled out. In places, the core of the fiber is exposed and appears as a dark line in the middle of the fiber. Some cuts were not made parallel with the fibers; hence, they were sliced at angles leaving points of fibers leading into the matrix. In Figure 20, a line of bubbles is visible in the middle of the matrix area (arrow A). They occur during manufacturing as bubbles left in between the plies as the laminate is pressed together. Each aspect of preliminary damage plays a role in the initiation and progression of fatigue failure due to thermal cycling.

To prepare for testing, the high temperature ceramic glue "clips" for the strain gage probes needed to be attached to the specimen. The wooden dowels used as dies had slits cut in one end to fit snuggly over the edge of the specimen. The centers of the dowels were placed exactly one-half inch on either side of the specimen's centerline and coated with a thin layer of light oil to act as a releasing agent for glue. The "clips" were molded in a triangular shape for better adherence to the specimen and the dowels were removed when the glue had hardened. Figure 17 shows the "clips" in place on the specimen. The final preparation made to the specimen was welding the three sets of Chromel-Alumel thermocouple wires to the surface of the sample.

Thermal Fatigue Testing

For the TF testing the computer program in Appendix A was used as shown. The temperature was cycled between 300°F and 800°F for these tests. A period of 48 seconds (0.8 minutes) was used as the Micricon 82300 is programmed in minutes. This temperature range and period were chosen after several trials to find the greatest temperature change in the least amount of time while maintaining a smooth triangular heating/cooling cycle. The uniform cooling of the specimen was the limiting factor for this TF testing system.

The temperature profile (solid line) established for these tests is shown in Figure 24. The temperature differs from the programmed value (dashed line) by maximum of 8°F (approximately 3% deviation). Variations were observed mainly when the electric cooling air valve opened and closed.

As mentioned earlier, strain was calculated from the displacement of the extensometer's quartz rods. Since the extensometer generates voltage, a calibration curve was generated to relate voltage to the displacement of the rod. The MTS calibrator accurately set the rods displacement while the data display showed the extensometer's voltage. These data points are plotted in Figure 25 and a straight line is fitted to the points by the least squares method. It can be seen from the plot that that displacement/voltage relation is exactly linear over the operational range of the gage.

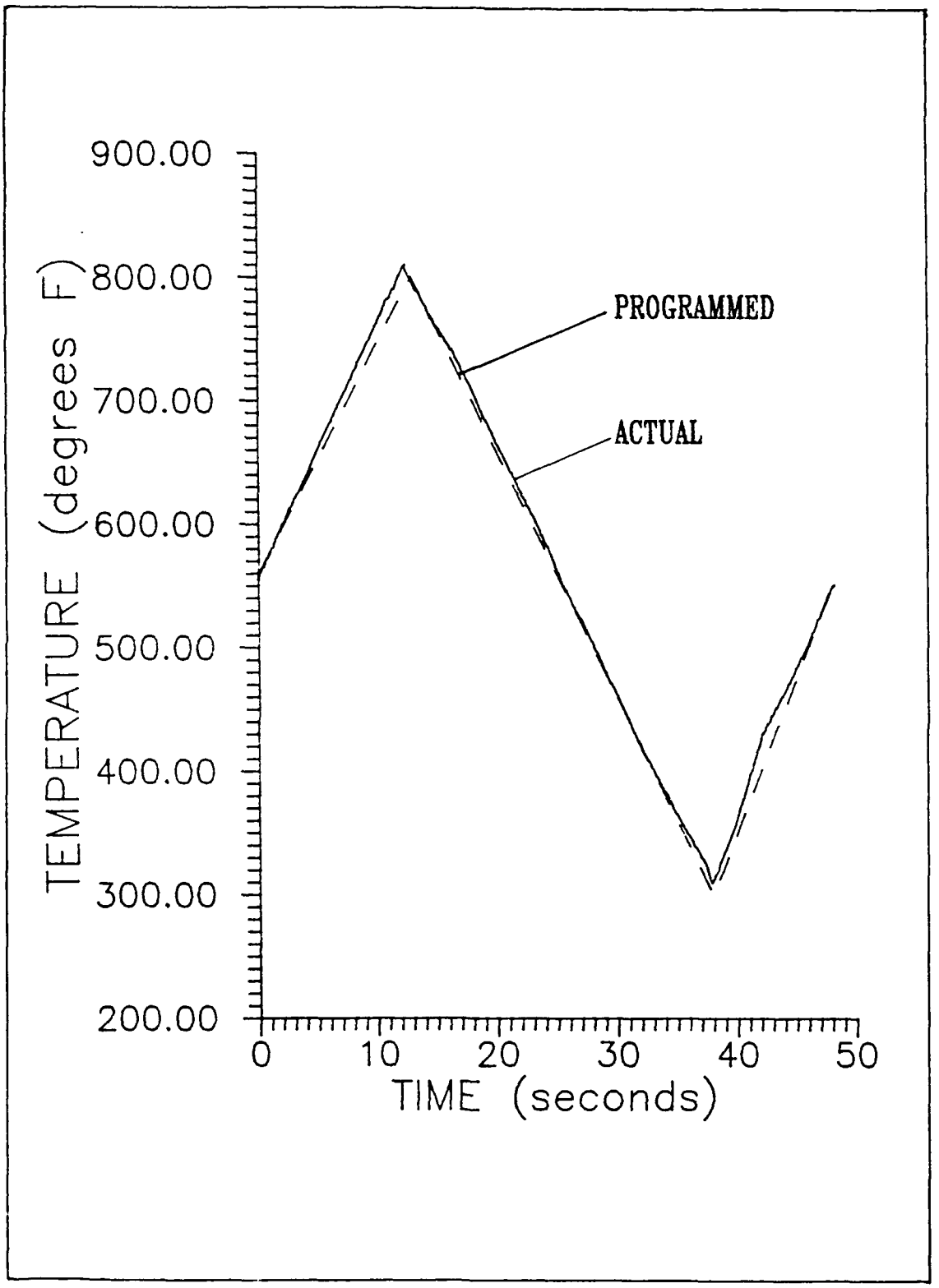

Figure 24. TF Test Temperature Profile

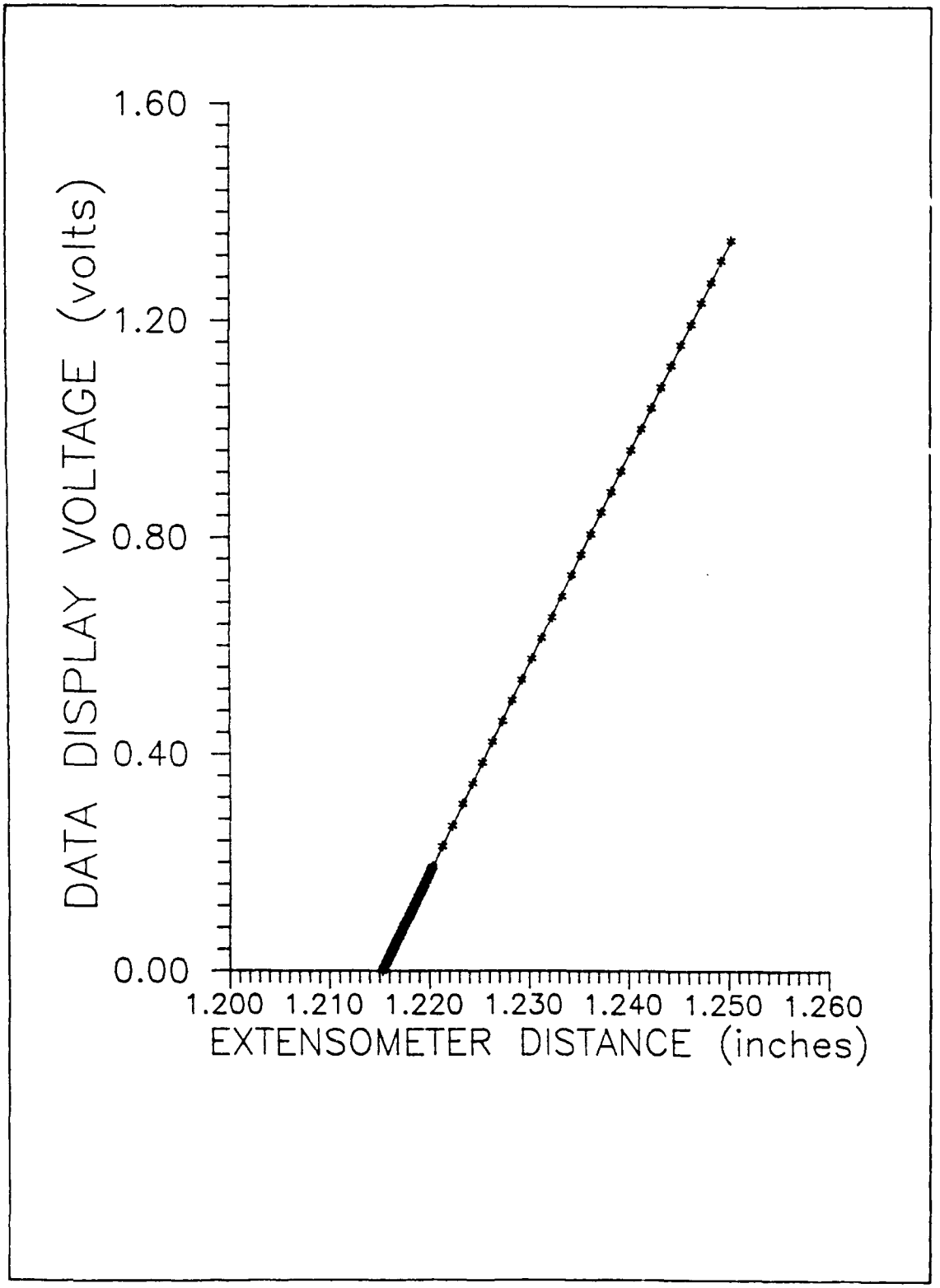

Figure 25. Extensometer Calibration Curve

A total of 10 tests were completed using the TF test system. Table 2 summarizes the tests. The effect of thermal cycling on Young's modulus, Poisson's ratio and CTE are discussed in the next section. The initiation and progression of the damage is documented as well as the variation in strain due to cycling.

Table 2 TF Tests Completed

Specimen #	Width (inch)	Thickness (inch)	Thermal Cycles
1	0.49	0.046	250
2	0.49	0.046	500
3	0.50	0.046	1000
4	0.50	0.046	1500
5	0.49	0.046	2000
6	0.47	0.046	2500
7	0.48	0.046	3000
8	0.49	0.046	5250
9	0.50	0.046	6000
10	0.49	0.046	16750

V. Results and Discussion

Thermal Strain and CTE Results

On every TF test the computer program in Appendix A was run to collect temperature and strain data every 25 cycles, except for test ten (16,750 cycles) which collected data every 100 cycles. As mentioned earlier, the program collected temperature data first for one complete cycle, then collected strain data from the extensometer voltage for one cycle. In this way, the actual temperature profile was checked for equivalence with the programmed profile. The data was used to examine how strain and CTE change over the accumulation of thermal cycles. The CTE, or coefficient of thermal expansion, is defined as the ratio of the change of length per unit length to the change in temperature or strain per change in temperature (6:195)

Figure 26 is a plot of the strain versus number of cycles for specimen 6 that was thermally cycled 2,500 times between 300°F and 800°F. The plot shows that the strain follows the triangular temperature profile exactly for the 48 second period. The maximum strain occurs at 800°F and the minimum strain occurs at 300°F, with a linear rise and fall during heating and cooling.

A unique phenonemon is observed in Figure 26. As evidenced by an increase in the mean strain, a slight expansion occurs in the sample from the first cycle to 600 cycles. It appears at first that an irreversible strain is generated as a function of thermal cycles. This

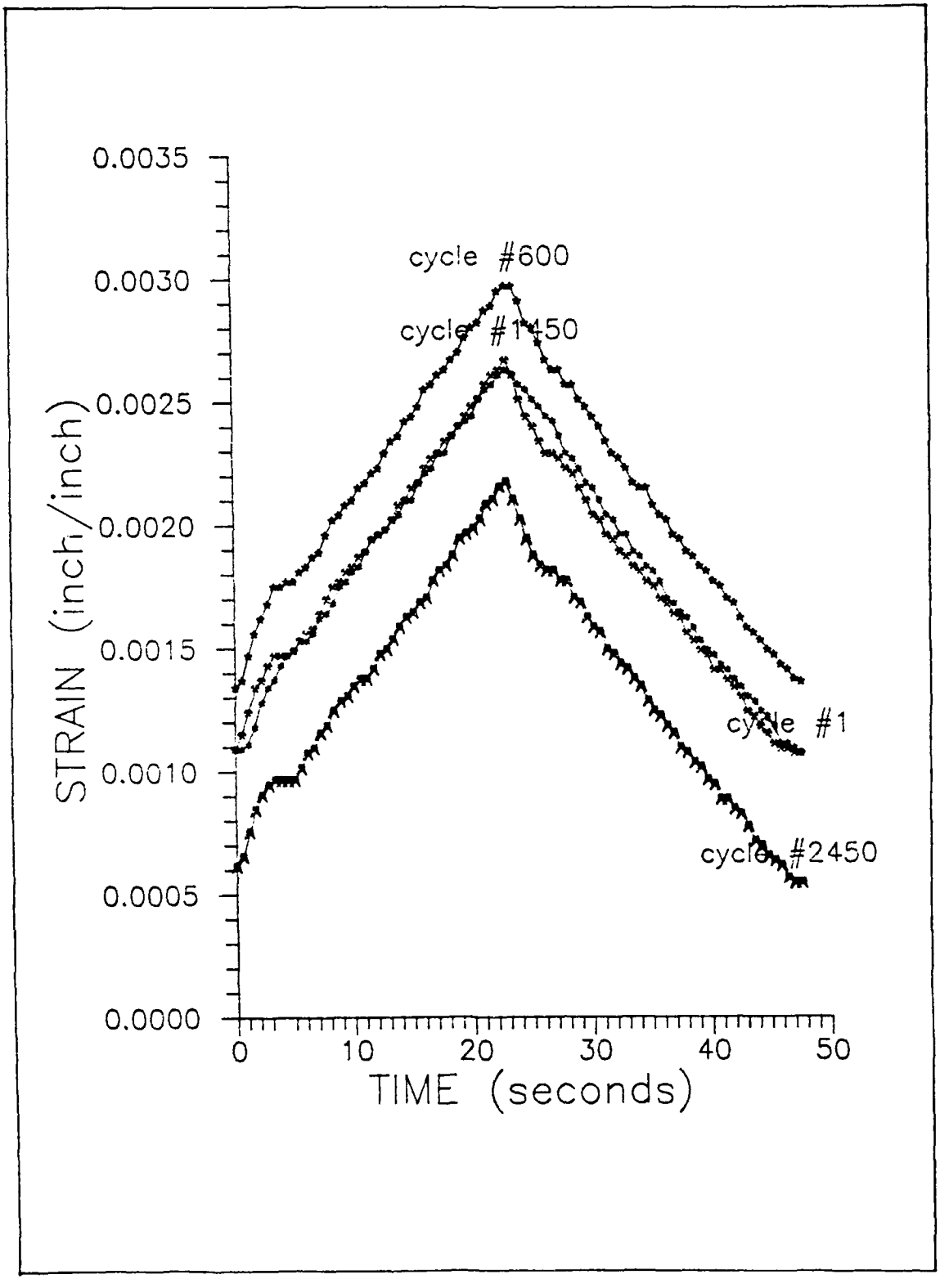

Figure 26. Strain versus Time Profiles, Specimen 6

expansion stops, however, and for the next 200 cycles the strain profile remains constant.

At 800 thermal cycles the specimen begins to compress as the number of cycles increases and continues to compress until it reaches a minimum at the end of the test. The mean strain now steadily drops as a function of thermal cycles. The expansion and compression were not a result of the temperature profile changing. The profile remained constant over the entire test and remained within the experimental fluctuation of 1 percent. The strain range stayed constant for the entire test.

Halford offers a possible explanation for the compression (16:9). He defines the compression of the specimen as ratcheting. Ratchet strains are unidirectional inelastic deformation that incrementally accumulate on each cycle of loading, and are associated with the thermal fatigue progess. Thermal strain ratchetting is a classical nonlinear material response characteristic of thermally cycled structures. It is an imbalance of thermal fatigue that results directly from the unsymmetric hysteresis loop response of thermally cycled materials. Ratchet strains may be composed of either time-independent plasticity or time-dependent creep.

Majumdar and Newaz of Battelle Memorial Institute performed thermo-mechancial fatigue tests on an angle-ply layup of SCS6/Ti-15-3 (26). When they conducted a thermal fatifue test (600°F to 1200°F) on their [0/+-45/90] laminate, they witnessed a similar irreversible compression

as a function of thermal cycles. However, the compression began after the first cycle and lasted until the 550th cycle. The specimen did not experience the expansion and increase of the mean stress; moreover, beyond 550 cycles the irreversible deformation reduced substantially and the maximum and minimum strains stabilized to a constant value. They believe the deformation may be related to residual stresses from processing.

The question remains for the investigation, what is the cause of the expansion in the first 600 cycles of thermal fatigue? It is possible that the unidirectional layup undergoes an inelastic deformation on each cycle that results in a permanent strain or expansion. It is not until enough thermal stress is accumulated, through thermal fatigue, to yield the material in a way that allows the residual stresses to become the dominating factor.

After the yielding, the unidirectional laminate may behave more similar to the angle ply which sustained higher temperatures over a greater range in the Battelle study (26). The effect of the residual stresses due to processing cause the compression of the material as shown by the strain measurements.

A second explanation of the thermal expansion lies in the high temperature ceramic glue clips that were molded onto the specimen to provide stops for the extensometer's quartz rods. The glue was allowed to cure overnight before the specimen was used in a test - even though it was hard to the touch in one hour. It is possible, during the first

600 to 800 cycles of the experiment that the glue continued to cure and dry out resulting in the clips shrinking. As the clips shrunk the quartz rods of the extensometer spread little by little every cycle until the glue was fully cured. This spreading of the rods appears as an expansion of the sample. Even though compression of the specimen could have begun after the first cycle, if the expansion was greater than the compression, the net result would be an expansion. Slowly the glue clips become stable, the expansion stops, and the compression of the sample is visible.

Since we were concerned about the reaction of the glue, we performed a pretest to measure the CTE of a known material, 7075-T6 aluminum. 7075-T6 aluminum is known to have a CTE of 14 x 10^{-6}/°F (6:223). The glue "clips" were molded onto the specimen for a 1 inch gage length and heated from room temperature to 561°F. The displacement was measured by the extensometer and converted to strain to calculate a CTE of 15 x 10^{-6}/°F. This is accurate to 7 percent of the actual CTE and acceptable for experimental work; therefore, there was no further concern over the integrity of the strain measurements

Figure 27 is another plot of the strain versus number of cycles for specimen 8 cycled 5,250 times. Again the same type of behavior is evident. In Figure 28 the mean strain and the strain range are plotted versus the number of thermal cycles for Specimen 8. The specimen's mean strain rises from the first cycle to the 525th cycle, causing expansion, then slowly, after stabilizing for one hundred cycles,

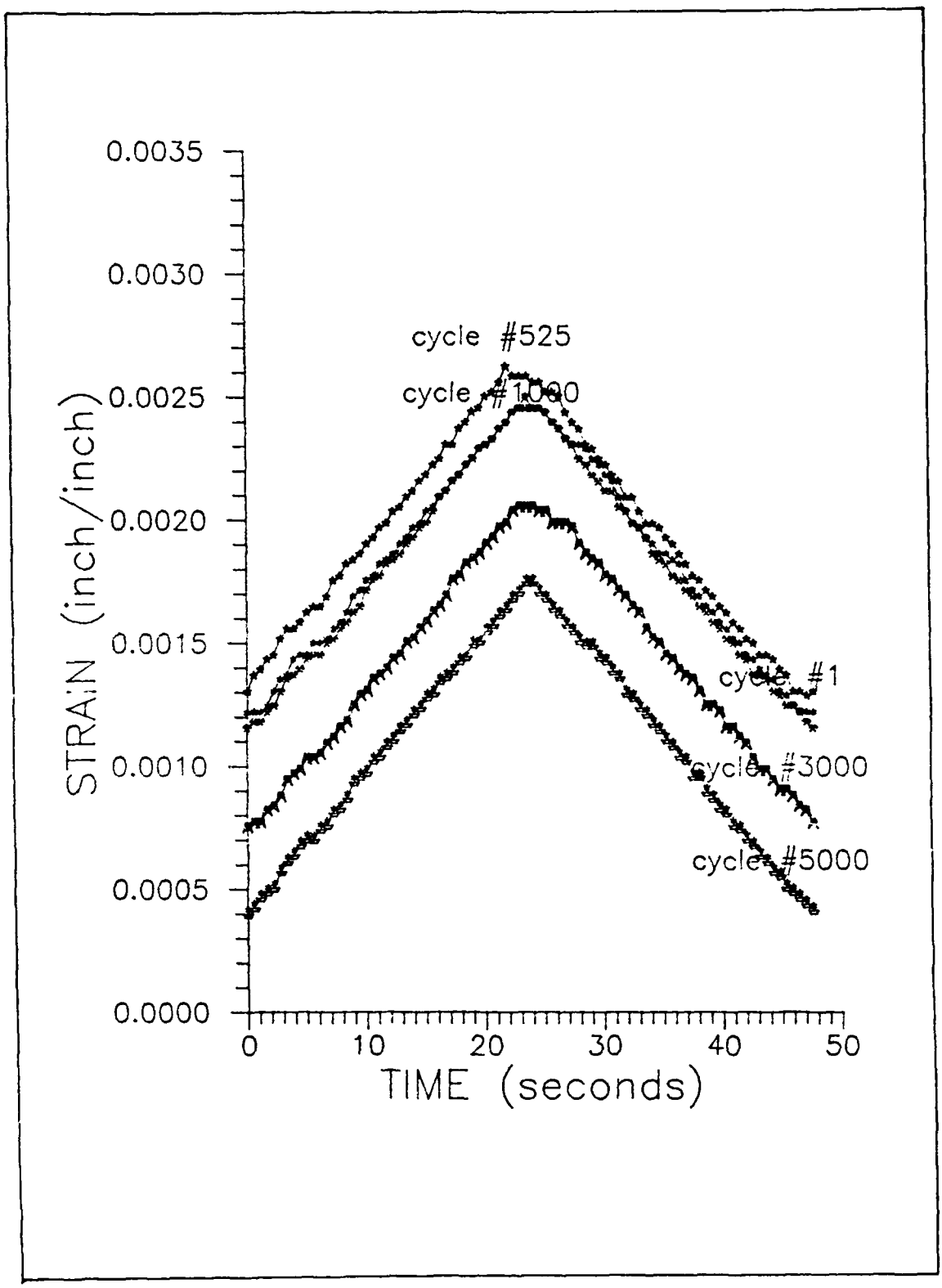

Figure 27. Strain versus Time Profiles, Specimen 8

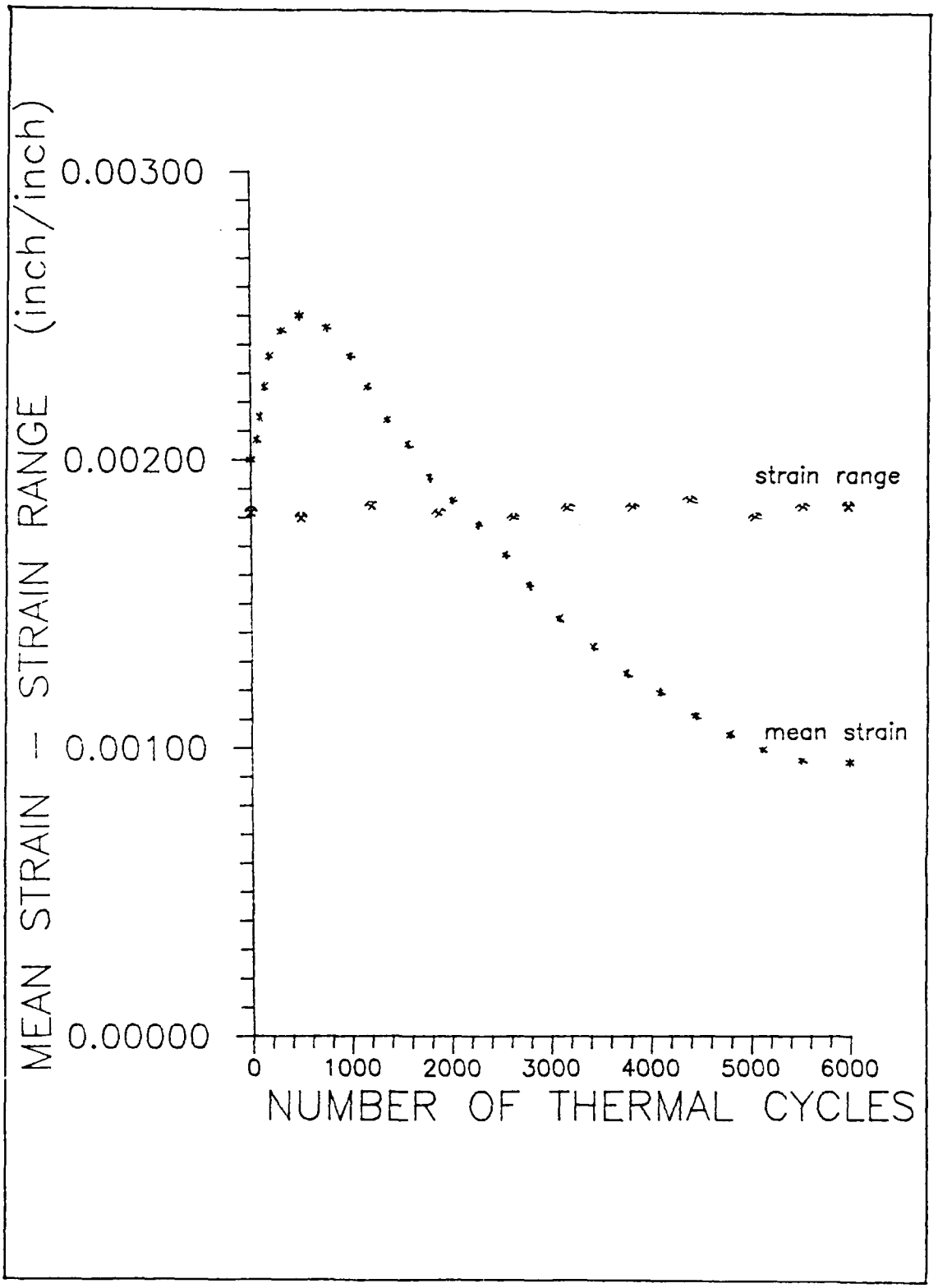

Figure 28. Mean Strain and Strain Range versus Thermal Cycles, Specimen 8

begins to drop causing a compression. The strain range stays constant throughout the expansion and compression process. The strain values match specimen 5 at each stage but specimen 8 shows that even beyond 2,500 cycles the compression continues until the end of the test at 5,250 cycles.

The other specimens showed similar trends and it was not until 6,500 cycles that the mean strain finally stabilized to a constant value. This was demonstrated in specimen 10 which was cycled 16,750 times.

Because CTE is defined as inch/inch/°F or strain/°F it is easily found from Figures 26 and 27. The CTE is calculated from the slope of the strain profiles. Since the slope is constant for all the strain profiles the CTE is constant. Figure 29 displays this fact. The average CTE is 0.34×10^{-5}/°F. METCAN predicts a CTE of 0.362×10^{-5}/°F for this laminate. The standard deviation is 0.008 for the Specimen 8 data.

As postulated earlier, the damage that occurs to cause the specimens to compress after 800 cycles and the mean strain to drop is a function of thermal cycles. Are the fibers debonding from the matrix thereby negating the effects of the matrix and driving the material characteristics of the ply toward the fiber characteristics? In the next section we examine the surface damage imposed to the material due to thermal cycles.

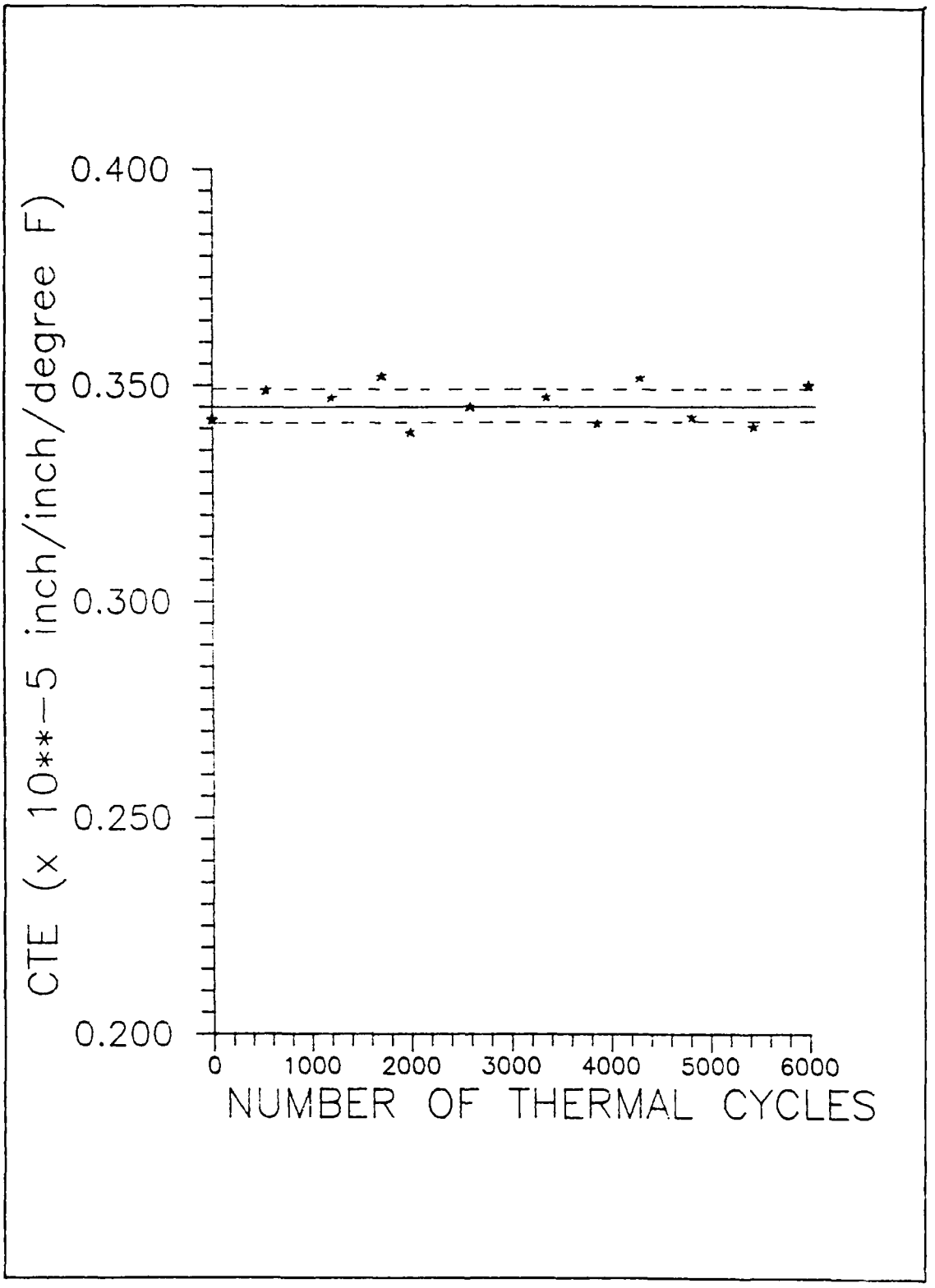

Figure 29. CTE versus Thermal Cycles, Specimen 8

Specimen Damage on the Edge

In order to characterize the natue of the initiation and progression of the thermal fatigue damage, specimen 9 was thermally cycled in increments. After each increment of 500 cycles, the specimen was removed from the testing system and viewed under a high power optical microscope to look for damage. Figure 30 is a summary of the uncycled damage seen earlier and a description of things to come.

Cracks formed in three distinct places along the edge. They first formed at the missing fiber tip at 1,500 cycles and in the seam bubbles. Next, the seam cracks connected and the fiber tip crack grew into the matrix at 3,000 cycles. Eventually cracks even formed inside the cavities left behind by the fiber at 6,000 cycles.

Figure 31 describes the meaning of the ply seam. A seam formed when the fibers were sandwiched between the foils of matrix material. During processing, bubbles were trapped in the seam.

The uncycled specimen suffered processing damage similar to that shown in Figures 20 through 23. Specimen 9 was then placed in the holding device and cycled. Over the first two increments the only visual change in the specimen was the appearance of oxidation on the specimen's surface. It wasn't until 1,500 cycles that cracks began to appear on the edge of the specimen. Figure 32 shows the initiation of cracks in the different places on the specimen. The oxidation on the specimen makes it difficult to see, but an effort was made not to alter the specimen in any way until the test was complete. No polishing of

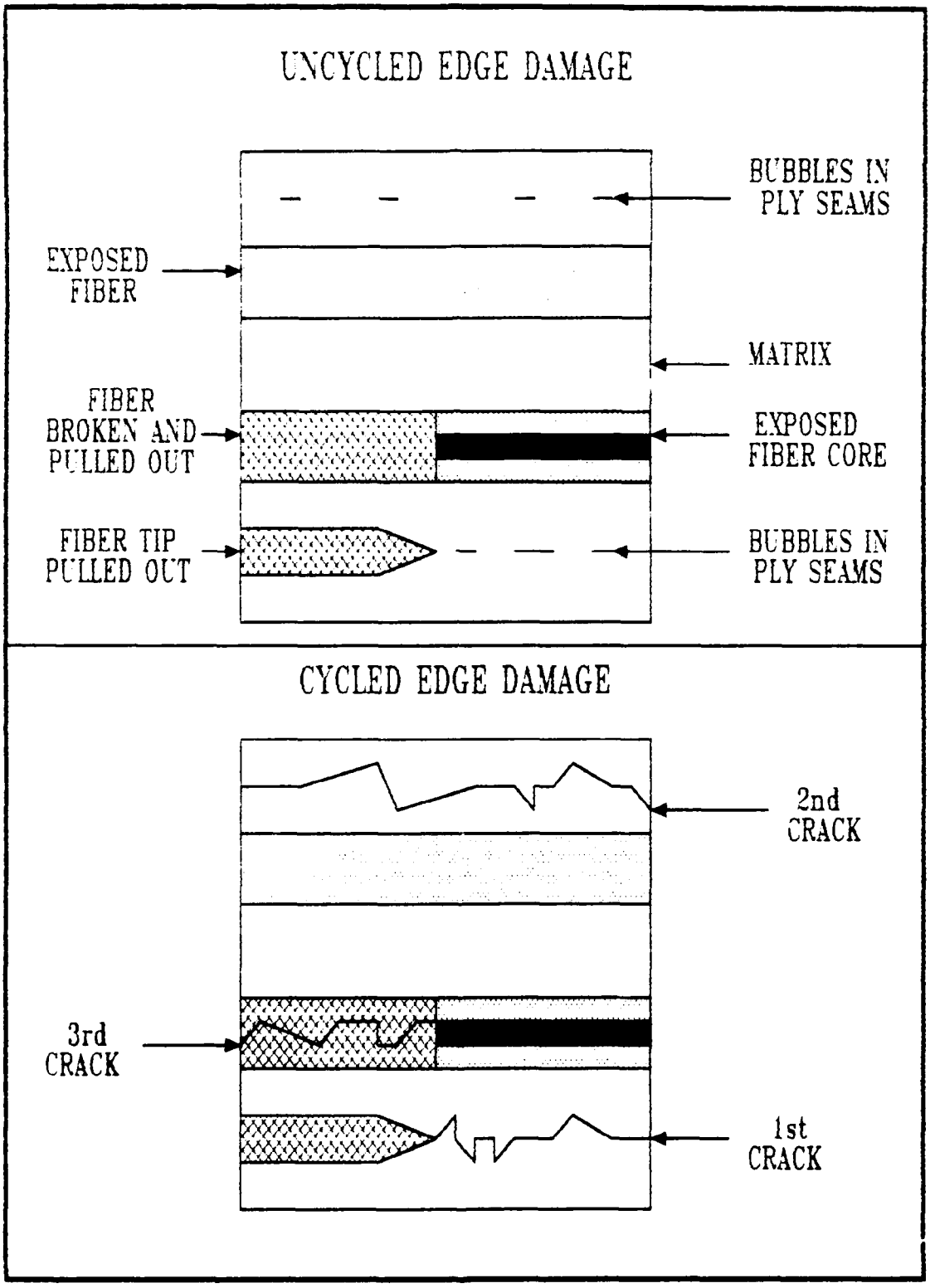

Figure 30. Comparison of Uncycled and Cycled Edge Damage

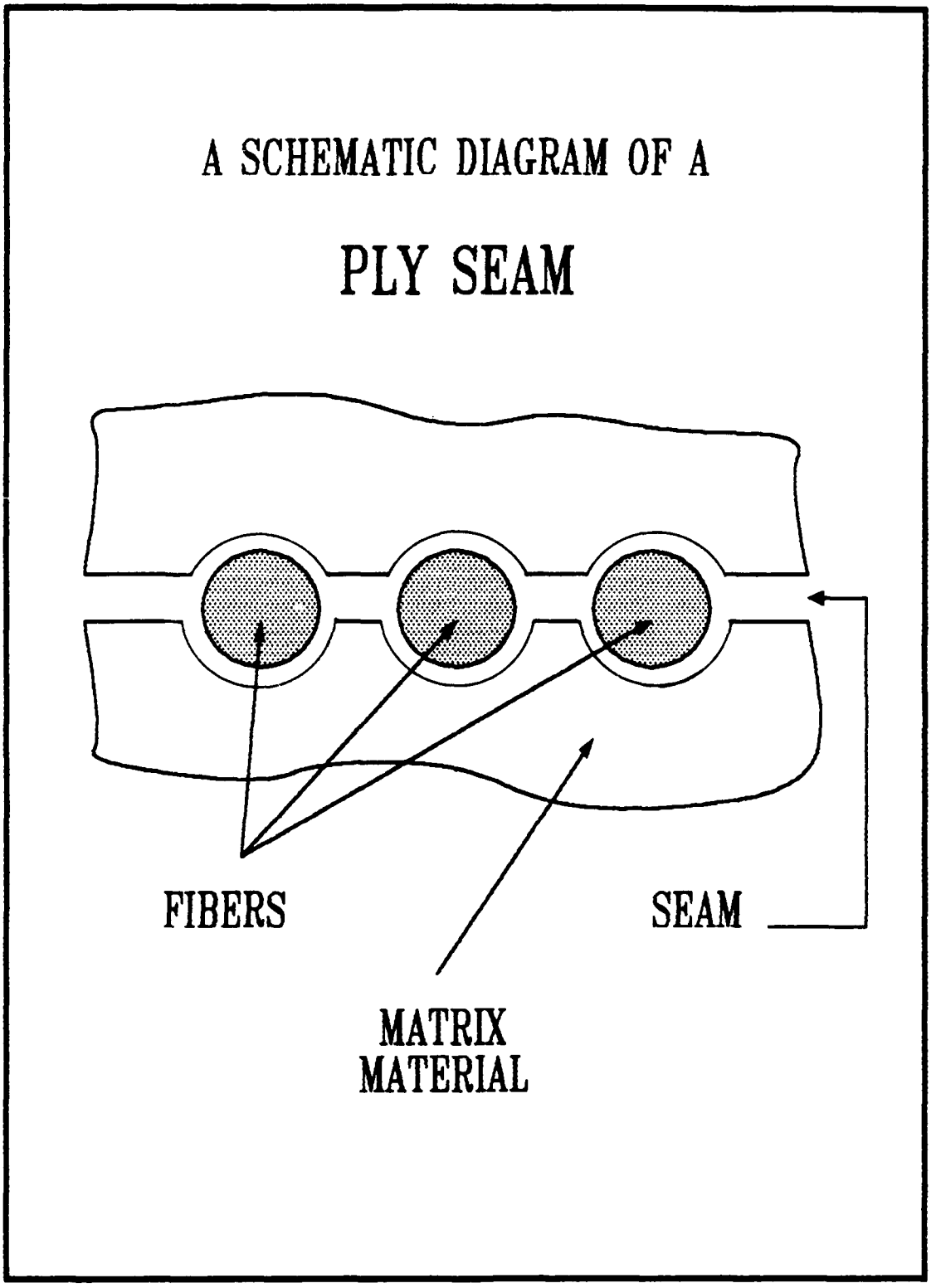

Figure 31. Ply Seam

the specimen was done during the cycling.

In Figure 32 there is a crack growing into the matrix at the point where the fiber was cut at an angle and the fiber was pulled out (arrow B). Secondly, where the bubbles or voids formed at the seam of the ply, cracks are forming (arrow C). It appears that the laminate is beginning to delaminate by the initiation of the cracks at the fiber edge. There is a third place where cracks were observed. They were observed inside the groove where a section of fiber was pulled out; however , these cracks are not visible in the photographs. Once again the seam line was exposed and here the cracks started to form.

After the accumulation of more thermal cycles, the progression of the damage was chronicled and the search for any new damage continued. Figure 33 shows the same edge area as Figure 32, but after 3,000 cycles and Figure 34 after 6,000 cycles. At the fiber pullout tip, the crack has grown longer and starts to connect with smaller cracks initiating at the bubbles along the seam (arrow D). Where the cracks began at the seam in the matrix, they are now longer and more of them are connected (arrow E). The cracks also get wider as thermal cycles increase.

Figure 35 through 37 are photographs of similar cracks after the edge of the specimen was diamond polished to remove oxidation. The cracks are much more visible as well as the seam line between the plies (designated by the line of bubbles in the matrix). Figure 36 is a closeup of the crack emanating from the fiber pullout tip. Damage initiated and progressed in the same manner in the rest of the

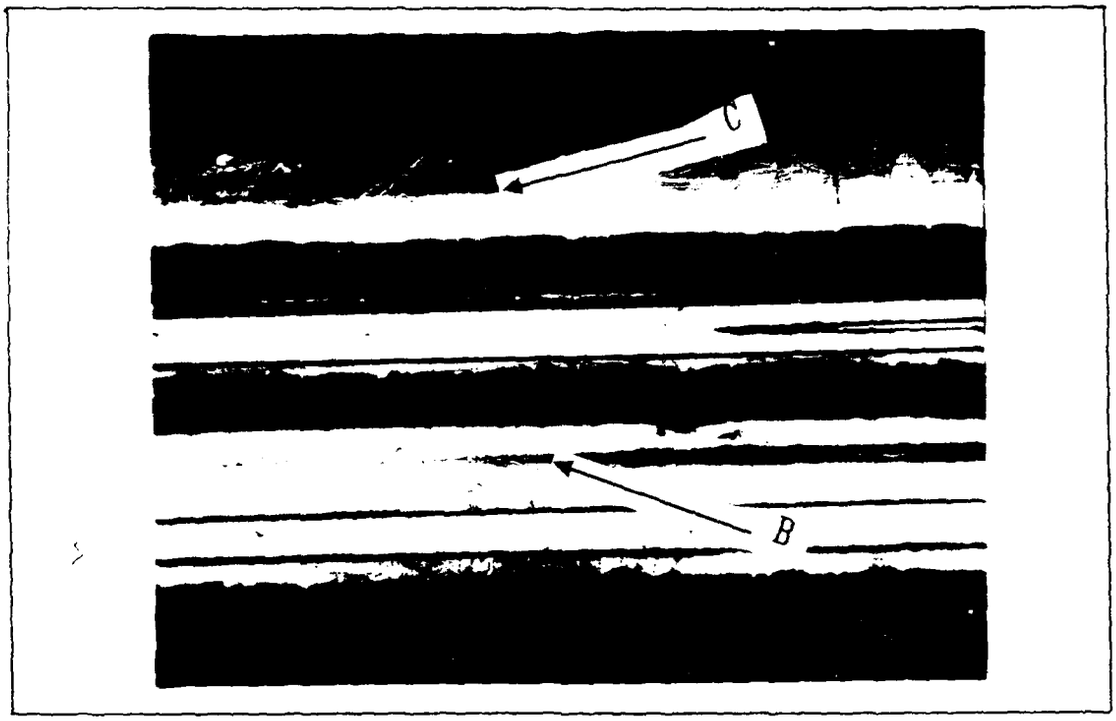

Figure 32. Specimen 9 at 1500 Cycles (50X)

Figure 33. Specimen 9 at 3000 Cycles (50X)

Figure 34. Specimen 9 at 6000 Cycles (50X)

Figure 35. Delamination Edge Cracks After Polishing (50X)

Figure 36. Fiber Tip Pullout Crack (100X)

Figure 37. Ply Delamination Cracks (50X)

specimens.

The only damage visible on the edge was cracking in the matrix. The cracks always formed along the seam and initiated at the fiber pullout tip or a bubble in the seam. The fiber never showed any cracking or damage. Whether or not any debonding of the fiber from the matrix occurred was not evident from the optical photographs. The cracks initiated at 1,500 cycles, which does not coincide with the 800 cycle change in strain from the expansion to compression. It is possible that the damage, such as cracks, initiates at a lower cycle count inside the laminate and grows outwards to the edge. The chance that a crack grew completely through the specimen from the edge to edge is unlikely. The cracks on one edge did not line up with the cracks on the opposite edge.

The next section tries to answer these questions by measuring the material characteristics and comparing the results to the number of thermal cycles. The initiation of damage may reveal itself by a change in the material characteristics as a function of applied thermal stresses.

Material Characteristics

After completion of the TF test two micro-measurements CEA-06-250UW-350 strain gages were applied to the heated zone of the sample. One was attached vertically and the other horizontally to measure Young's modulus and Poisson's ratio at room temperature. Figure 38

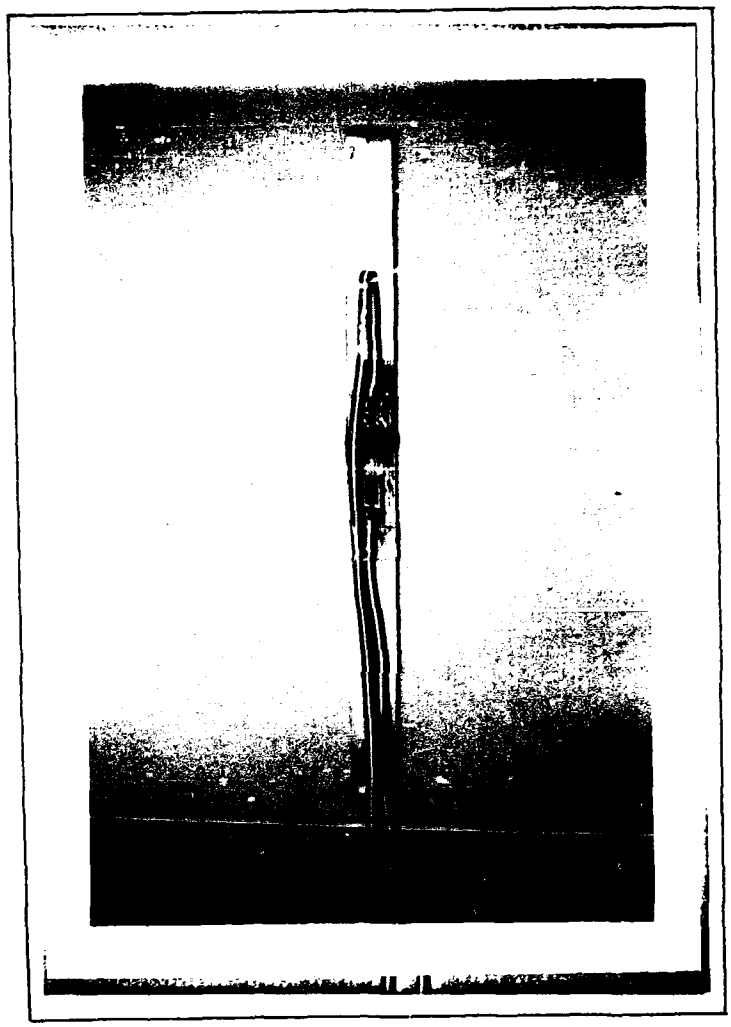

Figure 38. MMC Specimen Fitted with Strain Gages

shows the gages installed on the specimen.

In reference (24), Johnson et. al. studied the tensile and fatigue behavior of uniaxial and angle-ply SCS6/Ti-15-3 composites at room temperature. The author suggested that in the angle-ply system, the 0-degree plies played a significant role in controlling fatigue life. Johnson also reports that stiffness loss in continuous fiber reinforced MMCs can be a useful parameter for detecting fatigue damage initiation and accumulation. With this as our impetus, the specimens were placed in the 22 kip MTS machine and loaded to 850 pounds (37.7 ksi) or 17.3 percent of ultimate strength as reported in reference (23:40). The specimen was loaded to this level to stay in the linear regime of the stress-strain curve. The strains from the two strain gages were read directly from a BLH Electronics Digital Strain Indicator. The results are shown in Table 3.

Young's Modulus is calculated from the stress divided by the strain of the vertical strain gage. Poisson's Ratio is the negative of the horizontal strain divided by the vertical strain.

As shown in Figure 39, Young's modulus is fairly constant over this thermal cycle range. The average is 30.8 x 10^6 psi with a standard deviation of 0.008. Poisson's Ratio is also constant averaging 0.279 with a standard deviation of 0.009. METCAN predicts a modulus of 27.6 x 10^6 psi and Poisson's Ratio of 0.274. Johnson (24) found a modulus of 30.2 x 10^6 psi and v of 0.299.

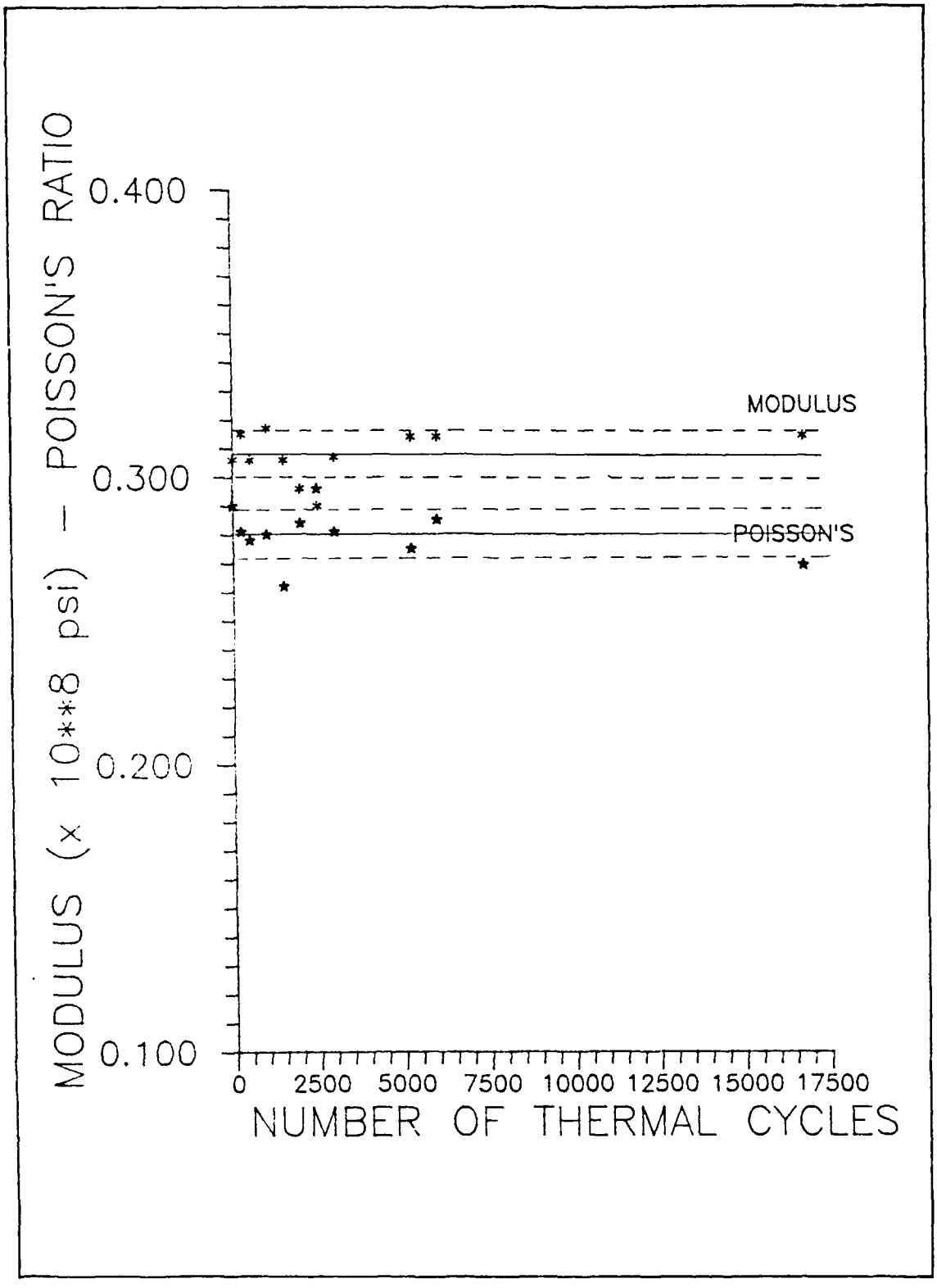

Figure 39. Modulus and Poisson's Ratio versus Thermal Cycles

Table 3 Young's Modulus and Poisson's Ratio Measurements

Specimen #	1	2	3	4	5
Cycles	250	500	1,000	1,500	2,000
E_1 (x10^6 psi)	31.5	30.6	31.7	30.6	29.6
ν_{12}	0.281	0.278	0.280	0.262	0.284
Specimen #	6	7	8	9	10
Cycles	2,500	3,000	5,250	6,000	16,750
E_1 (x10^6 psi)	29.0	30.7	31.4	31.4	31.4
ν_{12}	0.296	0.281	0.275	0.285	0.269
Uncycled Specimen : E_1 = 30.6 x 10^6 psi, ν_{12} = 0.290					

From this data no conclusion can be drawn about the correlation of these two material characteristics with thermal cycles, at least up to 16,750 cycles. According to Johnson's findings then, no significant fatigue damage has initiated or accumulated enough to affect the stiffness. However, some form of damage occured to cause the mean strain to fluctuate and the plies to delaminate at the edges.

The third material property examined to see if any changes occur as a function of thermal cycles is Ultimate Tensile Strength (UTS). METCAN predicts a UTS of 238 ksi for this ply layup of SCS6/Ti-15-3.

The UTS was found using the MTS machine. Both the upper and lower grip were clamped to the specimen and a loading rate was programmed into the MTS microconsole's function generator. A load rate of 50 pounds per second was applied to the sample and load versus strain was plotted on an X-Y recorder. Figure 40 shows the plot for the uncycled and Figure 41 for Specimen 8 (5,250 cycles).

These were two reasons for only testing two specimens for UTS. The first was the amount of material was limited, so specimens were precious and UTS testing rendered them useless afterwards. The second reason was, if the samples were going to be destroyed, it would be more beneficial to section them to view the interiors for damage. The results of sectioning are next topic of this chapter.

The uncycled specimen failed at a load of 6,267 pounds or 278 ksi. Specimen 8 failed at 5,557 pounds or 247 ksi. The accuracy of the UTS data is guestionable since both specimens broke at the grip and not in the center or heated zone. The wedge grip caused a stress concentration in the sample because no loading tabs were attached to the specimen ends to diffuse the load. Other studies have shown that UTS does decrease with thermal and thermo-mechanical cycles (24:40). The sharp point in the baseline curve denotes when the strain gage separated from the specimen surface.

Figure 42 shows the two curves laid one on top of one another. It is evident that the curves are linear and exactly the same below 2,300 pounds (102.0 ksi). E_1 is 31.8 x 10^6 psi. This checks with the data

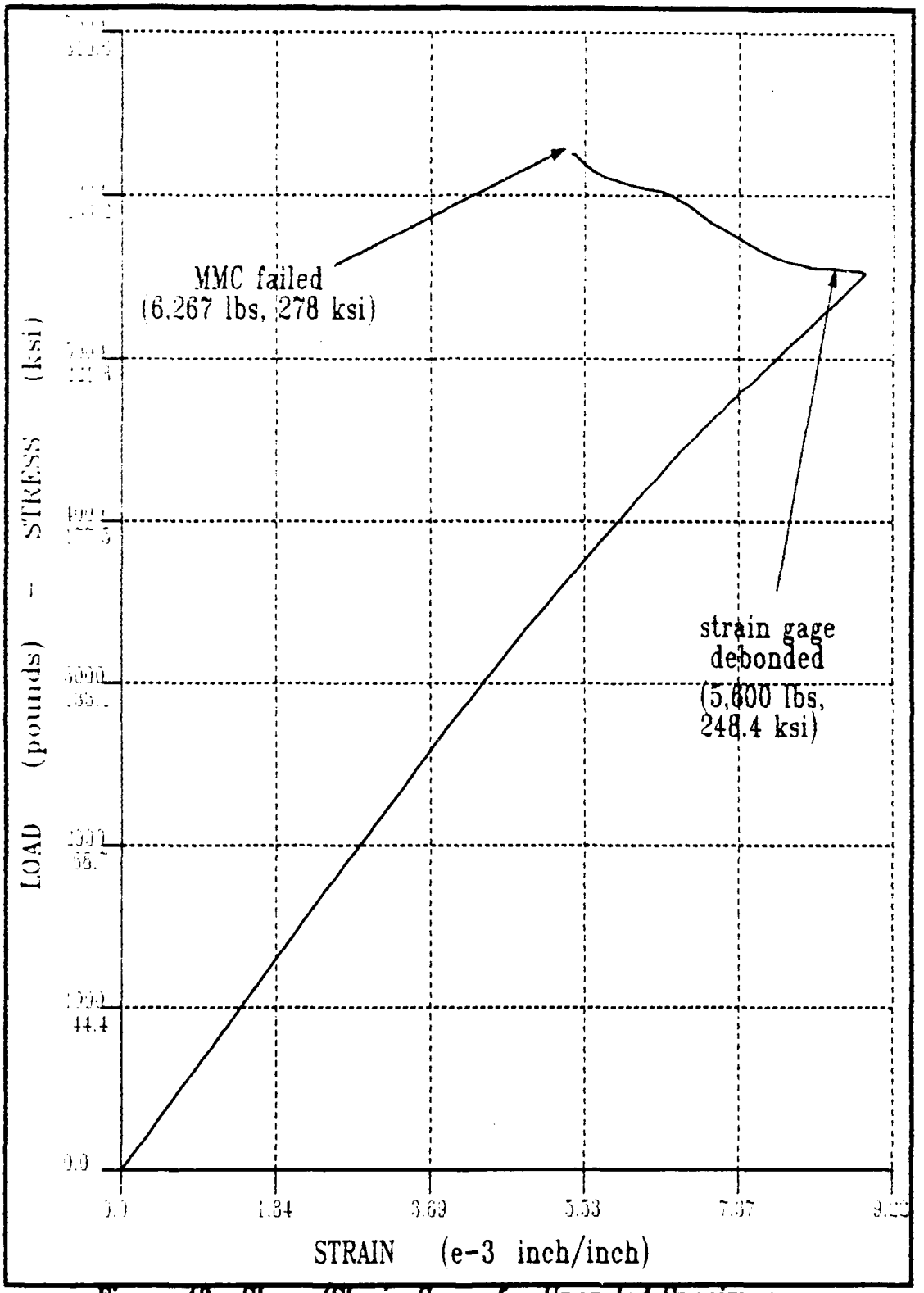

Figure 40. Stress/Strain Curve for Uncycled Specimen

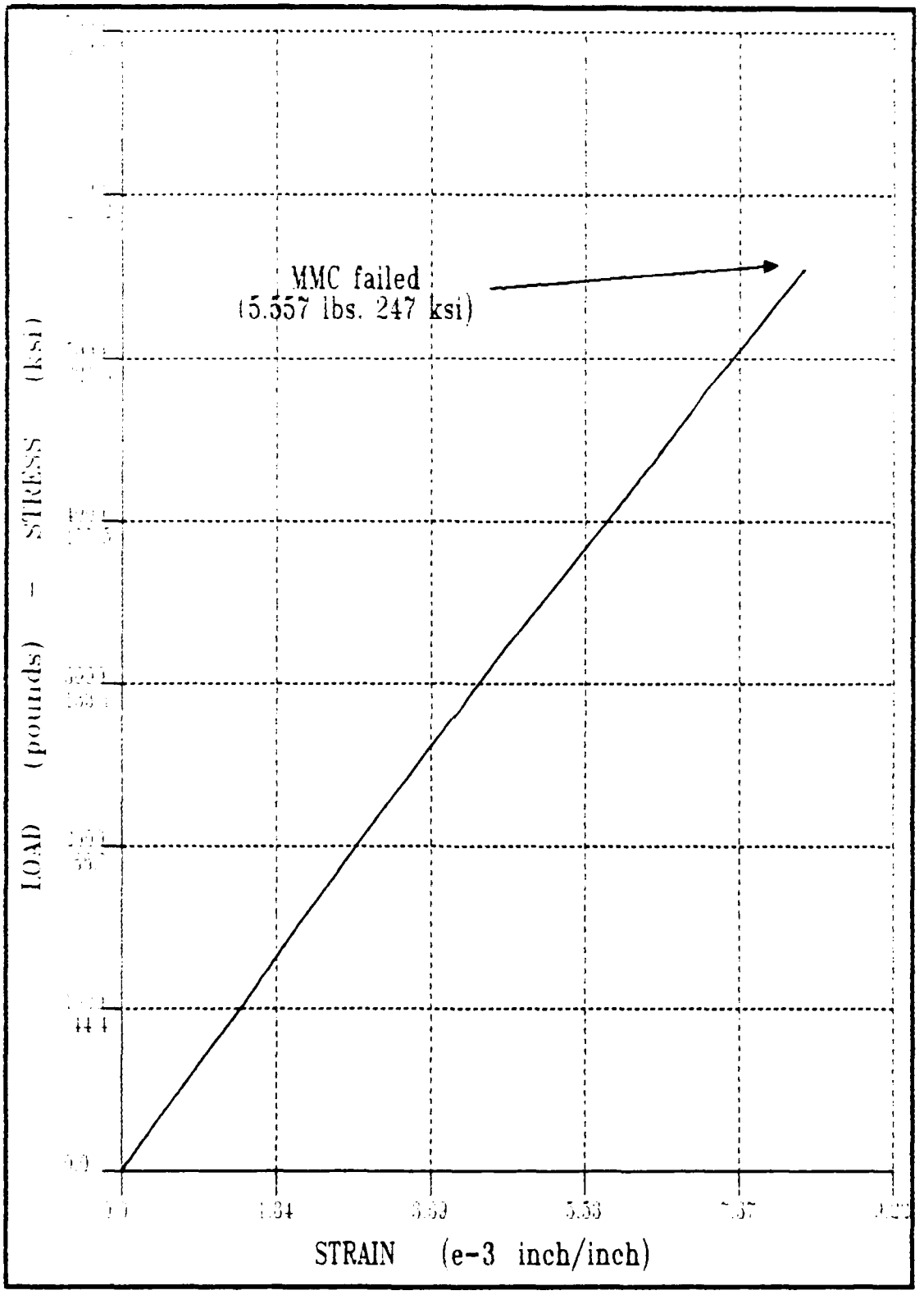

Figure 41. Stress/Strain Curve for Specimen 8 (5250 Cycles)

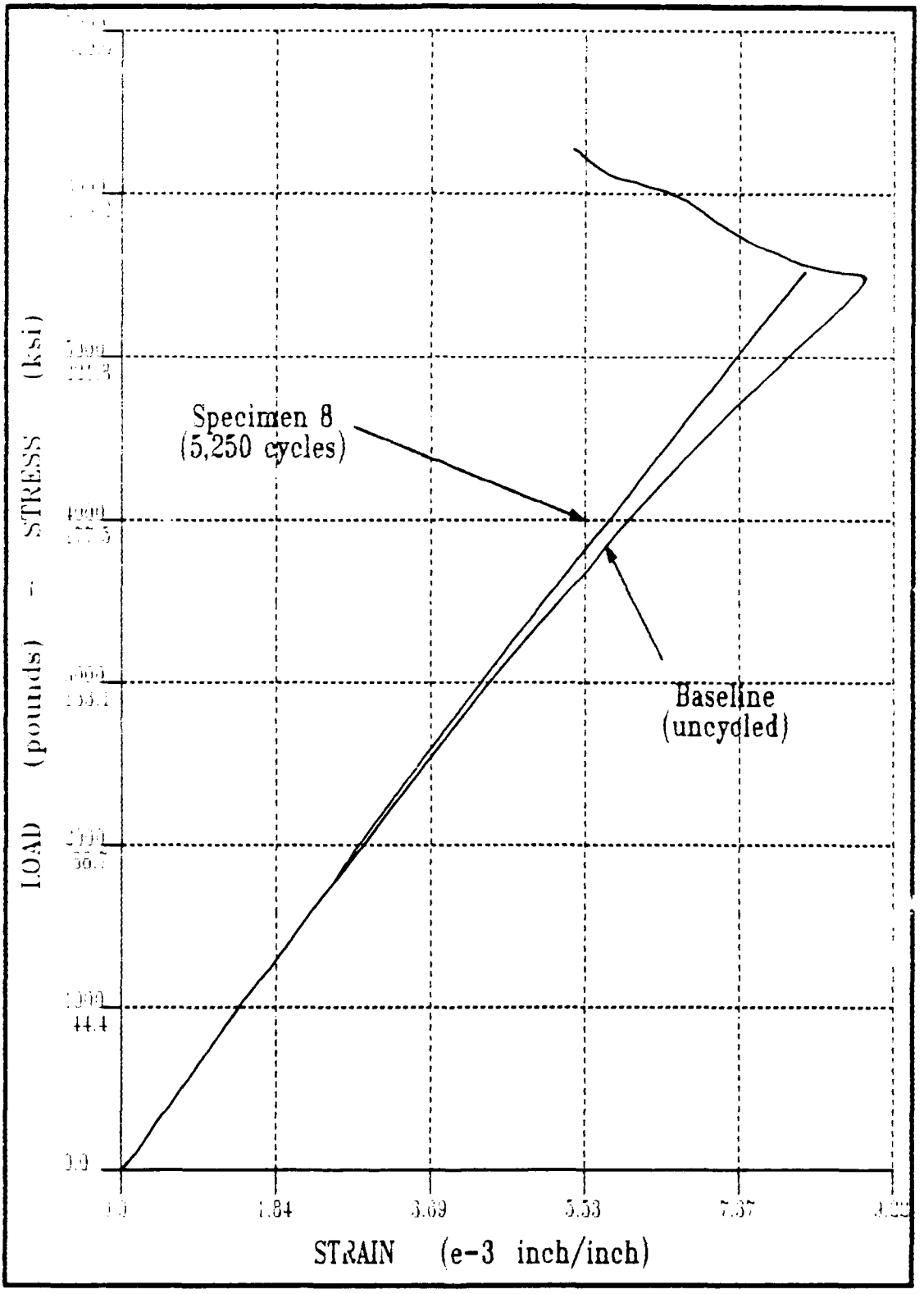

Figure 42. Comparison of Uncycled to Cycled Stress/Strain Curves

presented in the last section since the specimens were only loaded to 850 pounds (37.7 ksi), well below 2,300 pounds. Both specimens start nonlinear behavior at 2,300 pounds; however, the uncycled curves more and more as the load increases. Specimen 8 barely curves at all and the curve is almost linear above and below 3,300 pounds.

The comparison of these curves shows that thermal cycling does not affect the linear portion of the stress-strain curve. Since the specimens were loaded along the linear part of the curves, Young's modulus is constant. Thermal cycling does affect the nonlinear portion of the stress-strain curve. Thermal cycling causes the material to behave almost linearly up until it fails. Where the uncycled specimen displays some ductility and loses stiffness, the cycled material does not and stiffness remains much the same.

The residual thermal stresses are believed to cause the phenomenon in the stress/strain curves. Later in this chapter an analysis of residual stresses is done with METCAN and an explanation accompanies the plots. Residual stresses affect the other material characteristics as well and are also described. The next section deals with finding the initial fatigue damage and recording its history through Scanning Electron Microscope (SEM) photography.

Sectioning and SEM Photography

The following questions still remain:

When does thermal fatigue damage initiate and how does it progress?

Do cracks begin inside the specimen and work their way out to the edge?

Are the fiber and matrix debonding?

In order to answer these questions, several specimens were cut perpendicular to the fibers in the heated zone and the cross-section was viewed under a SEM. The specimens were sectioned with a six inch diameter diamond cutoff wheel and one quarter inch pieces were mounted in Epomet casting compound. The samples were polished with increasingly finer grades of diamond paste until clean. The last preparation necessary before SEM photography was a coating of carbon on the specimen.

Figure 43 diagramatically describes the uncycled and cycled fiber cross-sections. Before thermal cycling the reaction zone is smooth and a uniform color. A few radial cracks are present in the zone and the border between the outer coating and the zone is undifferentiated. After 500 cycles the reaction zone starts to change color and shape. At 1,000 cycles the radial cracks have broken up the reaction zone and

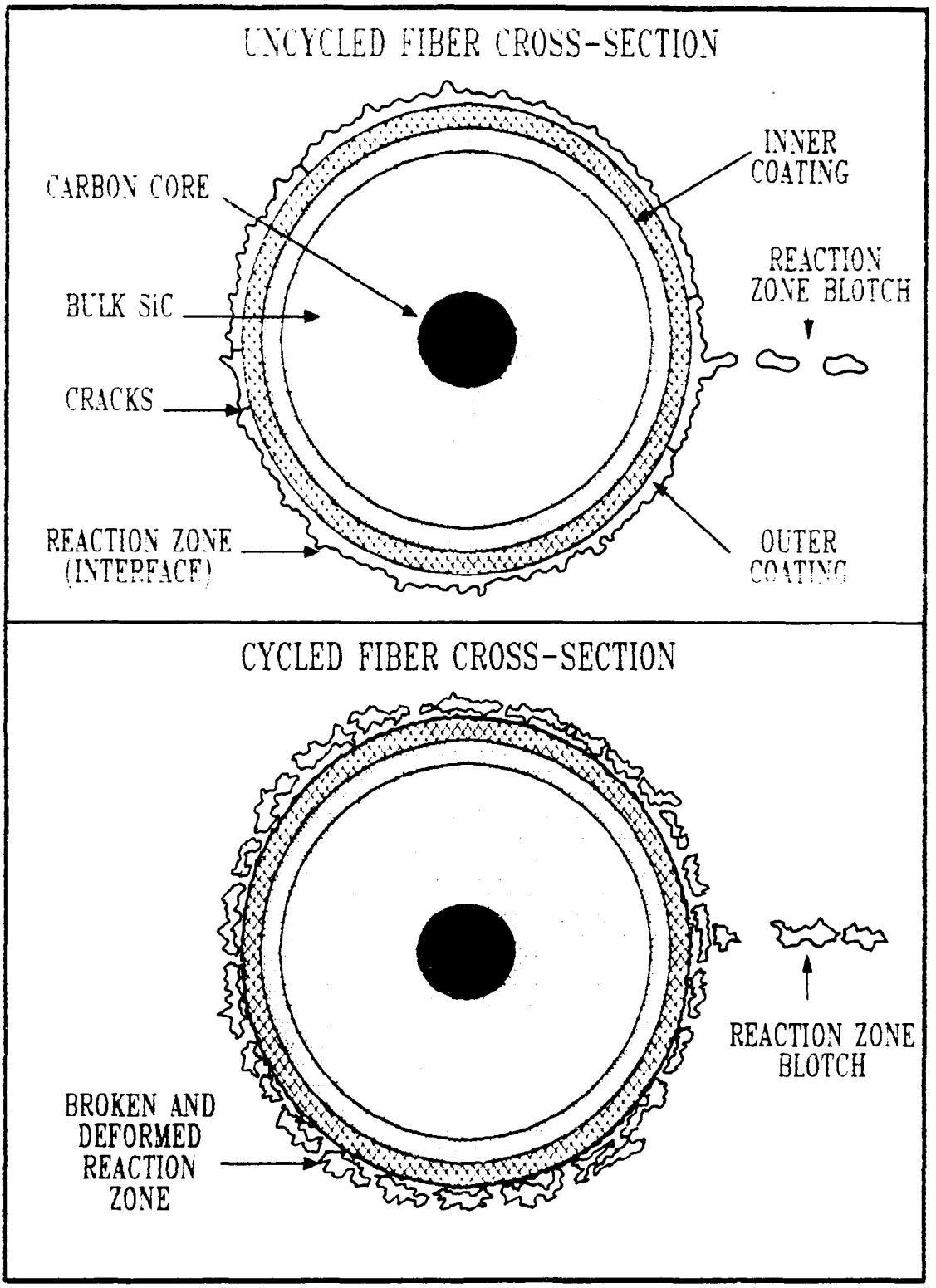

Figure 43. Comparison of Uncycled to Cycled Cross-Sections

the border at the outer coating is irregular. The actual pictures follow to verify Figure 43.

Figures 44 through 47 are photographs of an uncycled specimen at different locations and magnifications in the cross-sections. Figure 44 is a 90X magnification to give an overall picture of the uncycled cross-section. This view is useful to tell how uniformly spaced and how well lined up the fibers are. The bubbles along the seam of the plies that we thought were voids or air pockets on the specimen edge (eg. see Figure 30), are barely visible at this magnification. They are seen as small gray blotches lined up in between the fibers.

In Figures 45 the fiber cross-section fills the picture. The SCS6 fiber has an inner core of carbon surrounded by bulk SiC. The fiber is coated twice in layers of Si and C, the outermost layer being C. The outer coating protect the fiber during handling, and also are important in reducing residual stresses in the fibers during their fabrication (26:4). The two black rings around the fiber are the coatings.

The last gray area around the fiber is the fiber/matrix interface, or reaction zone, formed by the reaction between the constituents in the matrix, primarily Ti, with the fiber constituents, Si and C. Lerch et. al. (23) have shown that the reaction zone can have significant levels of carbides and silicides. Extending downward is a trail of blotches along the seam line having the same gray color as the reaction zone. We can conclude that these blotches are pieces of the reaction zone that got pushed into and trapped between the plies during

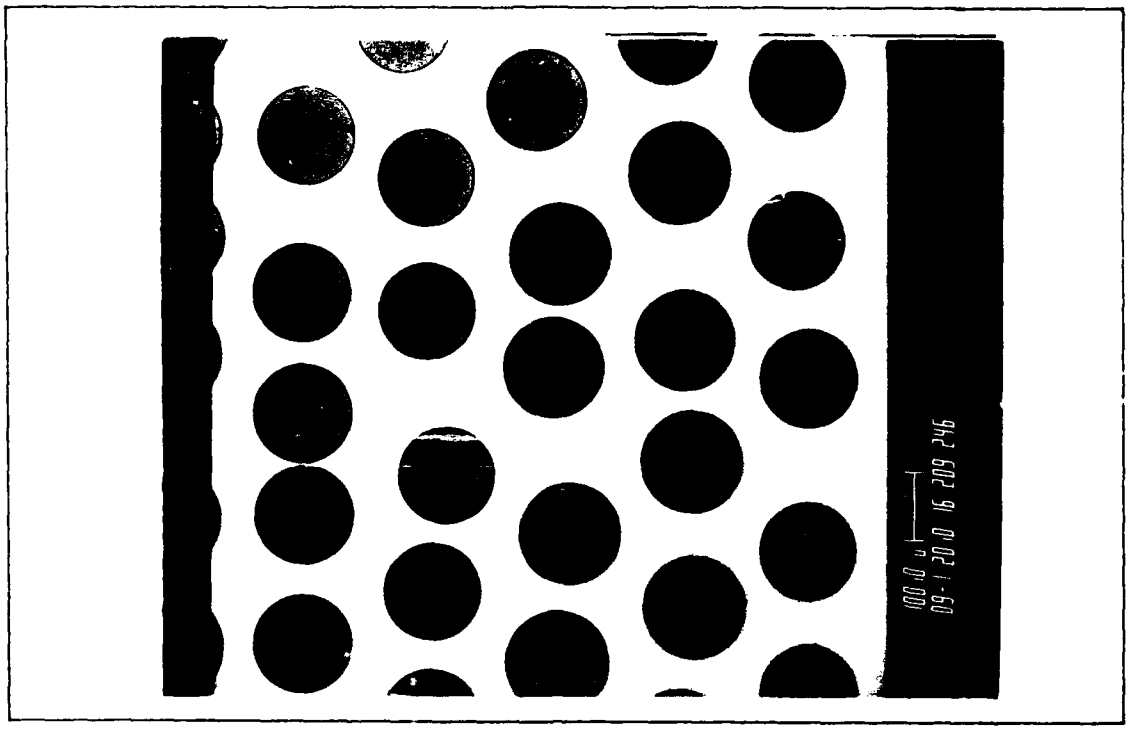

Figure 44. Uncycled Laminate Cross-Section (90X)

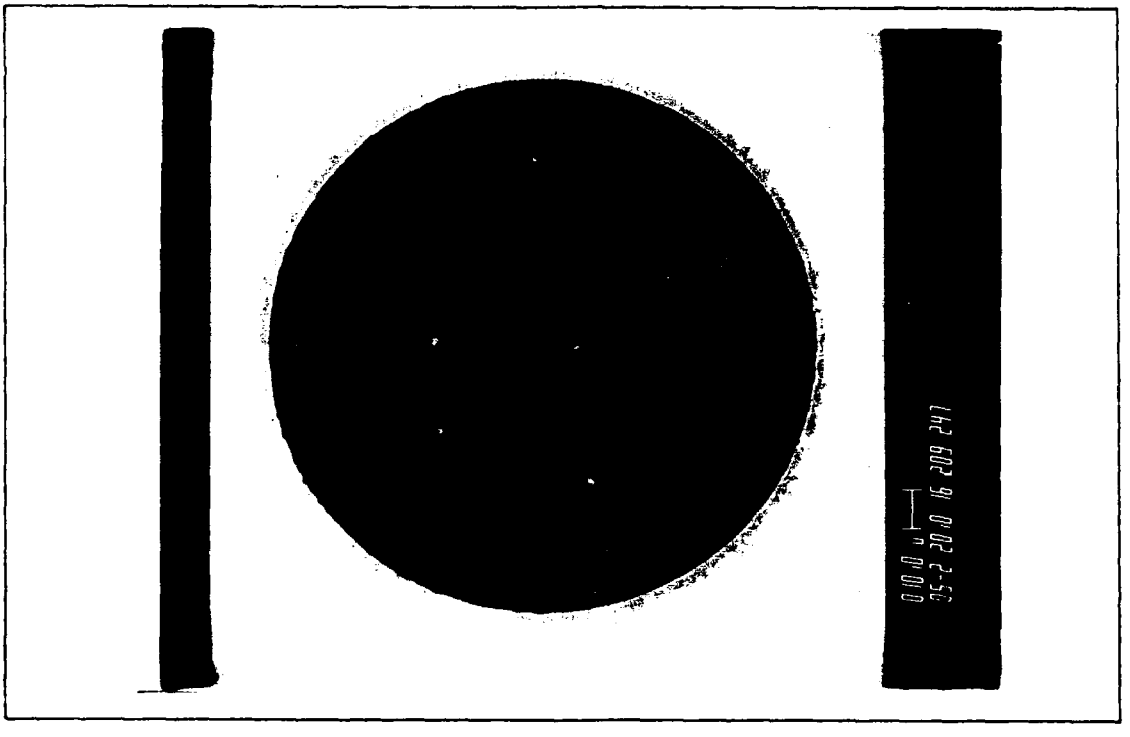

Figure 45. Uncycled Fiber, Coatings, and Interface (500X)

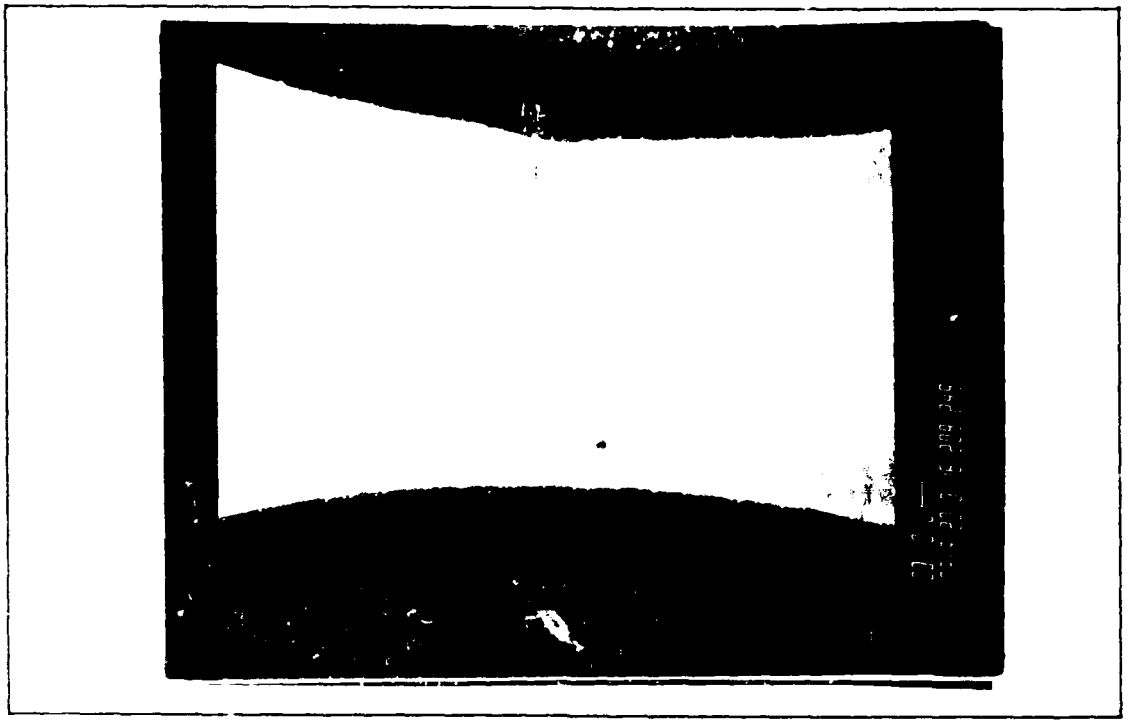

Figure 46. Uncycled Interface Radial Cracks (3000X)

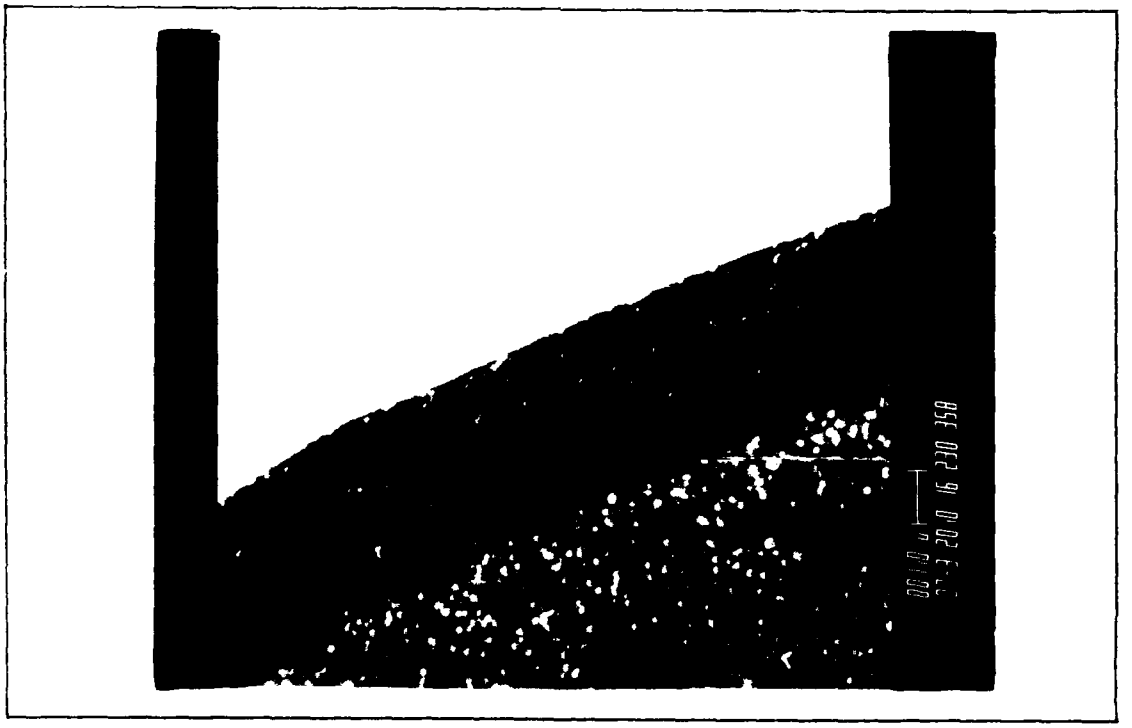

Figure 47. Uncycled Interface (7000X)

manufacturing of the laminate. We assume that the material in the blotches is the same as in the reaction zone since in SEM photography areas of like color have like density. Notice the reaction zone is a uniform color throughout and connected to the fiber.

Figure 46 shows two closely spaced fibers, their reaction zones and a reaction blotch between them. Also visible are several radial cracks in the reaction zone with two of them extending into the outer coating of the fiber. These radial cracks are found elsewhere around the fiber, but they are most common at the ply boundary when two fibers are close together.

Figure 47 is a 7000X magnification of the coating and reaction zone. The reaction zone is a solid shade of gray. There are no cracks here and the boundary between the coating and the reaction zone is very smooth.

The next specimen examined is specimen 1 cycled 250 times. The cross-section photographs look the same as the uncycled except for one detail. In Figure 48 the cracks in the reaction zone seem to have widened. The cracks have not extended into the matrix and the cracks in the fiber coating look the same. The reaction zone is still very uniform in color. The boundary between the reaction zone and the coating is hidden in Figure 48 due to a reflection that was unable to be attentuated.

Figures 49 and 50 are cross-sectional pictures of specimen 2 cycled 500 times. Figure 49 shows two close fibers with the reaction

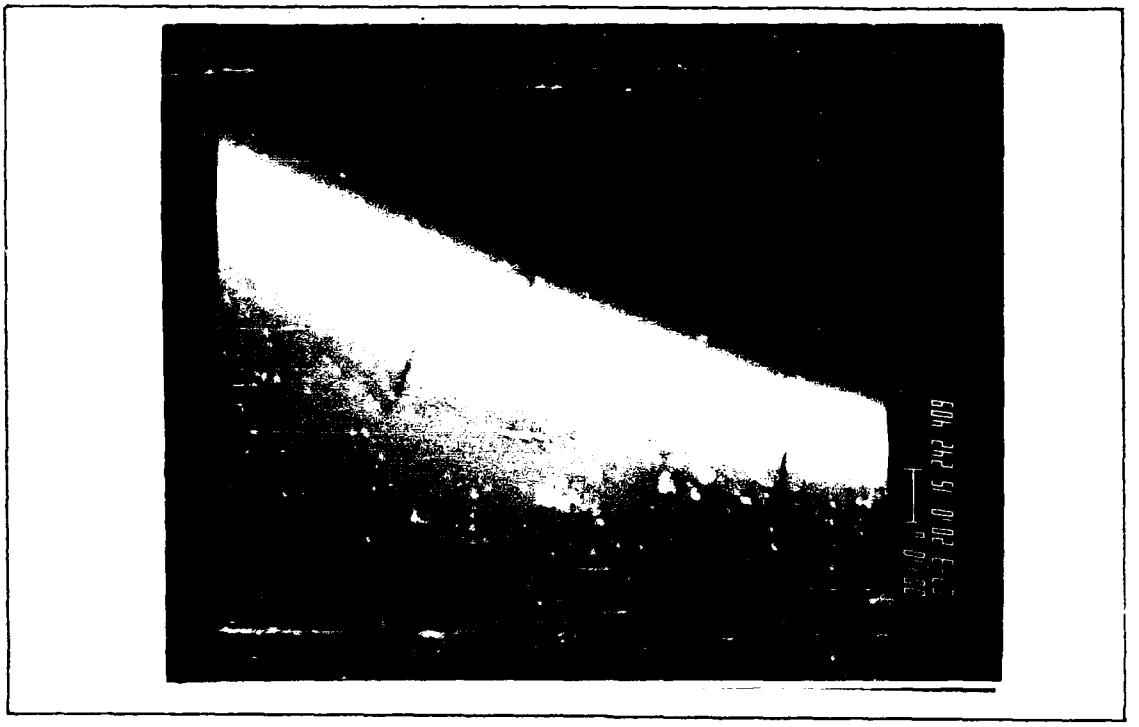

Figure 48. Radial Cracks After 250 Cycles (7000X)

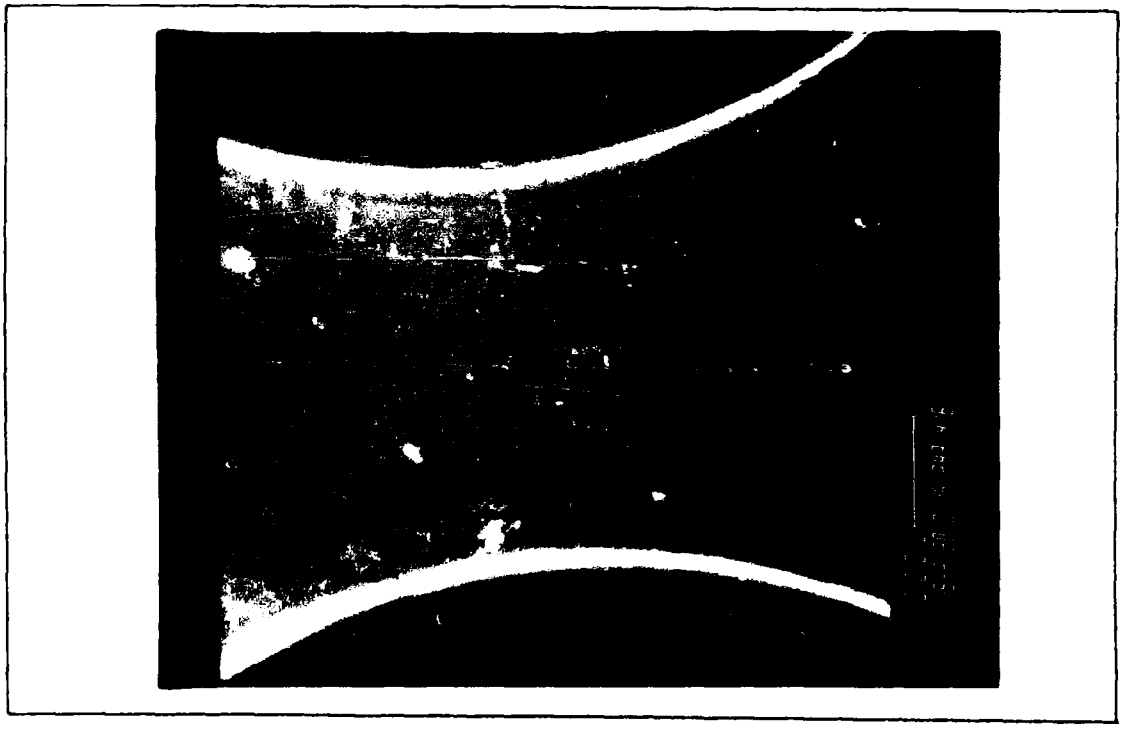

Figure 49. Radial Cracks of Closely Spaced Fibers After 500 Cycles (1500X)

zone blotches lined up between them. The radial cracks are still evident in the reaction zone and the outer coating but are still restricted inside them. The reaction zone looks uniform and forms a smooth border around the fiber coating. No cracks have grown into the matrix or have initiated there. Figure 50 is a closeup of Figure 49. At 5000X the reaction zone is not as uniform as it appears in Figure 49. Now there are two different shades to the reaction zone. The composition is changing in some way due to the effects of thermal cycles. The border between the coating and the interface is partially hidden again by the acute reflection, but it still appears smooth.

At 1,000 cycles, Figure 51 shows no cracking in the matrix of specimen 3. The reaction zone blotches are more easily seen here as well as some patchy areas in the interface region. Figure 52 exhibits a drastic change in the reaction zone. It is no longer the homogeneous buffer between the matrix and fiber. It appears to be breaking up and changing shape. Portions of it are becoming detached from fiber coating. Magnifying the area at 5000X shows a mottled reaction zone in Figure 53. The reaction zone blotch next to it also changed. Instead of being rounded, it now resembles a crystal shape. The border of the outer coating and reaction zone is getting uneven and irregular. The fiber and matrix are not debonding though. Figure 54 shows no spaces between the coating and interface. The radial cracks seen before, have contributed to the breakup of the interface through thermal fatigue.

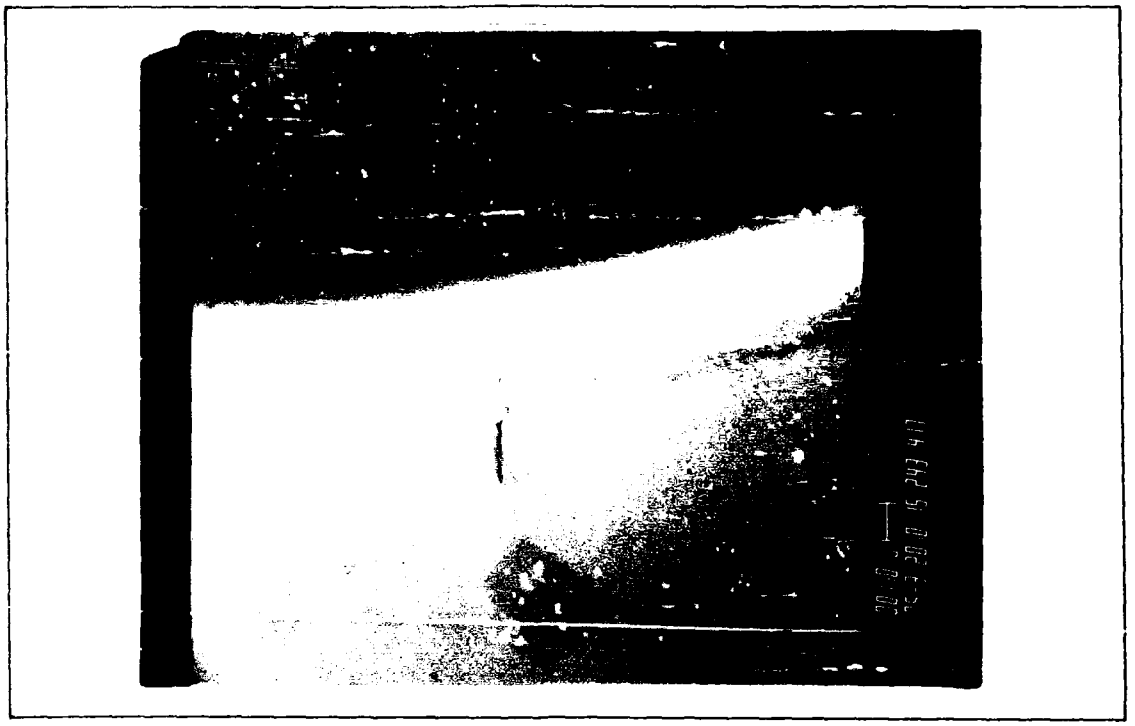

Figure 50. Radial Cracks After 500 Cycles (5000X)

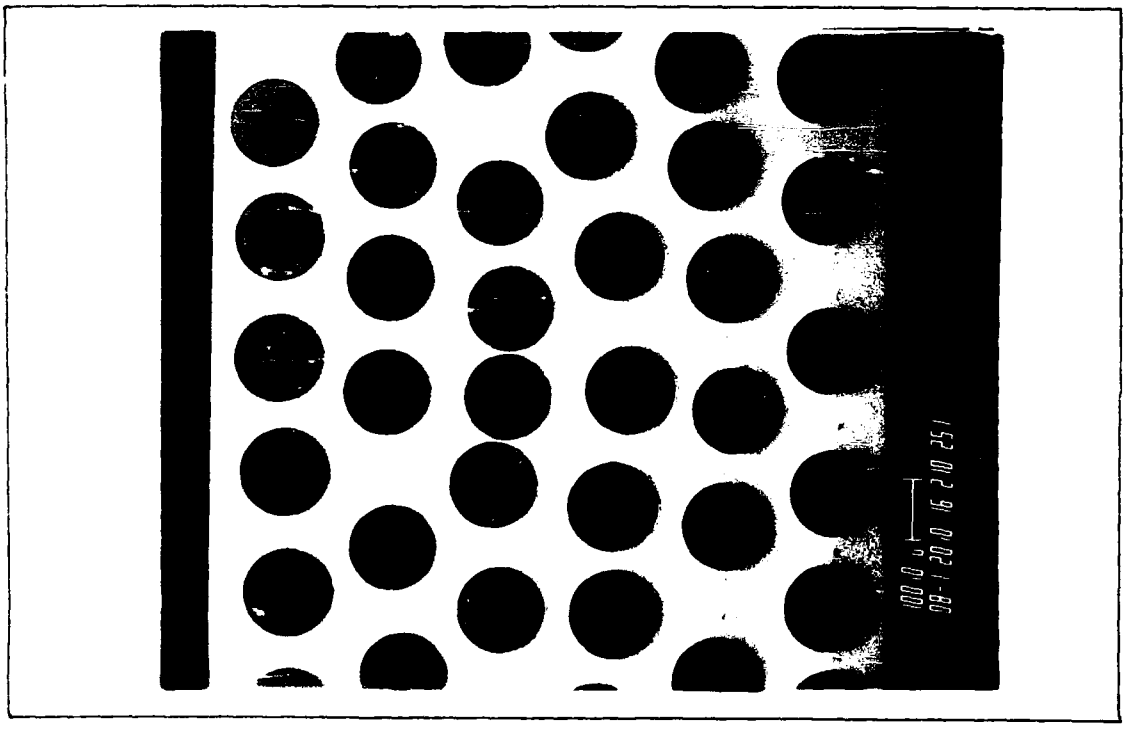

Figure 51. Cross-Section of Laminate After 1000 Cycles (1500X)

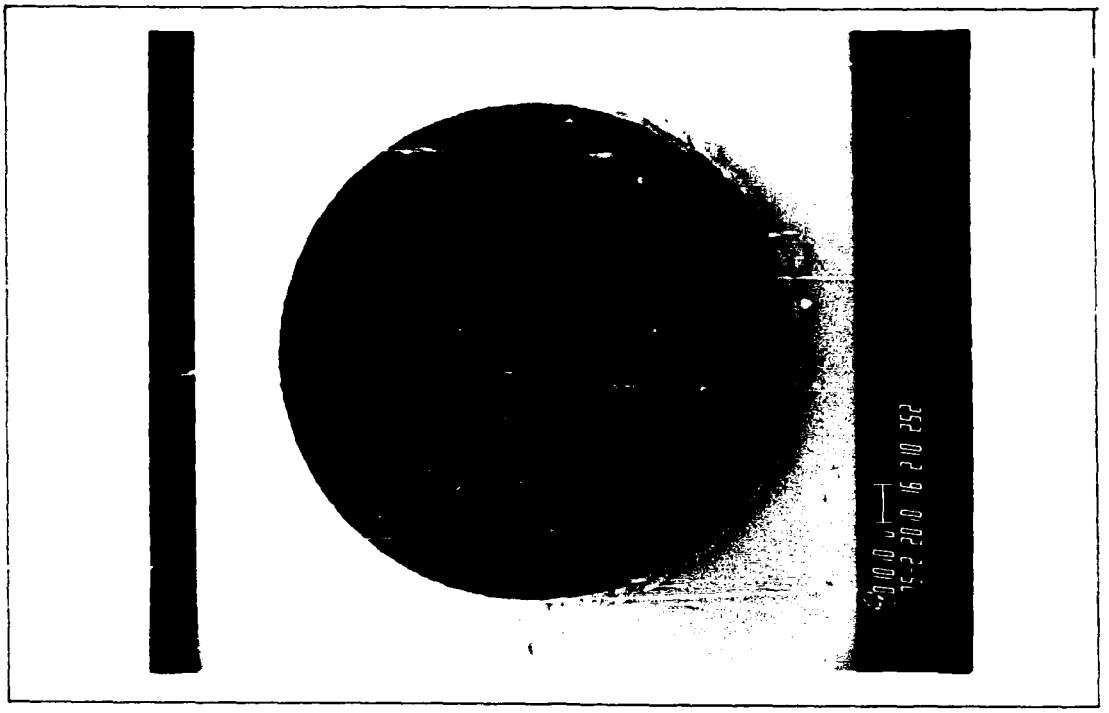

Figure 52. Fiber/Matrix Interface After 1000 Cycles (500X)

Figure 53. Reaction Zone After 1000 Cycles (5000X)

When the specimen is subjected to more thermal cycles, such as specimen 4 (1,500 cycles), not many changes take place. In Figure 55, the reaction zone is a little more damaged. The fiber coating and interface boundary is more irregular, but no cracks initiate inside the matrix. At this point, cracks were seen on the edge of the specimen. Figure 56 is a closeup of the crack that started at the edge and grew through the matrix towards the fiber. The damage to the reaction zone is worse here than anywhere else in the specimen. The matrix and fiber have even debonded near the edge crack, but are still attached on the opposite side of the fiber. The edge crack and ply delamination must be an edge effect resulting from stresses imposed when preparing the specimen. Missing fibers due to cutting play a key role in the formation of edge cracks. This will be discussed later in this chapter.

The degradation of the reaction zone is the first sign of damage due to thermal cycling. It initiates at 500 cycles and becomes signficant at 1,000 cycles. The reaction zone breaks up before any damage is evident on the surface of the specimen. The interface between the fiber and matrix is the probable cause of the change in material characteristics of a specimen undergoing thermal fatigue.

Let us continue to examine the damage progression. At 6000 cycles the extent of the damage has stabilized. Figure 57 shows the typical breaking up of the reaction zone and uneven boundaries, but this time a piece of the reaction zone has fractured and broken off. At 16,750

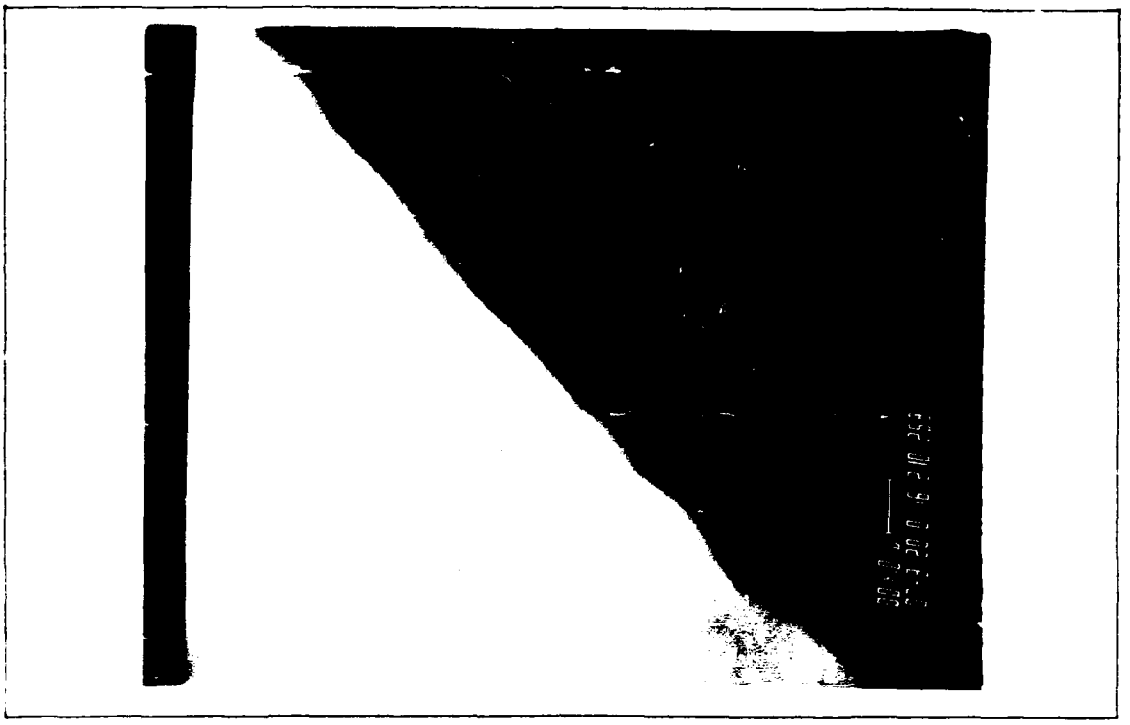

Figure 54. Reaction Zone After 1000 Cycles (7000X)

Figure 55. Reaction Zone After 1500 Cycles (7000X)

Figure 56. Edge Crack Cross-Section After 1500 Cycles (3000X)

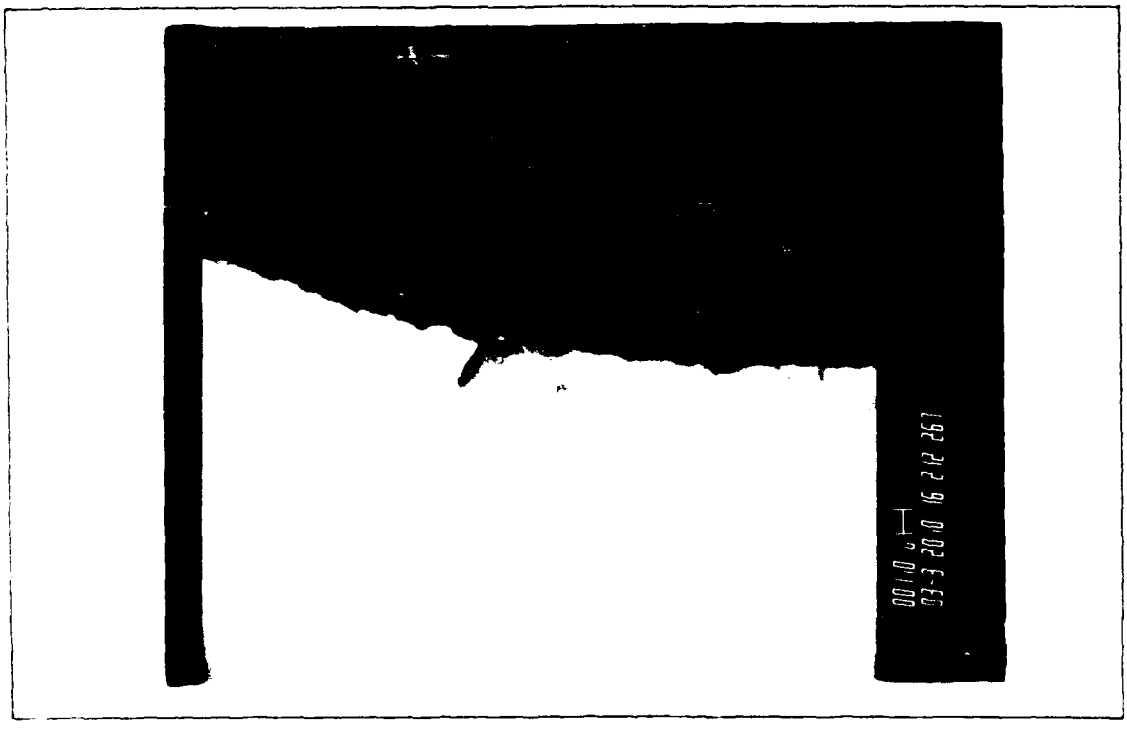

Figure 57. Reaction Zone Fracture After 6000 Cycles (3000X)

cycles, in Figure 58, there is not much change. The reaction blotch in the ply seam has the sharp edges seen earlier, but hasn't changed in any way. No cracks were observed in the matrix specimens up to this point. Even the edge cracks seen at 1,500 cycles stopped as they reached an interior fiber. It is predicted, however, that eventually cracks will form in the laminate.

The initiation point is forecast to start in the reaction zone or reaction zone blotches of closely spaced fibers and grow along the seam and around the fibers. The plies will delaminate and the fibers will debond from the matrix causing total laminate failure.

As yet, we have not discussed why the Young's Modulus remained constant for all the specimens even though damage initiated and progressed in the reaction zone. Neither have we discussed the effect of the residual stresses due to manufacturing on these topic areas. The next section addresses these areas with the aid of a computer code capable of performing a nonlinear analysis of fiber reinforced MMCs.

Residual Stress Analysis Using METCAN

The reason that Young's Modulus and Poisson's Ratio did not change as a function of thermal cycles may be related to residual thermal stresses. In order to incorporate thermal loading resulting from curing the material, it was necessary to account for the fact that the matrix will creep at elevated temperatures. Typically, significant creep is expected at temperatures above the homologous temperature,

Figure 58. Reaction Zone and Blotch After 16750 Cycles (5000X)

which is about 1/2 of the melting point expressed in absolute temperature (19:22). For the silicon carbide/titanium composite under study, the homologous temperature was approximately 1,100°F, while the material was processed at around 2000°F. It was assumed that during the cooling of the composite, any residual stresses that might be developed while cooling from 2,000°F to 1,100°F would be relieved by creep, and that no relaxation of residual stresses occurred while cooling from 1,100°F to room temperature. The temperature change during the cooling process was chosen to be 1000°F for convenience (19:23).

The computer code METCAN was used to calculate the current stresses in each ply due to residual thermal stresses. The residual thermal stresses come about after manufacturing from the variation in the fiber and the matrix CTEs. The stresses were given in the ply material axis system. For a $[0]_6$ layup the ply material axes are colinear with the laminate structural axis system. Axis 1 runs parallel with the 0 degree fibers. Axis 2 runs parallel to the ply and axis 3 runs perpendicular to the fiber and the ply. Radial and tangential stresses were desired; therefore, the following relations were used to transform σ_{22} and σ_{33} to σ_{rr} and $\sigma_{\theta\theta}$:

$$\sigma_{rr} = \sigma_{22} \cos^2 + \sigma_{33} \sin^2 + \sigma_{23} \sin 2 \quad (9)$$

$$\sigma_{\theta\theta} = \sigma_{33} \cos^2 + \sigma_{22} \sin^2 + \sigma_{23} \sin 2 \quad (10)$$

Since σ_{23} is zero and σ_{22} equals σ_{33} in the fiber and matrix, σ_{rr} equals $\sigma_{\theta\theta}$. Also, σ_{rr} and $\sigma_{\theta\theta}$ are constant from 0° to 90° for a given temperature in the laminate materials. METCAN predictd σ_{22} and σ_{33} due to the curing from 1,100°F to 70°F.

If we use METCAN to calculate the stresses in the fiber and matrix for the whole thermal profile we get Figure 59. The fiber is in compression and the matrix is in tension. At room temperature the fiber stress is -12.243 ksi and the matrix stress is 21.067 ksi. The residual stresses are -9.565 ksi and 16.458 ksi respectively at 300°F.

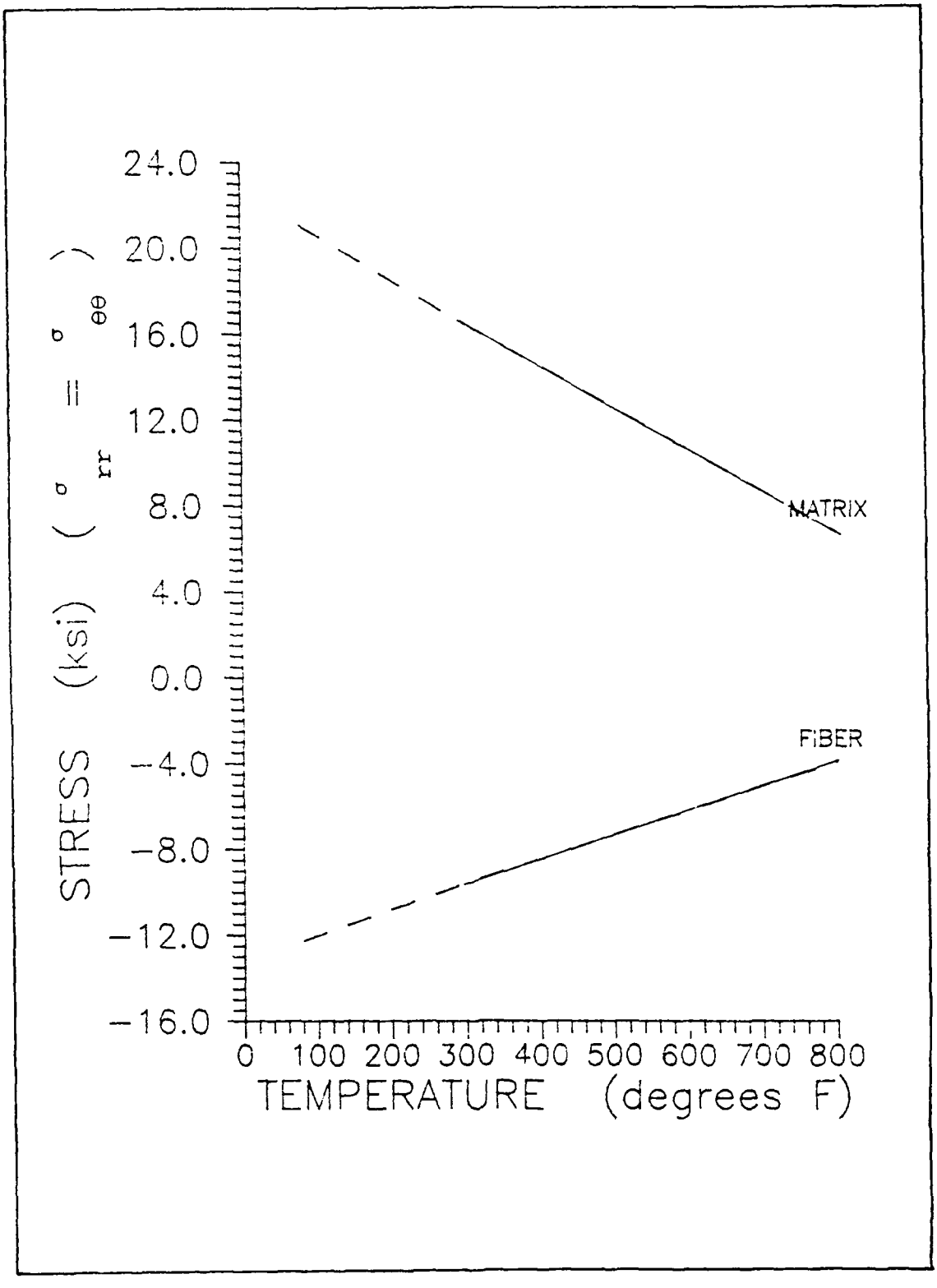

Figure 59. Fiber and Matrix Thermal Residual Stresses versus Temperature of Specimen

As temperature increases the stresses relax but do not completely vanish. A stress of 6.763 ksi is needed to overcome the matrix tension and -3.931 to overcome the fiber compression.

We have seen that the fiber/matrix interface is damaged after thermal cycling. Expectedly, the modulus should imitate this damage, but no change was observed at room temperature. The answer lies in the residual thermal stress due to curing. The compressive stress in the fiber and tensile stress of the matrix cause the fiber and matrix to rejoin upon cooling of the specimen. The residual stresses act to rebond the laminate together at room temperature. Due to the matrix choking the fiber, any separation at the interface was concealed as the material closed around itself at room temperature.

The residual thermal stresses explain why delamination cracking only occurred at the edges and not inside the laminate. Cracks always formed at the edge where a fiber was missing. The fiber/matrix union is the link that holds the laminate together. The residual tensile stresses of the matrix pulled the plies apart at the seam since the fiber was not there to hold them together. When the fiber/matrix union was intact inside the fiber, the matrix tensile stresses were not strong enough to separate the plies. Eventually, the accumulation of thermal fatigue will weaken the fiber/matrix bond (as we saw happening in the reaction zone) to allow total delamination through the laminate.

The residual thermal stresses are also the culprit of the more linear stress/strain curve for a cycled sample. As the thermal cycling

begins, cracks form and grow in the reaction zone. This damage relieves some of the residual stress in the laminate. In Figure 40, The uncycled specimen required a stress greater than 102 ksi for the material to react nonlinearly. The cycled specimen required a stress greater than 133 ksi for nonlinear behavior to occur. Even then, the nonlinearity was less than for the uncycled specimen.

It is believed therefore, that the stress must reach a threshold value before nonlinear deformation takes place. This threshold stress is comprised of the residual stress and the impinging load. The cycled sample needs more load to reach the threshold (i.e. the nonlinear regime), since the resulting damage has decreased the residual stress.

METCAN has the ability to specify the existence of a discrete interface between the fiber and matrix. To see what effects the interface has on the residual thermal stresses, METCAN was run again with the minimum interface thickness (5 percent of fiber diameter). The material properties of the interface were taken to be an average of the fiber and matrix properties. The reaction zone contains both fiber and matrix material , but the values found here are still approximate.

Figure 60 shows the radial and tangential stresses for the fiber, matrix, and interface from room temperature to 800°F. Again the radial and tangential stresses are equal since the shear stress is zero. The fiber is still in compression and the matrix and interface are in tension. The matrix and fiber stresses are about the same as Figure 59 when the interface was not included. The interface stress is

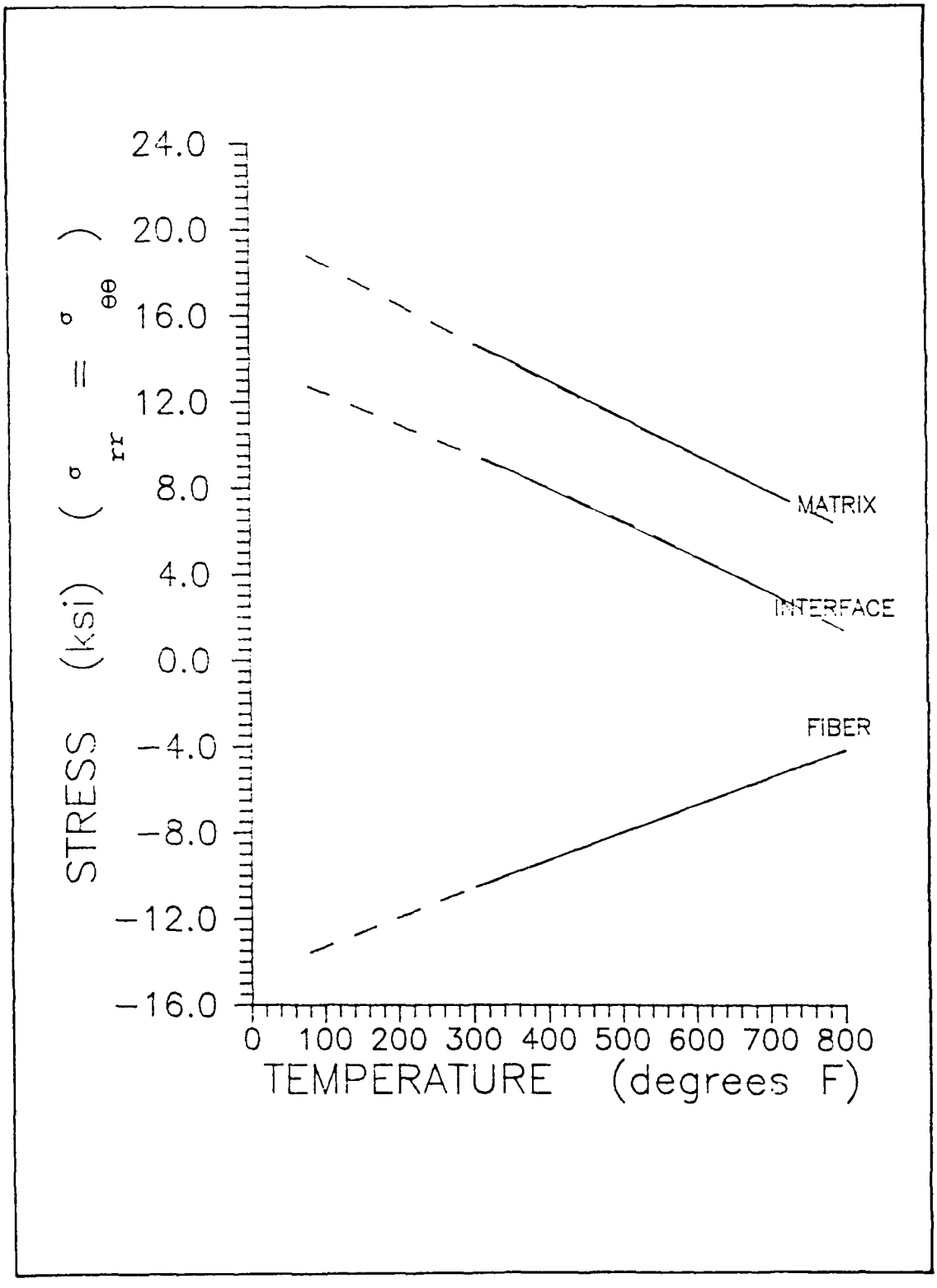

Figure 60. Fiber, Matrix, and Interface Thermal Residual Stresses versus Temperature of Specimen

12.890 ksi at room temperature. At 300°F the stress is 9.50 ksi and drops to 1.67 ksi at 800°F. These figures lead us to believe that the interface is a kind of buffer zone in between the fiber and matrix. The interface decreases the residual thermal stresses in the fiber and matrix slightly.

VI. Conclusions and Recommendations

This study discussed in detail the development of a setup for thermal fatigue (TF) testing of metal matrix composites (MMCs). The setup consists of a MTS servohydraulic loading machine modified to thermally load a specimen with a variety of temperature profiles. This setup utilizes a strain-gage type of extensometer to measure the thermal strain of the sample. A computer program for control of the acquisition of data has been developed for a triangular temperature profile. The modifications that can be made to the system to include mechanical fatigue were discussed.

To demonstrate the capability of the testing system, ten TF tests were run on an MMC. The MMC of interest was a $[0]_6$ ply layup of SCS6/Ti-15-3. The 7.0 inch by 0.5 inch by 0.046 inch specimens were cycled from a minimum of 250 to a maximum of 16,750 times between 300°F and 800°F. The results of these tests have been presented in this study.

The conclusions from this study can be summarized as follows:

1) Equipment was developed for TF testing of strips of MMCs.

2) The equipment used a strain-gage type of extensometer modified to measure displacement over a 1 inch gage length in the heated zone. The displacement was used to establish strain profiles during the thermal cycling.

3) The equipment was able to control temperature to within 3 percent of the programmed value during temperature cycling between 300°F and 800°F. Heating and cooling rates of 20.8°F/sec. were achieved on the MMC.

4) The computer program successfully directed the recording of temperature and strain profile data over the specified interval.

5) The mean strain changes as a function of thermal cycles. For approximately the first 550 cycles the mean strain increases indicating an expansion of the specimen. After 800 cycles the mean strain decreases showing a compression.

6) Conducted a systematic study of the initiation and progression of damage in a thermally cycled MMC.

7) Macroscopic damage occurs as cracking and ply delamination on the specimen edge around 1,500 cycles. This damage is an edge effect that occurs at the fiber tip pullout or at the ply seams.

8) Microscopic damage inside the specimen begins at 500 cycles. The damage formed as degradation of the fiber/matrix interface or reaction zone.

9) Young's Modulus, Poisson's Ratio, and coefficient of thermal expansion (at room temperature) were not affected by thermal cycling in this study even though damage was evident.

10) Ultimate tesile strength testing showed thermally cycled specimens stress-strain curves were more linear.

11) Analysis by the computer code METCAN showed thermal residual

stresses in the material as a result of processing. At high temperatures the stresses relaxed. At room temperature the stresses acted to rebond the material back together.

12) Plies delaminated at the edge because of residual tensile stresses in the matrix. Delamination occurred where fibers were missing since the laminate could not rebond itself.

Recommendations can be summarized as follows:

1) Temperatures should be read directly from the Micricon 82300, resulting in two temperature readings corresponding to the two quartz lamp heated areas. This requires computer connections and software to communicate with the Micricon. The system developed here reads the voltage in a type-K thermocouple and converts it to temperature, but it could read the voltage from only one thermocouple (corresponding to one area) at a time.

2) More thermal cycles need to be run with this temperature profile to see when the material completely fails and what the failure mode is.

3) Tests need to be run at higher temperatures with greater ranges and with the inclusion of mechanical fatigue to compare results.

4) Stain gages capable of surviving high temperatures are required to evaluate the stress-strain curves, and therefore Young's Modulus, at operating temperatures of the material. A change in modulus is an

indication of damage.

5) A model must be developed to predict the damage of MMC's on a microscopic level, since micrcscopic damage occurs before any change macroscopically or in the material's characteristics.

Appendix A

Software Written for the Computer Data Acquisition of a Metal Matrix Composite (MMC) Thermal Fatigue (TF) Test

This appendix describes the computer program developed for this thesis. The program acquires data from the equipment used in the TF testing of MMCs as presented in earlier chapters. The program:

1) Keeps track of cycle count at data samplings.
2) Records the temperature profile produced by the Micricon 82300 process controller at the designated cycle intervals.
3) Monitors the thermal strain profile by way of the extensometer at the designated cycle intervals.
4) Converts the respective voltages to temperature and strain and stores the data in specified files.

The output devices and their corresponding numbers used throughout the program are shown in Table 4. The IEEE-488 address numbers and their corresponding device names are shown in Table 5. A block diagram that describes the operation of the program is shown in Figure 61.

Table 4 Output Device Numbers

Output Number	Output Device Name
1	Com Port 2 for Data Display
2	Strain Data File
3	Temperature Data File
4	Temporary File for Extensometer Voltage

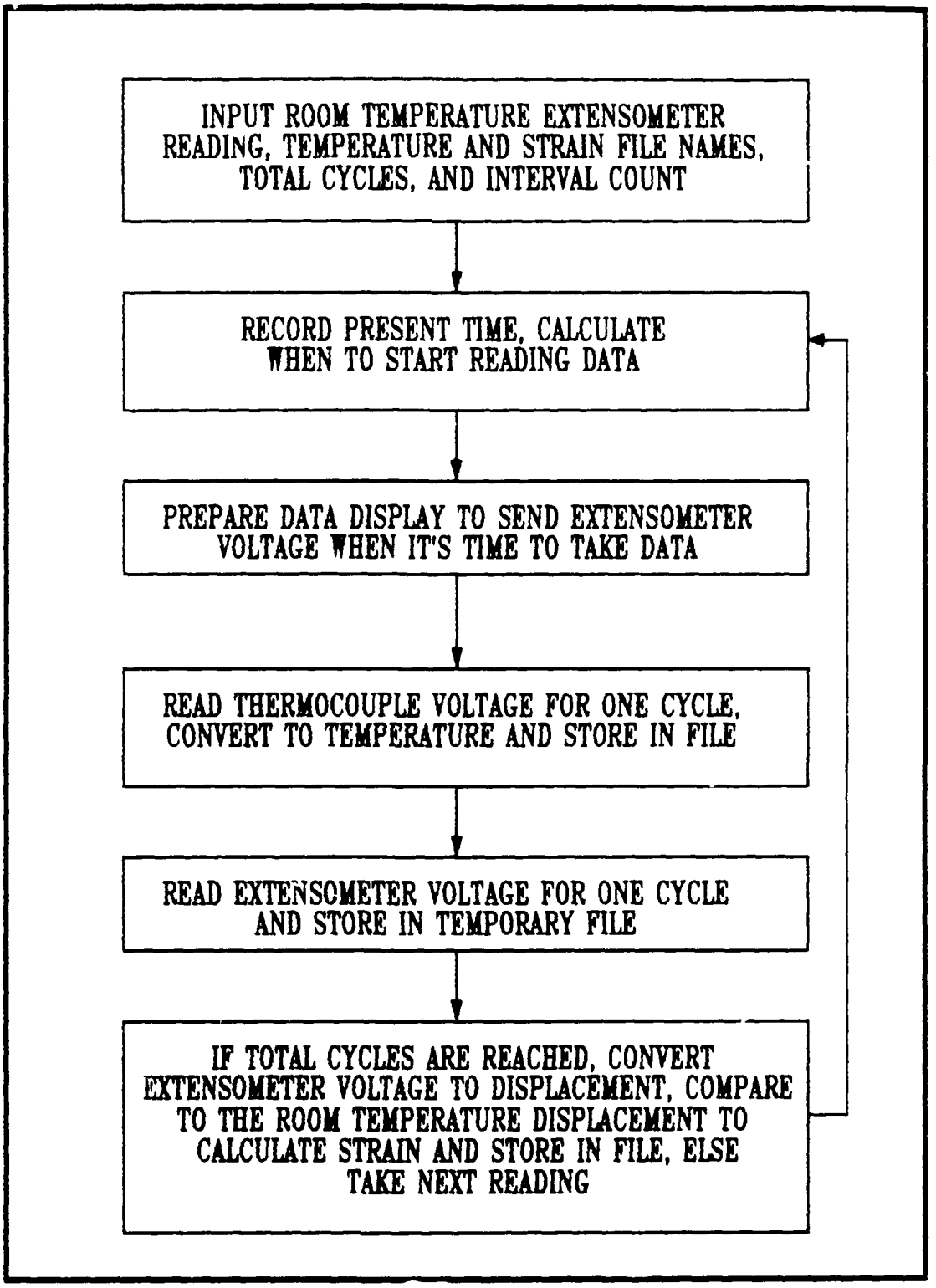

Figure 61. Block Diagram of the TF Testing Program

Table 5 IEEE-488 Address Numbers and Device Names

Address Number	Device Name
1	Z-248 Computer
24	HP 3437A Voltmeter

```
10 REM ************************************************************************
20 REM        DATA ACQUISITION FOR THERMAL CYCLING EXPERIMENTS ON MMC
30 REM ************************************************************************
40 REM
50 REM    This program:
60 REM      - reads voltage from the HP3437A voltmeter and converts it to temp.
70 REM      - reads voltage from the Data Display and converts it to strain
80 REM      - reads the temp data then the strain data at given intervals
90 REM      - shows a temperature profile if wanted
100 REM
110 REM ************************************************************************
120 REM
130 REM  Load the IEEE-488 software commands
140 REM
150 O!=0!
160 BUSSTA=&H4C5:CLR=&HA71:DCL=&H3A8:EOI=&H2BE
170 GTL=&H4A2:GTS=&H2AE:IFC=&H2D2
180 IFC3=&H315:INIT=&H321:LISTEN=&H6F5:LLO=&H3C8
190 LON=&H2C2:PASSCONT=&H609:PPDS=&H4D7:PPEN=&H3F8
200 PPOL=&H59C:PPU=&H3D8:READS=&H7FC:READB=&H7DE
210 RECECONT=&H645:REMOTE=&H6CE :SDC=&H3B8:SETTIMER=&HAA4
220 SPOL=&H4F9:TALK=&H7A3:TCA=&H24E:TCS=&H29E
230 TON=&H2CA:TRIG=&H4B3:ULON=&H2C6:UNL=&H36D
240 UNT=&H398:UTON=&H2CE:WRITES=&H8CB:WRITEB=&H8BB
250 XFER=&H99B
260 DEF SEG = 0
270 CSEG1=(256*PEEK(&H3C7))+PEEK(&H3C6)
280 DEF SEG=CSEG1
290 DIM TF(1000)
300 DIM AT(1000)
310 DIM X(1000)
320 REM
330 PRINT "*****************************************************************"
340 PRINT "       DATA ACQUISITION FOR THERMAL CYCLING OF MMC "
350 PRINT "*****************************************************************"
360 REM
```

```
370 PRINT : PRINT :PRINT "Start the THERMAL CYCLING!" : PRINT
375 PRINT "    Remember to run I488 before running this!!" : PRINT
380 PRINT "    For the HP3437A voltmeter, remember to:"
390 PRINT "         * turn on the voltmeter, amplifier and ice point"
400 PRINT "    For the Data Display, remember to:"
410 PRINT "         * turn on the power"
420 PRINT "         * turn off inputs 1 and 2"
430 PRINT "         * turn on input 3"
440 PRINT "         * Set Up Print to :"
450 PRINT "             * 0 - volts"
460 PRINT "             * 1 - dc"
470 PRINT "             * 0.560 sec intervals
480 PRINT "         * Set Peak Sensitivity to:"
490 PRINT "             * 0.1 for input #3" : PRINT : PRINT
492 INPUT "What's the room temp. extensometer reading?";EXROOM : PRINT
494 EXROOM=(EXROOM+46.834)/38.5364
500 INPUT;"Hit return to continue.";X$
510 PRINT: PRINT: PRINT:
520 REM
530 INPUT "Store temperature data in file?";NN$ : PRINT
540 OPEN NN$ FOR OUTPUT AS #3
550 INPUT "Store extensometer data in file?";NE$ : PRINT
560 OPEN NE$ FOR OUTPUT AS #2
570 INPUT "Total cycles?';TOTCYC : PRINT
580 INPUT "Cycle interval (>4)?";CYC : PRINT
590 REM
600 REM    Set up the inputs for the Data Display
610 OPEN"O",#4,"RAIN"
620 REM
630 XMIT$=""
640 PAUSELENGTH=10
650 FALSE=0
660 TRUE=-1
670 INPUTON=FALSE
680 DIM RECV$(256)
690 OPEN "COM2:600,E,7,1,CS,DS" AS #1      'Open COM2 to the Data Display
700 WHILE NOT EOF(1)                       'Clear the local buffer
710 BUFF$=INPUT$ (LOC(1),#1)
720 WEND
730 REM
740 REM  Set up the time interval to record data
750 REM
760 TIME$="01:00"
770 TOLD=TIMER
780 NUMCYC=NUMCYC+CYC
790 IF NUMCYC>TOTCYC THEN 1870
800 PRINT#3,  : PRINT#3,  : PRINT#3,NUMCYC
810 TNEW=TOLD+(48*CYC)
820 IF TNEW>80000! THEN 760
830 TT=TIMER
840 FOR K = 1 TO 2381
850 NEXT K
860 PRINT
```

```
870 IF TNEW-TT>0 THEN PRINT "   Cycle ";NUMCYC;"out of ";TOTCYC;" starts in ";TN
EW-TT;" sec."
880 IF TT>=TNEW THEN 890 ELSE 830
890 TOLD=TNEW
900 REM
910 REM   Put the Data Display in remote and clear the buffer
920 REM
930 XMIT$=CHR$(2):GOSUB 1960
940 WHILE NOT EOF(1)
950 BUFF$=INPUT$ (LOC(1),#1)
960 WEND
970 XMIT$="R"+CHR$(13):GOSUB 1960
980 REM
990 REM  ************ ************************************************************
1000 REM                Start collecting temperature data!
1010 REM  ************************************************************************
1020 REM
1030 I=0
1040 PRINT: PRINT "Just a minute...collecting temperature data."
1050 TIMEI=TIMER
1060 KV=0                                  'valve is initially closed
1070 DEF SEG=CSEG1
1080 I=I+1
1090 IF TIMER>(TIMEI+(1.5/.02083)) THEN 1400
1100 FOR K=1 TO 100
1110 NEXT K
1120 RDATA$="+.009620308                   "
1130 SYSCON%=1                            'IBM PC as system controller
1140 I488ADDR%=&H318
1150 DEVADDR%=1                           '488 controller device address
1160 CALL INIT(SYSCON%,I488ADDR%,DEVADDR%)     'initialize the system
1170 REM
1180 CALL LLO
1190 COMM$=" R1 T1"
1200 LISTEN$="24"
1210 EOI$=""
1220 CALL WRITES(LISTEN$,EOI$,COMM$)
1230 TALK$="24"
1240 LISTEN$=""
1250 CALL READS(TALK$,LISTEN$,EOI$,RDATA$,STATUS%)
1260 X=VAL(RDATA$)
1270 IF X<.001 THEN 1120
1280 AT(I)=TIMER
1290 X(I)=X
1300 IF I<5 THEN 1080
1310 IF KV=1 THEN 1360
1320 IF X(I)>X(I-4) THEN 1080
1330 KV=1
1340 REM
1350 GOTO 1070
1360 REM
```

```
1370 IF X(I)<X(I-4) THEN 1080
1380 KV=0
1390 GOTO 1070
1400 PRINT : PRINT "Hold on...converting temperature data."
1410 FOR J=1 TO I
1420 X = X(J)/10
1430 A0=.226584602#
1440 A1=24152.109#
1450 A2=67233.4248#
1460 A3=2210340.682#
1470 A4=-860963914.9#
1480 A5=4.83506*10^10
1490 A6=-1.18452*10^12
1500 A7=1.3869*10^13
1510 A8=-6.33708*10^13
1520 TC=A0+X*(A1+X*(A2+X*(A3+X*(A4+X*(A5+X*(A6+X*(A7+A8*X))))))
1530 TF(J)=TC*9/5+32.2
1540 NEXT J
1550 ATT=AT(1)
1560 K=I-1
1570 FOR J=1 TO K
1580 AT(J)=AT(J)-ATT
1590 PRINT #3, AT(J);TF(J)
1600 NEXT J
1610 REM
1620 REM ************************************************************************
1630 REM              Start collecting strain data!
1640 REM ************************************************************************
1650 REM
1660 XMIT$="O"+CHR$(13):GOSUB 1960
1670 PRINT : PRINT "Another minute...collecting extensometer data."
1680 INPUTON=TRUE
1690 FOR J = 1 TO 3
1700 FOR I = 1 TO 256
1710 IF LOC(1) > 164 AND INPUTON THEN OUT &H3FC,(INP(&H3F3) AND &HFE) : INPUTON=
FALSE
1720 IF LOC(1) <128 AND NOT INPUTON THEN OUT &H3FC,(INP(&H3FC) OR &H1) : INPUTON
=TRUE
1730 INPUT #1,RECV$(I)
1740 IF LOC(1) < 128 AND NOT INPUTON THEN OUT &H3FC,(INP(&H3FC) OR &H1) : INPUTO
N=TRUE
1750 NEXT I
1760 OUT &H3FC,(INP(&H3FC) AND &HFE) : INPUTON=FALSE
1770 FOR I = 1 TO 256
1780 PRINT #4,RECV$(I)
1790 NEXT I
1800 IF LOC(1) < 128 AND NOT INPUTON THEN OUT &H3FC,(INP(&H3FC) OR &H1) : INPUTO
N=TRUE
1810 NEXT J
1820 XMIT$="O"+CHR$(13) : GOSUB 1960
1830 GOTO 780
1840 REM
1850 REM   Get the Data Display out of remote and close files
1860 REM
```

```
1870 XMIT$=CHR$(3) : GOSUB 1960
1880 CLOSE #1 : CLOSE #4 : CLOSE #3
1890 PRINT : PRINT "*************************************************************"
1900 PRINT "          ";NUMCYC-CYC;" cycles completed!"
1910 PRINT : PRINT "          Temperature data in file: ";NN$
1920 PRINT "          Strain data in file: ";NE$
1930 PRINT "*************************************************************"
1940 GOSUB 2080
1950 END
1960 REM
1970 REM ***************************************************************************
1980 REM                  TRANSMISSION AND DELAY SUBROUTINE
1990 REM ***************************************************************************
2000 REM
2010 BUFFLENGTH=LEN(XMIT$)
2020 FOR BUFFPOSITION = 1 TO BUFFLENGTH
2030 XMITCHR$=MID$(XMIT$,BUFFPOSITION,1)
2040 PRINT #1,XMITCHR$;
2050 FOR DELAY = 1 TO PAUSELENGTH : NEXT DELAY
2060 NEXT BUFFPOSITION
2070 RETURN
2080 REM ***************************************************************************
2090 REM                EXTENSOMETER CONVERSION SUBROUTINE
2100 REM ***************************************************************************
2110 REM
2120 PRINT : PRINT "Hold on...just need to convert extensometer data."
2130 DIM N$(1000)
2140 OPEN"I",#4,"RAIN"
2150 TERV=.56
2160 FOR J = 1 TO TOTCYC/CYC
2170 NCYC=NCYC+CYC
2180 I=1 : TM=0
2190 FOR K = 1 TO 1000
2200 IF EOF(4) THEN END
2210 INPUT#4, N$(K)
2220 IF N$(K)="a" THEN IF K=1 GOTO 2330
2230 IF N$(K)="a" THEN IF K>5 GOTO 2340
2240 IF N$(K)="a" THEN IF N$(K-1)="a" GOTO 2330
2250 IF N$(K)<>"a" THEN IF N$(K-1)="a" THEN KK=K-1 : PRINT#2, : PRINT#2,NCYC
2260 IF K<>KK+I*4 GOTO 2330
2270 INCH=VAL(N$(K))
2280 INCH=(INCH+46.834)/38.5364
2285 STRAIN=(INCH-EXROOM)/EXROOM
2290 PRINT#2,USING "###.#####";TM;STRAIN
2310 TM=TM+TERV
2320 I=I+1
2330 NEXT K
2340 ERASE N$
2350 DIM N$(1000)
2360 NEXT J
2370 RETURN
```

Bibliography

1. Aveston, J. and others. "Single and Multiple Fracture," The Properties of Fiber Composites, 12: 12-26 (1971).

2. Bahei-El-Din, Y.A. Plastic Analysis of Metal-Matrix Composite Laminates. PhD dissertation. Duke University, 1979.

3. Bahei-El-Din, Y.A. and Dvorak, G.J. "Plasticity Analysis of Laminated Composite Plates," Journal of Applied Mechanics, 49: 740-746 (1982).

4. Bigelow, C.A. and others. "Mechanics of Composite Materials and Structures," The Third Joint ASCE/ASME Mechanics Conference, New York: ASME Press, 1989.

5. Bodner, S.R. "Review of a Unified Elastic-Viscoplastic Theory," Constitutive Equations for Plastic Deformation and Creep of Engineering Alloys (1987).

6. Broek, David. Elementary Engineering Fracture Mechanics. Netherlands: Martinus Nijhoff Publishers, 1986.

7. Budiansky, B. and others. "Matrix Fracture in the Fiber Reinforced Ceramics," Journal of Mechanical and Physical Solids. 34: 167-189 (1986).

8. Caruso, J.J. and Chamis, C.C. "Superelement Methods and Applications to Micromechanics of High Temperature Metal Matrix Composites," NASA TM - 2390, 1988.

9. Chamis, C.C. and Hopkins, D.A. "Thermoviscoplastic Nonlinear Constitutive Relationships for Structural Analysis of High Temperature Metal Matrix Composites," NASA TM - 87291, November 1985.

10. Complete Temperature Measurement Handbook and Encyclopedia. Omega Engineering Inc., Stamford CT, 1986.

11. Crowl, C.R. "Fatigue and Corrosion Fatigue Characteristics of Metal Matrix Composites," NASA TM - 1019, 1988.

12. Dvorak, G.J. and Bahei-El-Din, Y.A. "Elastic-Plastic Behavior of Fibrous Composites," Journal of the Mechanics and Physics of Solids, 27: 51-72 (1979).

13. Fundamentals of Process Control. Research Inc., Minneapolis MN, May 1981.

14. Gabb, T.P. and others. Isothermal and Non-Isothermal Fatigue Behavior of a Metal Matrix Composite. Submitted to Journal of Composite Materials, 1989.

15. Gayda, J.G. and others. "The Isothermal Fatigue Behavior of a Unidirectional SiC/Ti Composite and The Ti Alloy Matrix," NASA TM - 101984, April 1989.

16. Halford, G.R. Low-Cycle Thermal Fatigue. Lewis Research Center, Cleveland OH, February 1986.

17. Hartman, G.A. and Johnson, D.A. "D-C Electric-Potential Method Applied to Thermal/Mechanical Fatigue Crack Growth," Experimental Mechanics: 106-112 (March 1987).

18. Heil, Major Michael L. Crack Growth in Alloy 718 Under Thermal-Mechanical Cycling. PhD dissertation. School of Engineering, Air Force Institute of Technology (AU), Wright-Patterson AFB OH, November 1986.

19. Highsmith, A.L. and others. Local Stresses in Metal Matrix Composites Subjected to Thermal and Mechanical Loading. Presented at Symposium on Thermal and Mechanical Behavior of Ceramic and Metal Matrix Composites (ASTM), Atlanta GA, November 7, 1988.

20. Hopkins, D.A. and Chamis, C.C. "A Unique Set of Micromechanics Equations for High Temperature Metal Matrix Composites," NASA TM - 87154, November 1985

21. HP3437A Introductory User's Guide. Hewlett Packard, 1980.

22. IEEE-488 GPIB Controller Instruction Manual. Qua Tech Inc., Akron OH, undated.

23. Johnson, W.S. "Fatigue Testing and Damage Development in Continuous Fiber Reinforced Metal Matrix Composites," NASA TM - 100628, 1988.

24. Johnson, W.S. "Mechanical Characterization of SCS6/Ti-15-3 Metal Matrix Composites at Room Temperature," NASP TM - 1014, April 1988.

25. Kyno, T. and others. "Effects of Thermal Cycling on Properties of Carbon Fiber/Aluminum Composites," Journal of Engineering Materials and Technology, 110: 89-95 (April 1988).

26. Majumdar, B.S. and Newaz, G.M. Thermo-Mechanical Response and Damage in an Angle-Ply Metal Matrix Composite. Submitted to the Journal Engineering Materials and Technology ASME, October 1989.

30. Metal Matrix Composite Analyzer METCAN Version 2.0 User's Guide. NASA Lewis Research Center, Cleveland OH, September 1988.

31. Micricon Control PID Adjustments, Research Inc., Minneapolis MN, 1981.

32. Micricon Users Manual. Research Inc., Minneapolis MN, 1986.

33. Model 5305 Parabolic Strip Heater Rev B. Research Inc., Minneapolis MN, December 1985.

34. Mom, A.J.A. Operating Conditions and Materials Selection and Development in Gas Turbines. National Aerospace Laboratory (NLR) Amsterdam. The Netherlands, 17 Mar 1981.

35. Nimmer, R.P. "Fiber-Matrix Interface Effects in the Presence of Thermally Incuded Residual Stresses." GE TM - 944, October 1988.

36. Oleinik, A.S. and others. Heating Device For Rigs Used in Fatigue Testing of Specimens at Temperature Up to 1800°C. Academy of Sciences of the Ukrainia SSR, March 1983.

37. Pelloux, R.M. and Marchand, N. Thermal-Mechanical Fatigue Behavior of Nickel-Base Superalloys. Massachusetts Institute of Technology, Cambridge MS, March 1986.

38. Pernot, 2LT John J. Thermal-Mechanical Fatigue Testing of a Titanium-Aluminide Alloy. MS Thesis, AFIT/GAE/AA/87D-18. School of Engineering, Air Force Institute of Technology (AU), Wright-Patterson AFB OH, December 1987.

39. Series 632 High Temperature Extensometers. MTS Systems Corporation, Minneapolis MN, undated.

40. Wilson, D.A. and Warren, J.R. Thermal Mechanical Fatigue Crack Growth. Pratt & Whitney, West Palm Beach Florida, March 1985.

Vita

Captain Paul G. Ermer [redacted] he graduated from high school in Amherst, New York and attended the State University of New York at Buffalo. He received the degree of Bachelor of Science in Aerospace Engineering in May 1983. Upon completion of the OTS program in December 1983, he received a commission in the USAF. He then served as a High Energy Laser System Vulnerability Engineer at the Air Force Weapons Laboratory, Kirtland AFB, New Mexico until entering the School of Engineering, Air Force Institute of Technology, in May 1988.

[redacted]

REPORT DOCUMENTATION PAGE

Form Approved
OMB No. 0704-0188

1a REPORT SECURITY CLASSIFICATION UNCLASSIFIED	1b RESTRICTIVE MARKINGS
2a SECURITY CLASSIFICATION AUTHORITY	3 DISTRIBUTION / AVAILABILITY OF REPORT approved for public release; distribution unlimited
2b DECLASSIFICATION / DOWNGRADING SCHEDULE	
4 PERFORMING ORGANIZATION REPORT NUMBER(S) AFIT/GAE/ENY/89D-07	5 MONITORING ORGANIZATION REPORT NUMBER(S)
6a NAME OF PERFORMING ORGANIZATION School of Engineering 6b OFFICE SYMBOL (If applicable) AFIT/ENY	7a NAME OF MONITORING ORGANIZATION
6c ADDRESS (City, State, and ZIP Code) Air Force Institute of Technology Wright-Patterson AFB OH 45433-6583	7b ADDRESS (City, State, and ZIP Code)
8a NAME OF FUNDING / SPONSORING ORGANIZATION WRDC, Propulsion Lab 8b OFFICE SYMBOL (If applicable) WRDC/POTC	9 PROCUREMENT INSTRUMENT IDENTIFICATION NUMBER
8c ADDRESS (City, State, and ZIP Code) WRDC/POTC Wright-Patterson AFB OH 45433	10 SOURCE OF FUNDING NUMBERS PROGRAM ELEMENT NO. / PROJECT NO. / TASK NO / WORK UNIT ACCESSION NO

11 TITLE (Include Security Classification)
Investigation of the Failure Modes in a Metal Matrix Composite Under Thermal Cycling

12 PERSONAL AUTHOR(S)
Paul G. Ermer, Captain, USAF

13a TYPE OF REPORT	13b TIME COVERED	14 DATE OF REPORT (Year, Month, Day)	15 PAGE COUNT
MS Thesis	FROM _____ TO _____	1989 December	133

16 SUPPLEMENTARY NOTATION

17 COSATI CODES			18 SUBJECT TERMS (Continue on reverse if necessary and identify by block number)
FIELD	GROUP	SUB-GROUP	Thermal, Fatigue, MMC, Cracks, Reaction Zone, METCAN
21			

19 ABSTRACT (Continue on reverse if necessary and identify by block number)

Thesis Advisor: Shankar Mall
Professor of Aeronautics and Astronautics

20 DISTRIBUTION / AVAILABILITY OF ABSTRACT	21 ABSTRACT SECURITY CLASSIFICATION
☒ UNCLASSIFIED/UNLIMITED ☐ SAME AS RPT ☐ DTIC USERS	UNCLASSIFIED
22a NAME OF RESPONSIBLE INDIVIDUAL Dr. Shankar Mall	22b TELEPHONE (Include Area Code) (513) 255-5533 22c OFFICE SYMBOL AFIT/ENY

There is currently wide interest in producing a vehicle capable of hypersonic flight. Structural materials in such a vehicle must be able to withstand high temperatures and retain high stiffness. Metal matrix composites (MMCs) are rapidly becoming the strongest candidates for these applications and concurrently, the need to study the effects of thermal cycling on them. A titanium matrix composite with silicon carbide fibers (SCS_6/Ti-15-3) is the object of this study. A computer controlled testing system was designed to cycle the MMC from 300°F to 800°F while collecting strain and temperature data. A systematic study was undertaken to investigate the initiation and progression of the damage and its effect on mechanical properties as a function of applied thermal stresses.